ISSN 2413-5577

№ 1 Январь – Март 2023

Экологическая безопасность прибрежной и шельфовой зон моря

Ecological Safety of Coastal and Shelf Zones of Sea

No. 1 January – March 2023

ecological-safety.ru

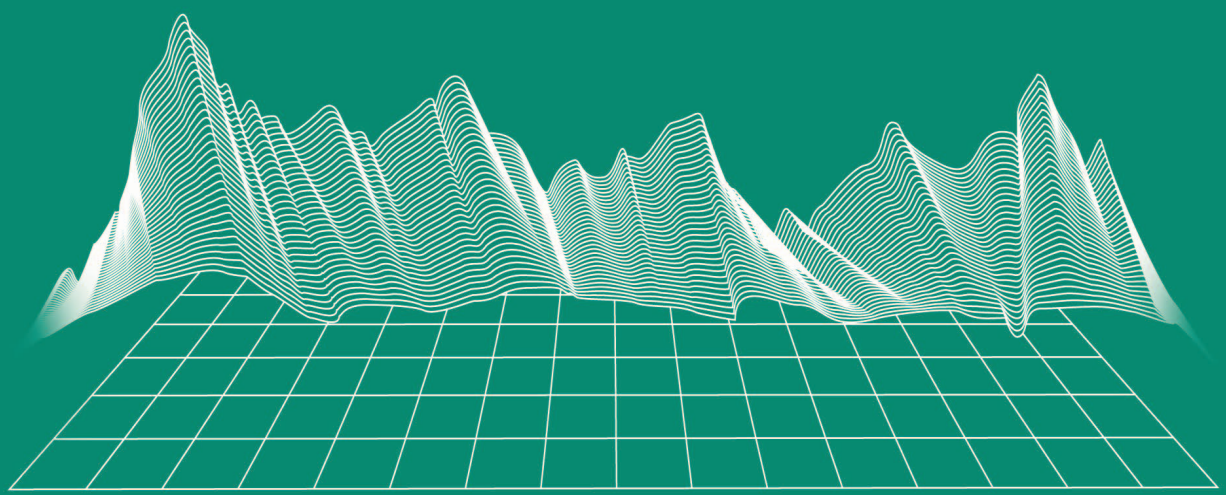

ISSN 2413-5577
No. 1, 2023
January – March

Publication frequency:
Quarterly
16+

ECOLOGICAL SAFETY OF COASTAL AND SHELF ZONES OF SEA

Scientific and theoretical peer reviewed journal

FOUNDER AND PUBLISHER:
Federal State Budget Scientific Institution
Federal Research Centre
"Marine Hydrophysical Institute of RAS"

The Journal publishes original research results, review articles (at the editorial board's request) and brief reports.

The Journal aims at publication of results of original scientific research concerning the state and interaction of geospheres (atmosphere, lithosphere, hydrosphere, and biosphere) within coastal and shelf areas of seas and oceans, methods and means of study thereof, ecological state of these areas under anthropogenic load as well as environmental protection issues.

The Journal's editorial board sees its mission as scientific, educational and regulatory work to preserve the ecological balance and restore the resource potential of coastal and shelf areas believing that despite the geographical limitations of the areas under study, the processes taking place within them have a significant impact on the waters of the seas and oceans and economic activity.

The Journal publishes original research materials, results of research performed by national and foreign scientific institutions in the coastal and shelf zones of seas and oceans, review articles (at the editorial board's request) and brief reports on the following major topics:
- Scientific basis for complex use of shelf natural resources
- Marine environment state and variability
- Coastal area state and variability; coast protection structures
- Monitoring and estimates of possible effects of anthropogenic activities
- Development and implementation of new marine environment control and monitoring technologies

The outcome of the research is information on the status, variability and possible effects of anthropogenic activities in the coastal and shelf marine areas, as well as the means to perform calculations and to provide information for making decisions on the implementation of activities in the coastal zone.

e-mail: ecology-safety@mhi-ras.ru

website: http://ecological-safety.ru

Founder, Publisher and Editorial Office address:
2, Kapitanskaya St.,
Sevastopol, 299011, Russia

Phone, fax: + 7 (8692) 54-57-16

EDITORIAL BOARD

РЕДАКЦИОННАЯ КОЛЛЕГИЯ

CONTENTS

№ 1. 2023 January – March, 2023

СОДЕРЖАНИЕ

№ 1. 2023 Январь – Март, 2023

Original article **DOI:** 10.29039/2413-5577-2023-1-6-19

Numerical Modelling of Upwelling near the South Coast of Crimea on 24–25 September 2013

V. V. Efimov, D. A. Iarovaya *, V. S. Barabanov

Marine Hydrophysical Institute of RAS, Sevastopol, Russia
* *e-mail: darik777@mhi-ras.ru*

Abstract
Using 2-km resolution coupled air-sea mesoscale model NOW (NEMO-OASIS-WRF), we studied a case of upwelling in the Black Sea near the South Coast of Crimea on 24–25 September 2013. The NOW model successfully reproduced a sharp decrease of sea surface temperature (SST) by 10 °C within two days. The high spatial resolution in the model allowed us to describe upwelling features resulting from the orography and shape of the coastline. In particular, we found small-scale areas of low SST near the coast where surface wind is directed along the coast to the right, for example over the sea near the coastal Crimean Mountains. At the same time the upwelling does not occur in the areas where the coastal wind has another direction, for example in the north-western part of Karkinit Bay, near the coast north to Sevastopol, and near the Azov coast. It is shown that there is a vertical circulation cell in the sea caused by the upwelling: a rise of the seasonal thermocline near the shore, outflow of warm water in the upper quasihomogenous layer and descend of water at the 30–50 km distance from the shore. We found that the coastal current has diurnal variation due to breeze circulation: the velocity component perpendicular to the coast reaches its maximum during the daylight hours, whereas velocity component directed along the coast reaches its maximum with a delay of 4–6 hours.

Keywords: mesoscale coupled modelling, wind upwelling, vertical structure of velocity and temperature fields in sea, seasonal thermocline, Black Sea, South Coast of Crimea

Acknowledgements: The work was performed under project no. 0555-2021-0002 “Fundamental studies of processes of interaction in the ocean – atmosphere system which determine the regional spatial-temporal variability of the natural environment and climate”.

For citation: Efimov, V.V., Iarovaya, D.A. and Barabanov, V.S., 2023. Numerical Modelling of Upwelling near the South Coast of Crimea on 24–25 September 2013. *Ecological Safety of Coastal and Shelf Zones of Sea*, (1), pp. 6–19. doi:10.29039/2413-5577-2023-1-6-19

Численное моделирование апвеллинга у Южного берега Крыма 24–25 сентября 2013 года

В. В. Ефимов, Д. А. Яровая *, В. С. Барабанов

Морской гидрофизический институт РАН, Севастополь, Россия
** e-mail: darik777@mhi-ras.ru*

Аннотация

При помощи совместной мезомасштабной модели море – атмосфера *NOW* (*NEMO-OASIS-WRF*) с разрешением 2 км изучен один из случаев ветрового прибрежного апвеллинга в Черном море у Южного берега Крыма 24–25 сентября 2013 г. Модель *NOW* успешно воспроизвела резкое понижение температуры поверхности моря на 10 °С в течение двух суток. Повышенное пространственное разрешение при моделировании позволило выделить особенности апвеллинга, связанные с рельефом и очертаниями береговой линии. В частности, выделены мелкомасштабные области понижения температуры там, где ветер направлен вправо вдоль берега, например над морем вблизи гор Южного берега Крыма. В то же время там, где прибрежный ветер имеет другое направление, апвеллинг отсутствует, например в северо-западной части Каркинитского залива, на побережье севернее Севастополя, а также на азовском побережье. Показано наличие в море вертикальной ячейки циркуляции, связанной с апвеллингом: подъем сезонного термоклина вблизи берега, отток теплой воды в квазиоднородном слое и опускание на расстоянии ~ 30–50 км от берега. Обнаружена суточная периодичность в изменении прибрежного течения, связанная с влиянием бризовой циркуляции: в дневные часы нормальная к берегу компонента скорости течения максимальна, а вдольбереговая достигает максимума с запаздыванием на 4–6 ч.

Ключевые слова: мезомасштабное совместное моделирование, ветровой апвеллинг, вертикальная структура полей скорости и температуры в море, сезонный термоклин, Черное море, Южный берег Крыма

Благодарности: работа выполнена в рамках проекта № 0555-2021-0002 «Фундаментальные исследования процессов взаимодействия в системе океан–атмосфера, определяющих региональную пространственно-временную изменчивость природной среды и климата».

Для цитирования: *Ефимов В. В., Яровая Д. А., Барабанов В. С.* Численное моделирование апвеллинга у Южного берега Крыма 24–25 сентября 2013 года // Экологическая безопасность прибрежной и шельфовой зон моря. 2023. № 1. С. 6–19. EDN SSUZXG. doi:10.29039/2413-5577-2023-1-6-19

Introduction

Upwellings in the near-surface coastal layer of the sea occur rather frequently near the South Coast of Crimea (SCC). The very physical mechanism of the coastal wind upwelling – the Ekman transport of water from the coast to the sea caused by the western alongshore wind – is quite obvious. In the warm season, this leads to the rise of cold deep waters and significant decreases in sea surface temperature (SST) [1]. As a result, near-surface waters are enriched with biogenic elements, and rich breeding ground for phyto- and zooplankton is formed. Sea temperature drops in coastal areas affect the weather and climate of the adjacent land.

However, this simple concept of wind Ekman upwelling in coastal areas is not always suitable for the description of specific natural phenomena. A number

of factors lead to the distortion of the spatial and temporal structure of coastal upwelling and in many cases to the emergence of new mechanisms concerning its occurrence. A simple picture of the development of wind upwelling becomes more complicated when taking into account the influence of bottom orography inhomogeneities in the coastal and shelf areas of the sea, seasonal and synoptic variability of the wind field, and features of the sea baroclinic layer. The local features of upwelling development in the coastal and open areas of the ocean were actively studied first analytically and then using numerical models, for example, in [2–6]. An overview of upwelling models can be found in [1)] [1].

When studying upwellings in the Black Sea, it is also necessary to take into account the relatively small size and isolation of the sea, as a result of which cold water areas will have small-scale spatial structure, and upwellings themselves can often occur in various parts of the coast. Variations of the bottom orography directed along the coast and large curves of the coastline significantly disrupt the two-dimensionality of coastal upwelling.

A number of numerical experiments are devoted to the study of upwellings in the northern part of the Black Sea [7, 8]. We should also note direct observations and numerical calculations of the development of upwelling off the eastern coast of the Black Sea – near Gelendzhik [9–13]. Recent works are often accompanied by illustrations of satellite observations of upwellings, which are especially well detected in the warm period of the year as areas of cold coastal waters. Among them, the recent work [14] should be pointed out with the review of a large number of upwelling satellite observations.

Satellite measurements of sea surface temperature currently have a fairly high spatial resolution of less than 1 km. At the same time, until recently, numerical experiments on the modelling of real cases of upwelling were mainly reduced to the modelling of the circulation of the entire Black Sea with rough spatial resolution, or the circulation was calculated in a local coastal model with high resolution, but with rough assignment of hydrometeorological characteristics at the open boundaries of the computational domains.

In this regard, it is of interest to conduct a coupled numerical simulation of upwelling development with increased spatial resolution, using a realistic coastline, bottom orography, and boundary conditions on the sea surface in the model. Recently, a numerical model of regional atmospheric circulation WRF [2)] and marine circulation model NEMO [3)] have been widely used. The first results of the use of a coupled air–sea model based on WRF and NEMO to study the response of the Black Sea to the 2005 quasitropical cyclone are described in [15].

[1)] Kraus, E.B., 1977. *Modelling and Prediction of the Upper Layers of the Ocean*. Oxford: Pergamon Press, 325 p.

[2)] Skamarock, W.C., Klemp, J.B., Dudhia, J., Gill, D.O., Barker, D.M., Duda, M.G., Huang, X-Yu, Wang, W. and Powers, J.G., 2008. *A Description of the Advanced Research WRF Version 3. NCAR Technical Note*. NCAR/TN-475+STR, 112 p. doi:10.5065/D68S4MVH

[3)] Madec, G. and the NEMO team, 2008. *NEMO Ocean Engine*. Note du Pôle de modélisation, No. 27. Technical Report. France: Institut Pierre-Simon Laplace. Available at: https://www.nemo-ocean.eu/doc/node1.html [Accessed: 30 March 2023].

In [16], this coupled model was used to study the characteristic response of the upper layer of the Black Sea to intense wind forcing.

This work is devoted to the description of the results of the modelling carried out with 2-km resolution in order to reproduce the interaction of the atmosphere and the sea during the upwelling in the Black Sea near the South Coast of Crimea on 24–25 September 2013. The task to consider in detail all the physical mechanisms responsible for the occurrence of upwelling in the Black Sea was not set. The development of upwelling for one specific synoptic situation is numerically reproduced, and small-scale features of its structure are identified.

Numerical Model

Coupled model NOW (NEMO-OASIS-WRF) consists of three following units: marine model NEMO, atmospheric model WRF and interface unit OASIS [17]. The computational area included the entire Black Sea. The horizontal computational grids in the marine and atmospheric models were identical to avoid interpolation during data exchange. The spatial resolution of the computational grids is 2 km. 37 vertical levels were used in the atmospheric model, 50 – in the marine one. Every two hours, sea surface temperature and surface current velocities are transmitted from NEMO to WRF, radiative heat fluxes (shortwave and longwave), sensible and latent heat fluxes, wind friction stress, as well as the difference between evaporated moisture and precipitation are transmitted from WRF to NEMO. To parameterize the atmospheric near-surface layer in WRF, the Revised MM5 Surface Layer Scheme was used, in which the sensible and latent heat fluxes from the surface are calculated using standard bulk formulas. To parameterize vertical turbulent mixing in NEMO, scheme $k - \varepsilon$ was used [18]. The exchange coefficients in this scheme are determined in terms of the turbulent kinetic energy and the dissipation rate, which is a prognostic quantity. The results of the NOW model were output in increments of 1 hour.

SST satellite images analysis showed the development of upwelling near Crimea on 24–25 September 2013 (Fig. 1). Coupled modelling started at 00:00 on September 21 and lasted 5 days. The initial and lateral boundary conditions for the atmospheric model were taken from the ERA5 reanalysis with a resolution of 0.25°. The initial conditions for the marine model (velocity, temperature, salinity and sea surface height fields), as well as the bottom orography, were taken from the Copernicus [4)] global reanalysis with a resolution of 1/12°. Generally speaking, for a more accurate reproduction of SST anomalies, preliminary adaptation of the marine and atmospheric models over a sufficiently long period of time is necessary. However, since the ERA5 reanalysis data are used as atmospheric forcing to obtain the Copernicus reanalysis, the initial conditions for the marine model

[4)] Copernicus Marine Service. *Global Ocean Physics Reanalysis*. 2023. [online] Available at: https://resources.marine.copernicus.eu/product-detail/GLOBAL_MULTIYEAR_PHY_001_030/INFORMATION [Accessed: 30 March 2023].

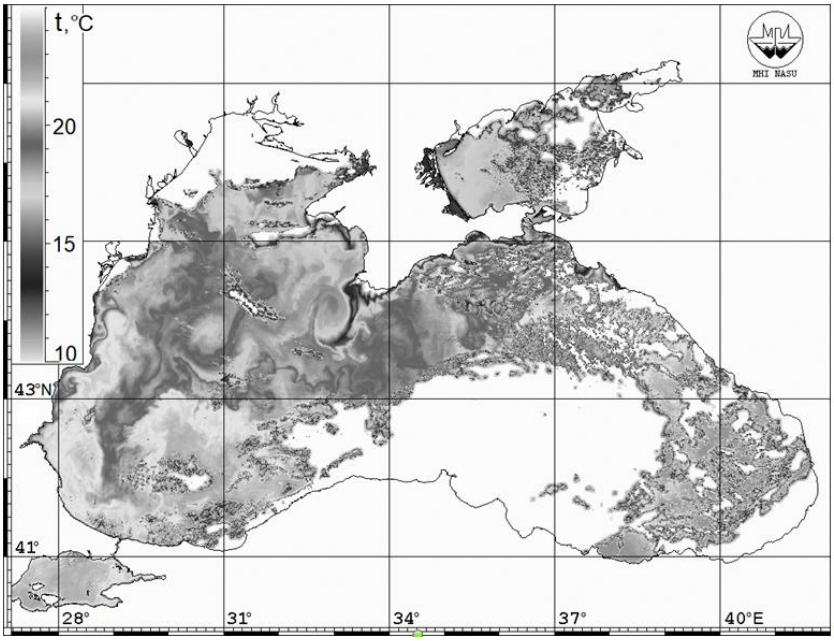

Fig. 1. A satellite image of the sea surface temperature for 25 September 2013 (Available at: http://dvs.net.ru/mp/data/1309/3SEP2504.GIF)

have already been largely adapted to the atmospheric fields from the WRF model, which reduces the adaptation calculation time. Pertinently, our task was to restore a more detailed spatial structure of wind upwelling in the coastal area of Crimea, which was not reproduced in the original reanalysis fields with a coarser resolution. Due to computational limitations, we did not use the ensemble forecasting method and settled on only one variant of the process development trajectory, taking into account that the following boundary conditions are decisive – orography, underlying surface type, coastline, etc.

Upwelling Development

Fig. 2 shows changes in sea surface temperature, zonal (alongshore) wind speed at a height of 10 m and surface air temperature at a height of 2 m in the coastal area at point *1* with coordinates 34.15°E, 44.4°N. This point will be further considered as characteristic of a relatively narrow coastal area of the sea near the South Coast of Crimea, where the 100 m isobath begins at a distance of about 10 km, 200 m – at a distance of 20 km, and 1,000 m – at a distance of 30 km from the coast. As reflected by Fig. 2, a slight decrease in the SST in the first two days was replaced by a sharp decrease by ~ 10 ºC associated with an increase in the near-surface wind speed and a decrease in the surface air temperature. Thus, Figure 2 clearly shows the episode of sharp local development of coastal wind upwelling near the South Coast on September 24–25, shown on a satellite image (see Fig. 1).

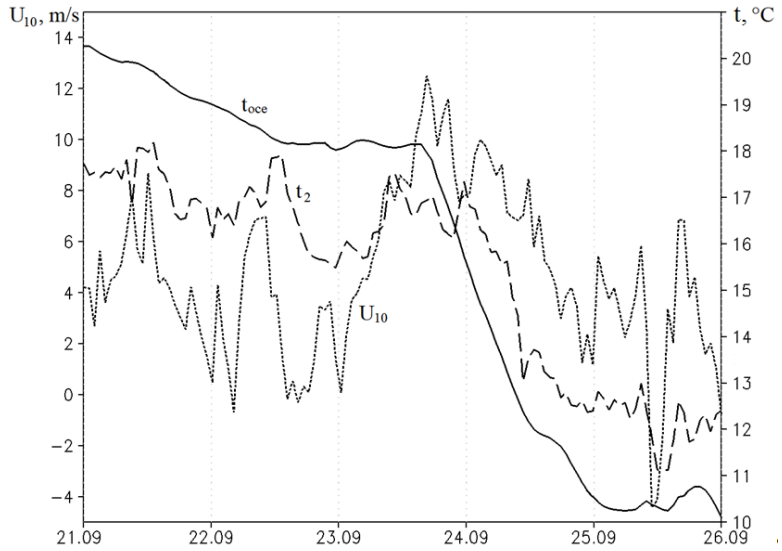

Fig. 2. Zonal (alongshore) wind speed at a height of 10 m, U_{10}, surface air temperature at a height of 2 m, t_2, and sea surface temperature t_{oce}, in the coastal area at point *1*

Horizontal Upwelling Structure

The SST distribution on the satellite image (see Fig. 1) refers to the most developed upwelling. Approximately for the same time, Fig. 3, *a* shows modelling results: the wind speed fields at a height of 10 m and the current velocity on the surface, as well as the air temperature field at a height of 2 m and SST. The same fields are shown on an enlarged scale with greater detail in Fig. 3, *b*. Note that the data in Fig. 3 refer to the night time, which is characterized by low overland temperatures.

As can be seen from Fig. 3, wind upwelling with minimum temperatures of ~ 11–12 °C occupies a relatively narrow coastal zone; the width of the upwelling area near the South Coast of Crimea makes ~ 30–50 km. At the same time, coastal upwelling has a small-scale spatial structure that reflects the curves of the coastline and spatial variations in wind direction relative to the coast. The increased resolution of the atmospheric model made it possible to identify small-scale inhomogeneities in the wind speed field, determined by the contours of the coast and relief, and, as a result, the local upwelling structure. In particular, we found small-scale areas of low SST near the coast where surface wind is directed along the coast to the right, for example over the sea near the coastal Crimean Mountains. At the same time the upwelling does not occur in the areas where the coastal wind has another direction, for example in the northwestern part of Karkinit Bay, near the coast north to Sevastopol, and near the Azov coast.

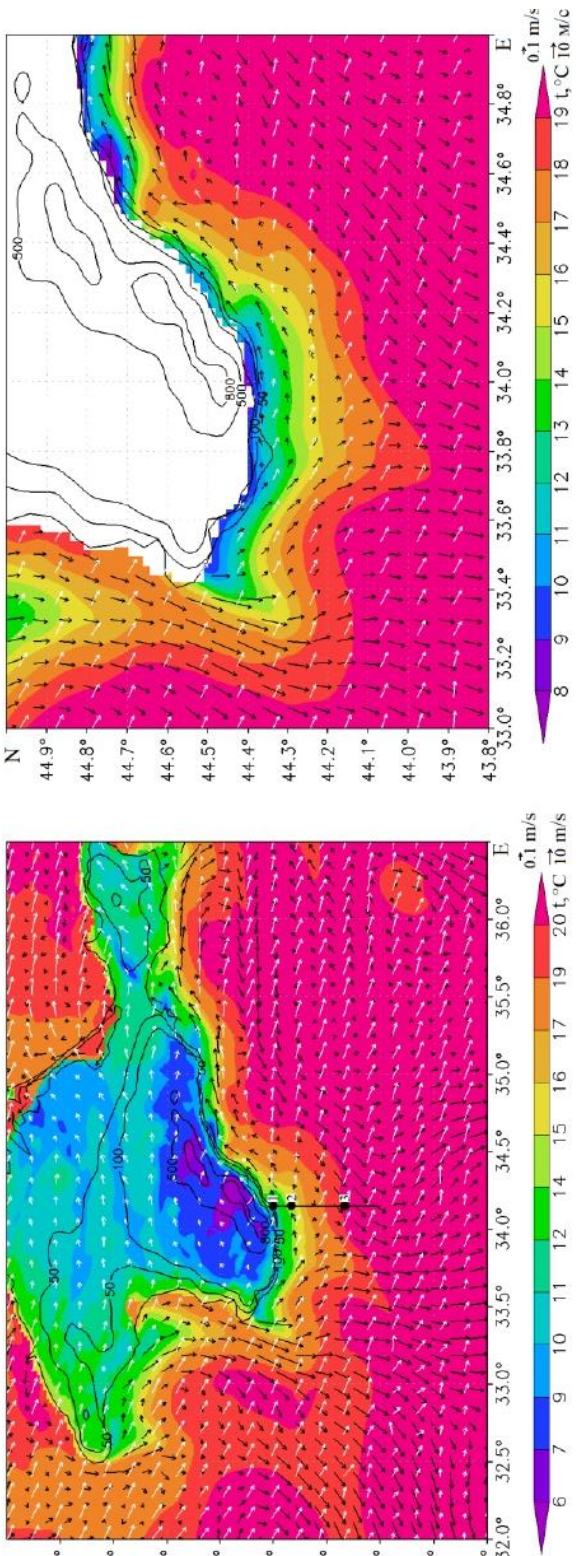

Fig. 3. Sea surface temperature and air temperature overland at a height of 2 m, vectors of near-water wind speed at a height of 10 m (white colour), and sea surface current velocities (black colour) for a mature upwelling event at 11:00 p.m. on 24 September (black line – the cross-section; numbers denote the points for which time series are built in Fig. 2 and vertical profiles in Fig. 4) (*a*); enlarged view of the selected area (overland air temperature is not shown) (*b*). The isolines show the terrain height (m)

The South Coast of Crimea is characterized by alternation of local zones of strong and weak upwelling (Fig. 3). In a general context, it should be noted that such zones of enhanced upwelling (filaments) are associated with sharp local changes in the contours of the coast in the form of capes [2].

It can also be seen from Fig. 3 that in the open sea the near-surface current velocity is generally directed along the normal to the near-water wind, and, for example, near the western coast of Crimea, this simple behavior is disrupted due to the features of the coastline.

Vertical Upwelling Structure

Numerical modelling makes it possible to examine the vertical structure of the velocity and temperature fields in upwelling in detail. On Fig. 4, at the cross-section at 34.15°E, the sea temperature and current velocity vectors (V_{oce}; $W_{oce}\cdot 10^3$) are shown, where V_{oce}, W_{oce} – meridional and vertical components, respectively. The area of cold upwelling extending from the coast for ~ 30 km, with a lower sea temperature and a reduced depth of the upper quasi-homogeneous layer, is clearly visible. The minimum temperature near the coast is about 11 °C. It should be noted that the narrow coastal area of shallow (< 60 m) depths here has a width less than the computational grid spacing (2 km) and, therefore, it is not shown in the figure.

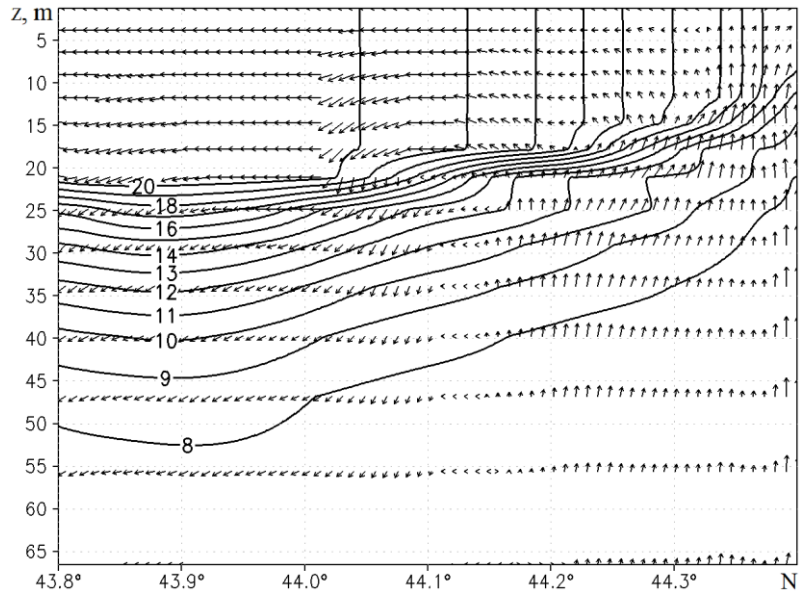

F i g . 4 . Sea temperature and current velocity vectors (V_{oce}, $W_{oce}\cdot 10^3$), where V_{oce} and $W_{oce}\cdot 10^3$ are meridional and vertical velocity components, at the cross-section at 34.15°E for a mature upwelling event at 6 p.m. on 24 September

Thus, numerical modelling made it possible to identify one more feature of the wind upwelling, namely, the development of a vertical circulation cell: a rise of water near the shore, outflow of warm water in the upper quasihomogenous layer and descend of water at the 30–50 km distance from the shore. This area of water descend is clearly visible from the velocity vectors shown in Fig. 4.

Fig. 5 shows vertical profiles of meridional velocity V_{oce}, and water temperature t_{oce}, at two points in the section shown in Fig. 3, *a*, – at point *2* (34.15°E, 44.3°N) and point *3* (34.15°E, 44°N). A velocity jump is seen in the thermocline area, indicating different mechanisms for the formation of velocity fields above and below the seasonal thermocline: in the area of the upper quasihomogeneous layer, the flow is an outflow of cold water, which forms the upwelling due to its rise near the coast from the thermocline area; in the area below the thermocline, the velocity profile reflects background geostrophic circulation not directly related to the upwelling. It is interesting to note that the temperature in the upper quasihomogeneous layer is constant, while the velocity profile is sloping. The latter is a consequence of the parametrization of vertical mixing in the NEMO model: the surface force of wind friction causes a linear velocity distribution in the underlying quasihomogeneous temperature layer. At the same time, the conditions for the formation of the upper quasihomogeneous temperature profile are satisfied.

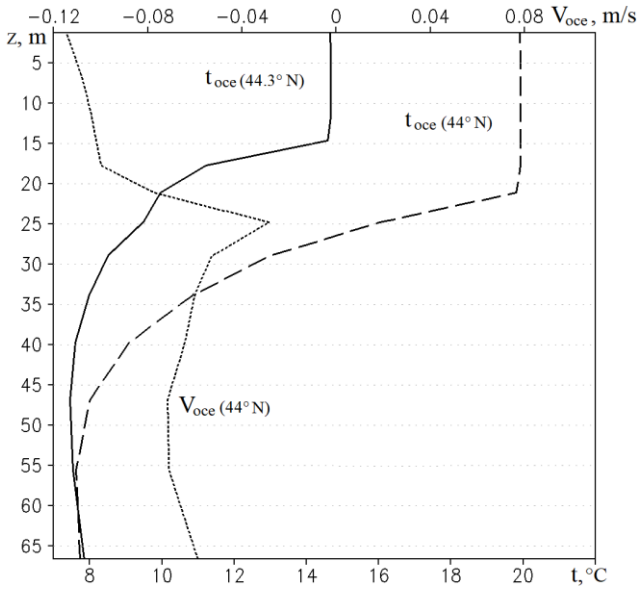

Fig. 5. Vertical profiles of water temperature, t_{oce}, at points *2* (solid line) and *3* (dashed line) as well as meridional velocity profile, V_{oce}, at point *3* (dotted line) at 3 a.m. on 25 September

Fig. 6 shows the velocity components and temperature in the upper layer of the sea along the section at 34.15°E, extended to 42.6°N. To compare, the right (northern) part of Fig. 6 refers to the upwelling, and the left (southern) part shows background fields not associated with the upwelling. The value of the zonal (along-shore) component of the surface current velocity varies from small positive values ~ 0.1 m/s near the shore to negative values ~ −0.15 m/s in the open sea. It is interesting to consider the behavior of the meridional velocity component, which is normal with respect to the coastline. As expected from general considerations, the velocity of this current normal to the coast, directed towards the open sea, is maximum at a certain distance from the shore (Fig. 6). It reaches a value of ~ 0.2 m/s. As can be seen from Fig. 6, the area of low (< 20 °C) temperature values of the near-surface layer of the sea is relatively small and extends from the coast to a distance of 50–60 km. In this case, the area where disturbances of the velocity fields are manifested is also traced at a greater distance from the shore.

This can be seen in Fig. 7, which shows how the meridional (directed along the normal to the shore) and zonal (alongshore) current velocities changed in time at the upper level of the model along the same section as in Fig. 6. The area of currents directed away from the shore with velocities reaching ~0.2–0.25 m/s at a distance of 40–60 km, as well as the area of currents directed towards the shore with lower velocities of ~ 0.1 m/s at a distance of 20–30 km, are clearly seen.

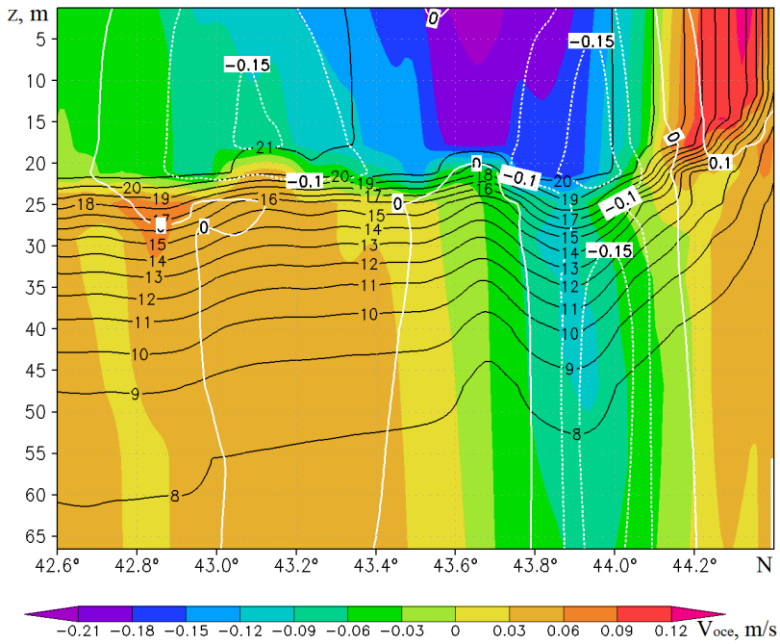

F i g . 6 . Meridional velocity, water temperature (black isolines), and zonal velocity (white isolines) along the cross-section at 34.15°E at 3 a.m. on 25 September

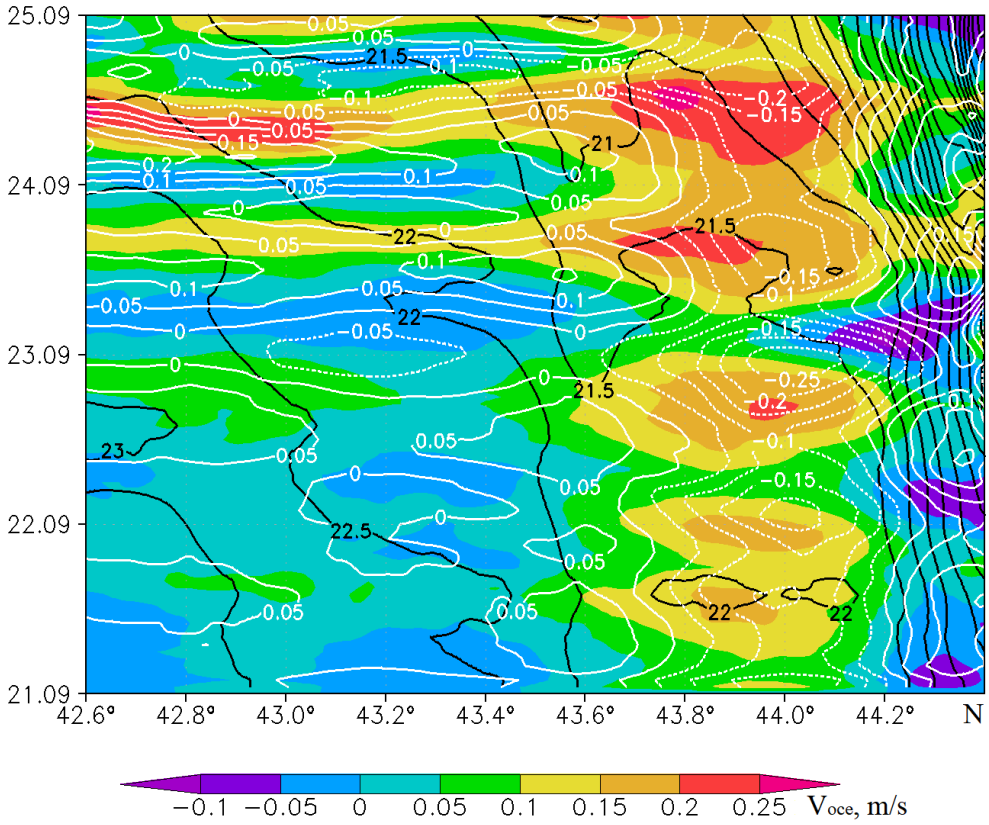

F i g . 7 . Time variation of the meridional (colour) and zonal (white isolines) current velocities as well as that of sea temperature (black isolines) at the upper level of the model (1.25 m) along the cross-section at 34.15°E. For illustrative purposes, the meridional velocity is shown opposite in sign

The diurnal variation of near-surface currents is traced. The maximum velocity directed away from the coast falls on the daytime hours (12–14 h), which corresponds to the time of maximum daily air heating and the daily variation of the coastal wind speed. The alongshore velocity component also experiences periodic diurnal fluctuations with a time delay of 4–6 h relative to the normal component. It can be confidently assumed that these coastal periodic changes in the velocity and temperature of the water are caused by the breeze circulation that develops in the warm period of the year in the area of the South Coast of Crimea [19]. We will not consider the physical mechanisms of the interaction of these two mesoscale processes, as this requires an increase in the spatial resolution of numerical models.

Conclusion

Using a 2 km resolution coupled numerical model, including the WRF atmospheric model and the NEMO marine model, the response of the upper layer of the Black Sea to an increase in wind speed in the coastal area of the South Coast of Crimea was reproduced. The numerical estimate of the SST decrease near the coast by ~10 °C, caused by cold upwelling, corresponds well to the satellite data.

The spatial structure of the fields of near-surface wind speed and air temperature, as well as the current velocity and sea temperature were obtained. The high spatial resolution in the atmospheric and marine models made it possible to identify small-scale inhomogeneities associated with inhomogeneities of the coast and coastal orography, which were not resolved in the reanalysis input data. The coastal upwelling area has a significantly heterogeneous alongshore spatial structure: there is no upwelling in the eastern, northeastern and northwestern parts of the Crimean coast.

The specific changes in the meridional (normal to the coast) and zonal (alongshore) components of the current velocity in upwelling were considered. The development of the alongshore current, as well as the current directed towards the sea, was shown. The latter is a part of the vertical cell of the upwelling circulation: the rise of cold waters near the coast, the spread towards the sea and further descend. The horizontal current velocities in this cell make 0.1–0.2 m/s near the surface, the vertical velocities of water rise in the coastal area make about 10^{-4}–10^{-3} m/s. Directly near the coast, diurnal velocity variations were found, associated with the influence of breeze circulation.

The analysis of the coupled modelling results showed that the NOW model was able to correctly reproduce such small-scale phenomena as wind upwelling near the Crimean coast, and could be used to numerically study the processes in the upper layer of the sea with high spatial resolution.

REFERENCES

1. Ivanov, V.A. and Mikhaylova, E.N., 2008. [*Upwelling in the Black Sea*]. Sevastopol: ECOSI-Gidrofizika, 92 p. (in Russian).
2. Brink, K.N., 1983. The Near-Surface Dynamics of Coastal Upwelling. *Progress in Oceanography*, 12(3), pp. 223–257. https://doi.org/10.1016/0079-6611(83)90009-5
3. Allen, J.S., 1973. Upwelling and Coastal Jets in a Continuously Stratified Ocean. *Journal of Physical Oceanography*, 3(3), pp. 245–257. https://doi.org/10.1175/1520-0485(1973)003<0245:UACJIA>2.0.CO;2
4. Preller, R. and O'Brien, J.J., 1980. The Influence of Bottom Topography on Upwelling off Peru. *Journal of Physical Oceanography*, 10(9), pp. 1377–1398. https://doi.org/10.1175/1520-0485(1980)010<1377:TIOBTO>2.0.CO;2
5. Philander, S.J.H. and Yoon, J.-H., 1982. Eastern Boundary Currents and Coastal Upwelling. *Journal of Physical Oceanography*, 12(8), pp. 862–879. https://doi.org/10.1175/1520-0485(1982)012<0862:EBCACU>2.0.CO;2

6. Peffley, M.B. and O'Brien, J.J., 1976. A Three-Dimensional Simulation of Coastal Upwelling off Oregon. *Journal of Physical Oceanography*, 6(2), pp. 164–180. https://doi.org/10.1175/1520-0485(1976)006<0164:ATDSOC>2.0.CO;2

7. Androsovich, A.I., Mikhailova, E.N. and Shapiro, N.B., 1995. Numerical Model and Calculation of the Water Circulation in the North-Western Black Sea. *Physical Oceanography*, 6(5), pp. 351–364. https://doi.org/10.1007/BF02197483

8. Kosnyrev, V.N., Mikhailova, E.N. and Stanichny, S.V., 1997. Upwelling in the Black Sea by the Results of Numerical Experiments and Satellite Data. *Physical Oceanography*, 8(5), pp. 329–340. https://doi.org/10.1007/BF02523759

9. Zatsepin, A.G., Silvestrova, K.P., Kuklev, S.B., Piotoukh, V.B. and Podymov, O.I., 2016. Observations of a Cycle of Intense Coastal Upwelling and Downwelling at the Research Site of the Shirshov Institute of Oceanology in the Black Sea. *Oceanology*, 56(2), pp. 188–199. https://doi.org/10.1134/S0001437016020211

10. Ginzburg, A.I., 1995. [On Variable Jet Currents in the Southwest Part of the Black Sea]. *Issledovanie Zemli iz Kosmosa*, (4), pp. 10–16 (in Russian).

11. Ginzburg, A.I., Kostianoy, A.G., Soloviev, D.M. and Stanichny, S.V., 1998. Cyclonic Upwelling Eddies off the South-West Crimea. *Issledovanie Zemli iz Kosmosa*, (3), pp. 83–88 (in Russian).

12. Divinsky, B.V., Kuklev, S.B. and Zatsepin, A.G., 2017. Numerical Simulation of an Intensive Upwelling Event in the Northeastern Part of the Black Sea at the IO RAS Hydrophysical Testing Site. *Oceanology*, 57(5), pp. 615–620. https://doi.org/10.1134/S0001437017040038

13. Polonskii, A.B. and Muzyleva, M.A., 2016. Modern Spatial-Temporal Variability of Upwelling in the North-Western Black Sea and off the Crimea Coast. *Izvestiya RAN. Seriya Geograficheskaya*, (4), pp. 96–108. (in Russian).

14. Stanichnaya, R.R. and Stanichny, S.V., 2021. Black Sea Upwellings. *Sovremennye Problemy Distantsionnogo Zondirovaniya Zemli iz Kosmosa*, 18(4), pp. 195–207. doi:10.21046/2070-7401-2021-18-4-195-207 (in Russian).

15. Iarovaya, D.A., Efimov, V.V., Barabanov, V.S. and Mizyuk, A.A., 2020. Response of the Black Sea Upper Layer to the Cyclone Passage on September 25–29, 2005. *Russian Meteorology and Hydrology*, 45(10), pp. 701–711. https://doi.org/10.3103/S1068373920100040

16. Iarovaia, D.A. and Efimov, V.V., 2021. Development of Cold Sea Surface Temperature Anomalies in the Black Sea. *Izvestiya, Atmospheric and Oceanic Physics*, 57(4), pp. 413–424. https://doi.org/10.1134/S0001433821040228

17. Valcke, S., 2013. The OASIS3 Coupler: A European Climate Modelling Community Software. *Geoscientific Model Development*, 6(2), pp. 373–388. https://doi.org/10.5194/gmd-6-373-2013

18. Rodi, W., 1987. Examples of Calculation Methods for Flow and Mixing in Stratified Fluids. *Journal of Geophysical Research: Oceans*, 92(C5), pp. 5305–5328. https://doi.org/10.1029/JC092iC05p05305

19. Efimov, V.V., 2017. Numerical Simulation of Breeze Circulation over the Crimean Peninsula. *Izvestiya, Atmospheric and Oceanic Physics*, 53(1), pp. 84–94. doi:10.1134/S0001433817010042

Submitted 14.11.2022; accepted after review 23.01.2023;
revised 1.02.2023; published 24.03.2023

About the authors:

Darya A. Iarovaya, Senior Research Associate, Marine Hydrophysical Institute of RAS (2 Kapitanskaya St., Sevastopol, 299011, Russian Federation), Ph.D. (Phys.-Math.), **ResearcherID: Q-4144-2016**, **ORCID ID: 0000-0003-0949-2040**, **Scopus Author ID: 57205741734**, *darik777@mhi-ras.ru*

Vladimir V. Efimov, Head of the Atmosphere and Ocean Interaction Department, Marine Hydrophysical Institute of RAS (2 Kapitanskaya St., Sevastopol, 299011, Russian Federation), Dr.Sci. (Phys.-Math.), professor, **ResearcherID: P-2063-2017**, **Scopus Author ID: 6602381894**, *vefim38@mail.ru*

Vladislav S. Barabanov, Senior Research Associate, Marine Hydrophysical Institute of RAS (2 Kapitanskaya St., Sevastopol, 299011, Russian Federation), Ph.D. (Phys.-Math.), **ResearcherID: C-6007-2013**, **Scopus Author ID: 7006247713**, *wbarbs@gmail.com*

Contribution of the authors:

Darya A. Iarovaya – numerical modelling, processing and interpretation of the modelling results, preparation of the illustrations

Vladimir V. Efimov – task statement, participation in the result discussion, critical analysis of the article

Vladislav S. Barabanov – participation in the result discussion

All the authors have read and approved the final manuscript.

Original article **DOI**: 10.29039/0233-7584-2023-1-20-30

Influence of Upwelling on River Plume Development in the Coastal Zone of the North-Western Black Sea Shelf Based on Numerical Modelling

M. V. Tsyganova *, E. M. Lemeshko, Yu. N. Ryabtsev

Marine Hydrophysical Institute of RAS, Sevastopol, Russia
* *e-mail: m.tsyganova@mhi-ras.ru*

Abstract
In a south wind, coastal upwelling can be observed off the western coast of the Black Sea. In the same area, the hydrological structure of waters is strongly influenced by river runoff, which forms a river plume, and a southward longshore current. The paper studies the evolution of the plume on the northwest shelf of the Black Sea and its interaction with upwelling based on numerical modelling. The impact of upwelling development under the influence of the south wind on plume propagation was studied using a three-dimensional sigma-coordinate numerical model (POM-type) to calculate the circulation in the coastal zone taking into account the river runoff. The calculations were performed for a rectangular region for the cases of both uniform depth and typical water stratification of the northwestern shelf. The last case was sampled for May condition, when, on average, the Danube plume development is maximal. It is obtained that the joint dynamics of upwelling and river plume are closely related to the stratification of coastal waters. In the case of unstratified shelf waters, the thin plume layer enhances upwelling and downwelling on the inshore and offshore sides of the river plume, respectively. The results allowed studying the peculiarities of river water transformation during winds that cause the development of coastal upwelling. Estimates of the time of bottom water rise near the coast under the action of south winds with different wind speeds and shelf water stratification parameters retrieved from numerical modelling data can be used to develop regional upwelling indices based on satellite data on the sea surface temperature and wind speed.

Keywords: Black Sea, river plume, upwelling, numerical modelling, shelf, coastal zone, river runoff

Acknowledgements: The work was performed under state assignment on topic no. FNNN-2021-0005.

For citation: Tsyganova, M.V., Lemeshko, E.M. and Ryabtsev, Yu.N., 2023. Influence of Upwelling on River Plume Development in the Coastal Zone of the North-Western Black Sea Shelf Based on Numerical Modelling. *Ecological Safety of Coastal and Shelf Zones of Sea*, (1), pp. 20–30. doi:10.29039/2413-5577-2023-1-20-30

Влияние апвеллинга на развитие речного плюма в прибрежной зоне северо-западного шельфа Черного моря на основе численного моделирования

М. В. Цыганова *, Е. М. Лемешко, Ю. Н. Рябцев

Морской гидрофизический институт РАН, Севастополь, Россия
** e-mail: m.tsyganova@mhi-ras.ru*

Аннотация

При южном ветре у западного побережья Черного моря наблюдается проявление прибрежного апвеллинга. В этом же районе сильное влияние на гидрологическую структуру вод оказывают сток рек, который формирует речной плюм, и вдольбереговое течение, направленное на юг. Целью данной работы является изучение эволюции плюма на северо-западном шельфе Черного моря и его взаимодействие с апвеллингом на основе численного моделирования. Влияние развития апвеллинга под действием ветра южных румбов на распространение плюма исследовалось с помощью трехмерной сигма-координатной численной модели *POM*-типа для расчета циркуляции в прибрежной зоне с учетом стока реки. Расчеты проведены для прямоугольной области для случаев как однородной по глубине, так и типичной для мая (когда в среднем наблюдается максимальное развитие плюма Дуная) стратификации вод северо-западного шельфа. Получено, что совместная динамика апвеллинга и речного плюма тесно связана со стратификацией прибрежных вод. В случае нестратифицированных вод шельфа тонкий слой плюма усиливает апвеллинг и даунвеллинг на береговой и морской сторонах речного плюма соответственно. Полученные результаты позволили изучить особенности трансформации речных вод в период действия ветров, вызывающих развитие прибрежного апвеллинга. Оценки времени подъема придонных вод у берега при действии южных ветров с различными скоростями ветра и параметрами стратификации вод шельфа по данным численного моделирования могут быть использованы для разработки региональных индексов апвеллинга на основе спутниковых данных о температуре поверхности моря и скорости ветра.

Ключевые слова: Черное море, речной плюм, апвеллинг, численное моделирование, шельф, прибрежная зона, речной сток

Благодарности: работа выполнена в рамках государственного задания по теме FNNN-2021-0005.

Для цитирования: *Цыганова М. В., Лемешко Е. М., Рябцев Ю. Н.* Влияние апвеллинга на развитие речного плюма в прибрежной зоне северо-западного шельфа Черного моря на основе численного моделирования // Экологическая безопасность прибрежной и шельфовой зон моря. 2023. № 1. С. 20–30. EDN SYKFPE. doi:10.29039/2413-5577-2023-1-20-30

Introduction

The northwestern part of the Black Sea is characterized by a vast shelf and significant river runoff, as well as a variety of morphological types of plumes in the area of the Danube delta and the Dnieper-Bug Estuary [1]. Therefore, the northwestern shelf is a unique testing ground for studying the dynamics of river plumes of various types [2]. The long-term archival hydrological observations of this region make it possible to verify numerical models of river plumes.

With a southerly wind, upwelling is observed along the western coast of the Black Sea. The hydrological structure of the waters in this region is strongly

influenced by river runoff, which is a source of nutrients necessary for phytoplankton bloom. In the case of alongshore upwelling in the summer, a decrease in the oxygen content occurs in the coastal zone, which can cause fish to die [3]. Both of these phenomena are closely related to plume dynamics. Therefore, it is necessary to understand how the distribution of river waters changes with the development of coastal upwelling.

The origin and evolution of upwelling in the Black Sea were studied based on the analysis of *in situ* and satellite data [4–9] and numerical simulation [10, 11]. The satellite data make it possible to recognize colder waters [7, 10, 11], but the high variability and transport of river waters in the region of the northwestern shelf significantly complicate the study of processes by such methods [12, 13]. Therefore, it is important to use numerical simulation along with *in situ* and remote sensing data [14].

The development of upwelling near the northwestern Black Sea coast occurs under the influence of southerly winds. The long-term statistics of upwelling formation, obtained based on the analysis of remote sensing data on sea surface temperature, showed that during the extended summer period there are from 3 to 10 intense upwelling events with a total duration of 35 to 65 % of the length of the summer period, respectively [7]. From a comparison of the in-situ and satellite data analyses, it was concluded that the upwelling evolution has a significant effect on the river plume propagation [15].

The coastal upwelling occurrence is compensated by the geostrophic current and the freshwater plume associated with it. The study of the coastal upwelling and river plume dynamic interaction is of particular interest. River waters with low salinity create pressure gradients that cause surface geostrophic currents that arise in the coastal zone in an anticyclonic direction (in the Northern Hemisphere) from the mouth [16]. The river plume can weaken the development of the upwelling if the wind is too weak to disturb the haline stratification. The change in the stratification of shelf waters is an important factor that determines the plume and upwelling dynamics, affecting the plume thickness, the transfer of desalinated water to the inner shelf area, and the bottom transfer of denser bottom waters towards the coast [17].

Therefore, this work is devoted to the study of joint dynamics of the development of upwelling and river plume, identification of patterns of the influence of upwelling on the transformation of river waters on the sea shelf during the development of coastal upwelling.

Materials and methods

The temperature and salinity fields were selected from the MHI hydrological database (http://bod-mhi.ru/) for wind conditions with wind speeds of less than 3 $m \cdot s^{-1}$. Based on the spatial distribution of temperature and salinity isolines, the river runoff evolution in the Danube Delta region was estimated and the dy-namics of the river plume was studied. The characteristic time during which the plume reaches the southern boundary of the northwestern shelf is about five days, which corresponds to the obtained estimates based on the approach [2].

The effect of upwelling development under the action of southerly winds on plume propagation was studied using numerical modeling based on a three-dimensional POM-type sigma-coordinate numerical model previously adapted and tested for the northwestern shelf of the Black Sea to calculate the circulation in the coastal zone, taking into account the river runoff [18, 19]. The calculations were carried out for a rectangular area for the cases of both uniform in depth and typical for the month of May (when on average the Danube plume develops its maximum) stratification of the waters of the northwestern shelf.

The model parameters were selected in such a way that they corresponded to the area where the Danube inflows into the Black Sea. The model was adapted for a rectangular area and the conditions of the northwestern shelf of the Black Sea. The computational domain coordinates: 28°–31°E и 43°–46°N, the number of grid nodes along the X axis = 51, the number of grid nodes along the Y axis = 171, the grid step is 2 km, the time step is 2 min, the number of sigma horizons is 25. At the initial moment of calculation, the fresh water inflow is included near the mouth of the Danube.

For the first version of the calculations, a homogeneous stratification was set: salinity of the shelf waters was 18 PSU, the temperature was 18 °C, and the salinity of the inflowing water in the area of the Danube mouth was 6 PSU, the water temperature at the mouth was 10 °C, the river discharges corresponded to the climatic values for April–May (8000 $m^3 \cdot s^{-1}$). On the shelf, a steady southward background current was set; its velocity amounted to 5 $cm \cdot s^{-1}$ [19]. For the second version of the calculations, the climatic values of temperature and salinity near the area of the Danube delta for May were used: on the surface, the shelf water temperature was set to 15.75 °C, the salinity was 12 PSU, the temperature at the bottom was 6.5 °C, the salinity was 18.25 PSU [20]. The thermocline was at a depth of 20 m, the halocline was at a depth of 12 m, and the bottom depth was 40 m. The river discharge, temperature, and salinity were the same as in the first version of the calculations.

Results

Under the influence of the south wind at a speed of 5 $m \cdot s^{-1}$ and the flow rate of the river Q equal to 8000 $m^3 \cdot s^{-1}$, the plume is extended from the coast in a northeasterly direction on the 10^{th} day (Fig. 1).

At the same time, the development of coastal upwelling blocks the propagation of the alongshore current of desalinated waters from the plume area to the south. To understand the role of stratification, we compared the results of calculations for the cases without stratification (Fig. 1) and the cases with stratification (Fig. 2). For the case without stratification, the upwelling develops after 3–5 days, but it does not manifest itself in the surface temperature field due to uniformity of its depth distribution (Fig. 1, *b*). Nevertheless, the alongshore current directed to the north develops at a speed of 5–10 $cm \cdot s^{-1}$, which blocks the initial propagation of the plume to the south, and over time, the plume extends into the inner shelf area, which is traced both by salinity (Fig. 1, *a*) and by water surface temperature, since the temperature of river waters is lower than the temperature of shelf waters by 8 °C (Fig. 1, *b*).

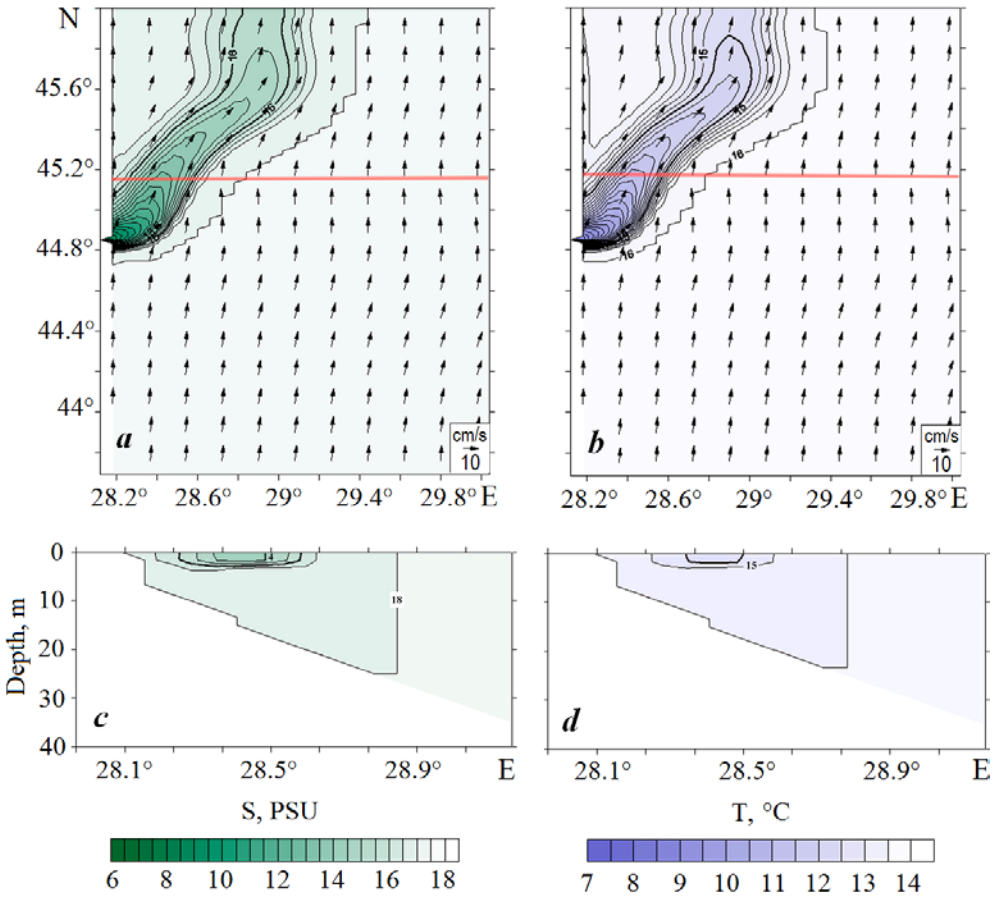

Fig. 1. Surface salinity (*a*) and temperature (*b*) of water from modelling data on the 10th day for uniform stratification influenced by the south wind with a speed of 5 m·s^{-1}. The red line (*a*, *b*) denotes zonal sections of salinity (*c*) and temperature (*d*) fields along 45.18° N latitude

The plume width determined from the position of the 16 PSU isohaline along the transect line at 45.18°N is approximately 25 km; in the temperature field, this corresponds to the plume boundary along the 16 °C isotherm (Fig. 1, *a*, *b*). At the same time, the thickness of the plume is about 5 m, which is seen in the zonal sections of the fields of salinity (Fig. 1, *c*) and temperature (Fig. 1, *d*).

For the case with stratification, the upwelling acquires a well-developed form on the 10th day: the 8 °C isotherm, which characterizes the bottom waters, reaches the surface up to 28.6°E (~ 20 km from the coast), except for the area in the region of the river delta (Fig. 2, *b*).

The upwelling pushes the plume toward the shelf, position of the 10 °C isotherm shifts to the east, and on the 10th day it reaches a longitude of 28.9°E

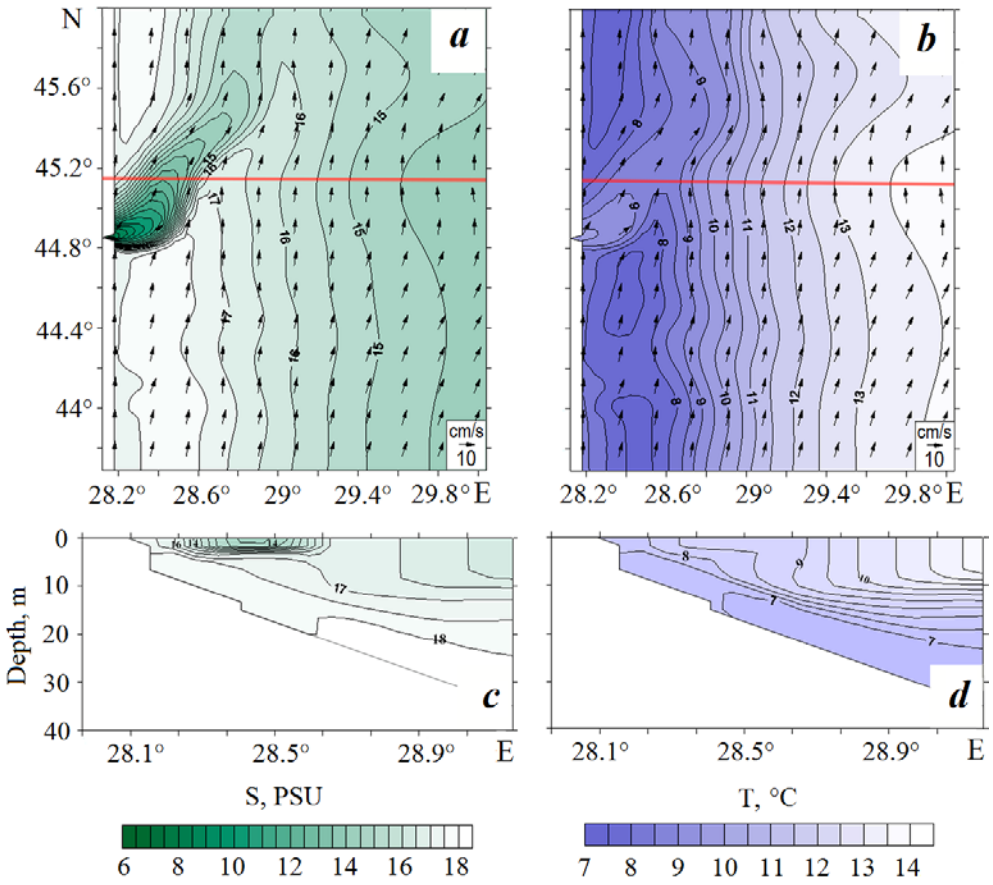

Fig. 2. Surface salinity (*a*) and temperature (*b*) of water from modelling data on the 10th day with shelf water stratification influenced by the south wind with a speed of 5 m·s^{-1}. The red line (*a*, *b*) denotes zonal sections of salinity (*c*) and temperature (*d*) fields along 45.18°N latitude

(Fig. 2, *b*) ~ 55 km from the shore, which in the salinity field corresponds to the position of the 17 PSU isohaline characterizing the bottom waters of the shelf (Fig. 2, *a*). Thus, due to small contrasts between the temperature of the river and the waters of the shelf, the plume identification from satellite data on the sea surface temperature does not contribute to the statistics of upwellings and plumes. When analyzing the results of numerical modelling, the salinity field is used in this case. In addition, unlike the first case without stratification (Fig. 1, *d*), the plume is not distinguished in the temperature field and on the zonal section (Fig. 2, *d*). On the 10th day, the plume elongates to the northeast, and the width of it along the 16 PSU isohaline increases compared to the first case and amounts to 30 km.

On the zonal section along 45.18°N it can be seen that on the 10th day the rise of bottom waters (18 PSU isohaline) reaches a depth of 17 m, the 17 PSU isohaline comes to the surface at a distance of ~ 8 km from the shore (Fig. 2, *c*). In contrast to the plume waters, the position of the bottom waters is clearly distinguished on the zonal sections in the temperature field: the 7 °C isotherm reaches a depth of 10 m, and the 8 °C isotherm comes to the surface at a distance of 8–10 km from the shore (Fig. 2, *d*).

The evolution of coastal upwelling over time is shown in Fig. 3. For calculations with stratification typical for May conditions, the development of coastal upwelling is observed already on the 2nd–3rd day. On the 3rd day, the bottom waters with a temperature of 7–8 °C form a tongue of cold waters, which rises along

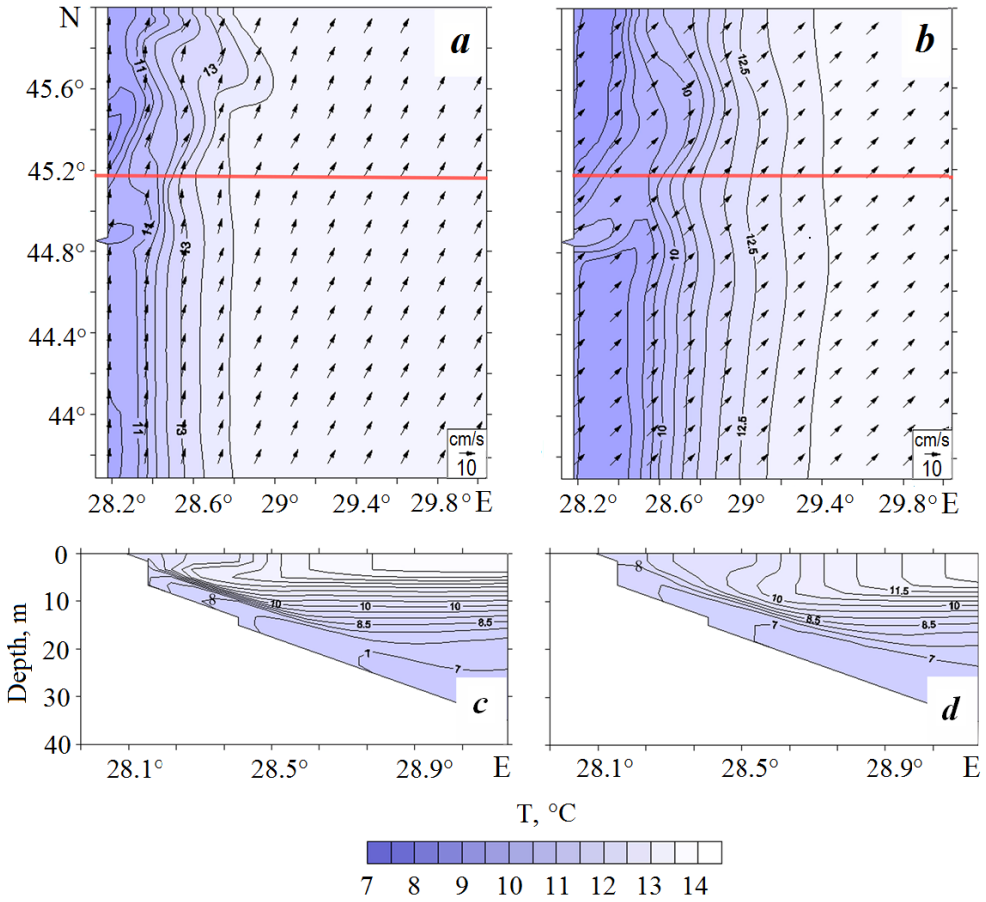

Fig. 3. Surface salinity of water from modelling data with shelf water stratification influenced by the south wind with a speed of 5 m·s^{-1}. The red line (*a*, *b*) denotes zonal sections of temperature fields on the 3d (*c*) and 7th (*d*) day along 45.18°N latitude

the slope of the depths and reaches a depth of 10 m (Fig. 3, *c*). On the 7th day, the 8 °C isotherm reaches a depth of 3 m (Fig. 3, *d*), and on the 8th day it comes to the surface. The 10 °C isotherm emerges on the surface near the coast on the 3rd day (Fig. 3, *c*) and masks the position of a plume with a temperature of 10 °C in the temperature field. The waters with a temperature of 10–11 °C occupy the entire alongshore coastal area and are well manifested in the surface temperature field (Fig. 3, *a*). Over time, the 10 °C isotherm shifts to the east and on the 7th day reaches 28.6°E ~ 35 km from the coast (Fig. 3, *b*).

The development of upwelling in time was also analysed based on the variability of the isohaline positions in the zonal section through the plume region along 45.18° N. The rise time of bottom waters, characterized by a salinity of 17 PSU, along the entire coast was on average 5 days for a wind speed of 5 $m \cdot s^{-1}$. At the same time, the rise of bottom waters occurs along the coastal slope and, after 5 days, their transfer develops in the surface Ekman layer to the shelf area. Based on numerical simulation data, it is possible to obtain detailed estimates of the rate of water rise during the development of coastal upwelling for various values of wind speed, bottom slope angle, and shelf water stratification parameters. The advection time t_{ad} of bottom waters along the shelf slope is directly proportional to the product of the difference between the depths of the pycnocline occurrence H_0 and the depth of the rise of the isopycna (isotherm) H_1 characterizing the bottom waters in the process of upwelling development:

$$t_{ad} = \frac{\rho \cdot f \cdot d \cdot (H_0 - H_1)}{\alpha \cdot \tau}, \quad (1)$$

where ρ is sea water density; f is Coriolis parameter; d is bottom layer thickness; α is bottom slope angle; τ is wind stress. The equation (1) gives a theoretical estimate of the advection time as a function of the bottom slope and wind stress. For the parameters characteristic of the northwestern shelf and the wind stress corresponding to a wind speed of 5 $m \cdot s^{-1}$, we obtain a value of 3 days. If the time of action of the south wind is less than the advection time according to the formula (1), in this case less than 3 days, then cold waters do not have time to reach the surface. Thus, upwelling will not manifest itself in the sea surface temperature field, which must be taken into account when analyzing satellite data.

The advection time t_{ad} is inversely proportional to the wind stress. For the same value of the bottom inclination angle α, numerical calculations were carried out for the case with shelf water stratification and different south wind speeds – 7 $m \cdot s^{-1}$ and 9 $m \cdot s^{-1}$. At a wind speed of 7 $m \cdot s^{-1}$, on the 5th day, the 17 PSU isohaline reaches the surface (Fig. 4, *a*), and the tongue of cold water rises along the slope to a depth of 5 m, according to the position of the 8 °C isotherm (Fig. 4, *b*). For a wind speed of 9 $m \cdot s^{-1}$ on the 5th day, saline waters (17 PSU) occupy a larger area on the surface (Fig. 4, *c*), and cold waters (less than 8 °C) are on the surface, the width of the upwelling zone along this isotherm is 30 km (Fig. 4, *d*).

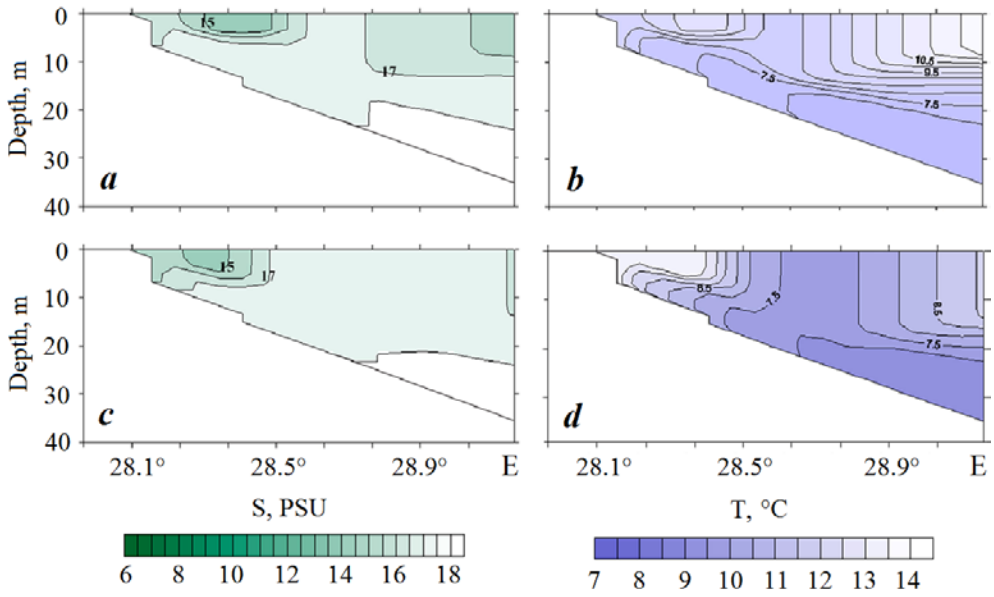

Fig. 4. Zonal sections along 45.18° N latitude: salinity (*a*, *c*) and temperature (*b*, *d*) of water from modelling data with shelf water stratification on the 5th day influenced by the south wind with a speed of 7 m·s^{-1} (*a*, *b*) and 9 m·s^{-1} (c, *d*)

Conclusions

The results obtained made it possible to study the features of the river water transformation during the action of winds that cause the development of coastal upwelling. The plume propagation due to Ekman transport is analyzed depending on the shelf water stratification and wind speed. It was found that the joint upwelling and river plume dynamics is closely related to the stratification of coastal waters. In the case of unstratified shelf waters, a thin layer of plume enhances upwelling and downwelling on the inshore and offshore sides of the river plume, respectively. The upwelling intensity increases when the plume reaches its boundary. In this case, the maximum transport of water towards the shelf is 1.5 times greater than the Ekman transport. After the plume passes through the upwelling region, the water transport is regulated by alongshore density variations.

The regularities of plume dynamics obtained under the conditions of upwelling development manifest themselves in the field of sea surface temperature, which makes it possible to use model estimates of the advection time t_{ad} for interpreting satellite data on sea surface temperature. The estimates of the rise time of bottom waters near the shore under the action of southerly winds with different wind speeds and shelf water stratification parameters based on numerical modelling data can be used to develop regional upwelling indices based on satellite data on sea surface temperature and wind speed.

REFERENCES

1. Horner-Devine, A.R., Hetland, R.D. and MacDonald, D.G., 2015. Mixing and Transport in Coastal River Plumes. *Annual Review of Fluid Mechanics*, 47, pp. 569–594. doi:10.1146/annurev-fluid-010313-141408
2. Lemeshko, E.M. and Tsyganova, M.V., 2021. Investigation of Danube River Plume Formation and Propagation Based on Numerical Modeling. In: MSU, 2021. *InterCarto. InterGIS. GI support of sustainable development of territories: Proceedings of the International conference*. Moscow: MSU, Faculty of Geography, 2021. Vol. 27, part 3, pp. 32–41. doi:10.35595/2414-9179-2021-3-27-32-41 (in Russian).
3. Kondratev, S.I., 2019. Three Typical Hydrological-Hydrochemical Situations near the Danube River Mouth Based on the Marine Hydrophysical Institute Research Expeditions in 1997-2013. *Physical Oceanography*, 26(4), pp. 326–340. doi:10.22449/1573-160X2019-4-326-340
4. Bogdanova, A.K. and Korpachev, L.N., 1959. [Upsurge and Downsurge Circulation and its Role for the Hydrological Regime of the Black Sea]. *Meteorologiya i Gidrologiya*, (4), pp. 26–32 (in Russian).
5. Borovskaya, R.V., Panov, B.N., Spyrydonova, E.O., Leksikova, L.A. and Kyrylova, M.V., 2005. Black Sea Near-Coastal Upwelling and Interannual Variability of Its Intensity. In: MHI, 2005. *Ekologicheskaya Bezopasnost' Pribrezhnoy i Shel'fovoy Zon Morya* [Ecological Safety of Coastal and Shelf Zones and Comprehensive Use of Shelf Resources]. Sevastopol: MHI. Iss. 12, pp. 42–48 (in Russian).
6. Ginzburg, A.I., Kostianoy, A.G., Soloviev, D.M. and Stanichny, S.V., 2000. Coastal Upwelling in the North-West Black Sea. *Earth Observation and Remote Sensing*, 15(6), pp. 933–948.
7. Stanichnaya, R.R. and Stanichny, S.V., 2021. Black Sea Upwellings. *Sovremennye Problemy Distantsionnogo Zondirovaniya Zemli iz Kosmosa*, 18(4), pp. 195–207. doi:10.21046/2070-7401-2021-18-4-195-207
8. Zatsepin, A.G., Silvestrova, K.P., Kuklev, S.B., Piotoukh, V.B. and Podymov, O.I., 2016. Observations of a Cycle of Intense Coastal Upwelling and Downwelling at the Research Site of the Shirshov Institute of Oceanology in the Black Sea. *Oceanology*, 56(2), pp. 188–199. https://doi.org/10.1134/S0001437016020211
9. Silvestrova, K.P., Myslenkov, S.A. and Repkov, D.S., 2022. Wind Upwelling Forecast for the Russian Black Sea Coast. *Hydrometeorological Research and Forecasting*, (1), pp. 89–107. https://doi.org/10.37162/2618-9631-2022-1-89-107
10. Divinsky, B.V., Kuklev, S.B. and Zatsepin, A.G., 2017. Numerical Simulation of an Intensive Upwelling Event in the Northeastern Part of the Black Sea at the IO RAS Hydrophysical Testing Site. *Oceanology*, 57(5), pp. 615–620. https://doi.org/10.1134/S0001437017040038
11. Oguz, T., La Violette, P.E. and Unluata, U., 1992. The Upper Layer Circulation of the Black Sea: Its Variability as Inferred from Hydrographic and Satellite Observations. *Journal of Geophysical Research: Oceans*, 97(C8), pp. 12569–12584. doi:10.1029/92JC00812
12. Mikhailova, E.N., Muzyleva, M.A., Polonskii, A.B., Soloviev, D.M. and Stanichny, S.V., 2009. [Spatial and Temporal Variability of Upwelling Characteristics in the Northwestern Part of the Black Sea and off the Crimean Coast in 2005–2008]. In: MHI, 2009. *Monitoring Systems of Environment*. Sevastopol: ECOSI-Gidrofizika. Issue 12, pp. 318–321 (in Russian).
13. Osadchiev, A.A., 2021. *River Plumes*. Moscow: Scientific World, 285 p.

14. Zavialov, P.O., Makkaveev, P.N., Konovalov, B.V., Osadchiev, A.A., Khlebopashev, P.V., Pelevin, V.V., Grabovskiy, A.B., Izhitskiy, A.S., Goncharenko, I.V., Soloviev, D.M. and Polukhin, A.A., 2014. Hydrophysical and Hydrochemical Characteristics of the Sea Areas Adjacent to the Estuaries of Small Rivers of the Russian Coast of the Black Sea. *Oceanology*, 54(3), pp. 265–280. doi:10.1134/S0001437014030151

15. Kubryakov, A.A., Stanichny, S.V. and Zatsepin, A.G., 2018. Interannual Variability of Danube Waters Propagation in Summer Period of 1992–2015 and Its Influence on the Black Sea Ecosystem. *Journal of Marine Systems*, 179, pp. 10–30. https://doi.org/10.1016/j.jmarsys.2017.11.001

16. Fong, D.A. and Geyer, W.R., 2002. The Alongshore Transport of Freshwater in a Surface-Trapped River Plume. *Journal of Physical Oceanography*, 32(3), pp. 957–972. https://doi.org/10.1175/1520-0485(2002)032<0957:TATOFI>2.0.CO;2

17. Alory, G., Da-Allada, C.Y., Djakouré, S., Dadou, I., Jouanno, J. and Loemba, D.P., 2021. Coastal Upwelling Limitation by Onshore Geostrophic Flow in the Gulf of Guinea Around the Niger River Plume. *Frontiers in Marine Science*, 7, 607216. doi:10.3389/fmars.2020.607216

18. Ivanov, V.A. and Fomin, V.V., 2010. *Mathematical Modeling of Dynamical Processes in the Sea – Land Area.* Kiev: Akademperiodika, 286 p.

19. Tsyganova, M.V., Lemeshko, E.M. and Ryabcev, Yu.N., 2016. Modelling of Hydrofront Forming on the Danube Mouth Area. In: MHI, 2016. *Ecological Safety of Coastal and Shelf Zones of Sea*. Sevastopol: MHI. Iss. 3, pp. 26–31 (in Russian).

20. Ivanov, V.A. and Belokopytov, V.N., 2013. *Oceanography of the Black Sea*. Sevastopol: ECOSI-Gidrofizika, 212 p.

Submitted 20.12.2022; accepted after review 23.01.2023;
revised 1.02.2023; published 24.03.2023

About the authors:

Marina V. Tsyganova, Junior Research Associate, Marine Hydrophysical Institute of RAS (2 Kapitanskaya St., Sevastopol, 299011, Russian Federation), **ORCID ID: 0000-0003-2398-1756, ResearcherID: S-5426-2018, SPIN-code: 2256-0620**, *m.tsyganova@mhi-ras.ru*

Evgeny M. Lemeshko, Senior Research Associate, Marine Hydrophysical Institute of RAS (2 Kapitanskaya St., Sevastopol, 299011, Russian Federation), Ph.D. (Phys.-Math.), **SPIN-code: 3836-5786, ResearcherID: S-7815-2018, Scopus AuthorID: 6508300982**, *eugeny.lemeshko@mhi-ras.ru*

Yuri N. Ryabtsev, Research Associate, Marine Hydrophysical Institute of RAS (2 Kapitanskaya St., Sevastopol, 299011, Russian Federation), **ORCID ID: 0000-0002-9682-9969, SPIN-code: 7853-4597**, *ruab@mail.ru*

Contribution of the authors:

Marina V. Tsyganova – collection, systematization, and analysis of literature, performance of numerical experiments, processing, analysis, and description of the study results, preparation of the text and graphic material for the article

Evgeny M. Lemeshko – problem statement, processing, analysis, and description of the study results, preparation of the article text

Yuri N. Ryabtsev – development of the mathematical model, selection and justification of methods for equation solution, mathematical model correction

All the authors have read and approved the final manuscript.

Original article **DOI**: 10.29039/2413-5577-2023-1-31-47

Morphodynamics of Sevastopol Bays under Anthropogenic Impact

T. V. Efremova *, Yu. N. Goryachkin

Marine Hydrophysical Institute of RAS, Sevastopol, Russia
* *e-mail: efremova@mhi-ras.ru*

Abstract

The degradation of the Crimean shores under the influence of the anthropogenic factor has become a serious problem to overcome which significant efforts and financial resources are spent. The purpose of the article is to consider retrospectively the morphodynamics of Sevastopol bays under the influence of anthropogenic activity. We used materials of MHI RAS observations, satellite and aerial photographs, literary sources as well as a range of maps and plans, mainly of the 19th century. It is shown that the natural environment of Sevastopol bays has changed significantly as a result of anthropogenic activity. The greatest impact is noted in the area of Sevastopol Bay, where the shores have been subjected to significant anthropogenic impact (the removal of cliffs, concreting of the coastline, construction of piers, etc.). The shores, which can be classified as untransformed, have survived only on 1.1 km (or 3 %) of the original length of the coastline. The outer shores of the coastal bays have preserved their natural state to the greatest extent. Only 1.3 km (17 %) were subject to anthropogenic impact consisting in cutting and planning of cliffs and erection of coastal protection and beach-retaining structures. The shores of the coastal bays themselves were subject to a much greater impact. Only one of them preserves the average level of technogenic impact, whereas in three of them it is the maximum, and in three others it is extreme. Out of 33.5 km of the inner perimeter of the bays, about 10 km (30 %) remain relatively unchanged. It is noted that by now only 0.3 km or 10 % of the pre-existing shores with sandy beaches have remained in the region under consideration. It is observed that as a result of anthropogenic activity, the Sevastopol group of salt lakes, which were previously used medicinally, has been almost destroyed.

Keywords: Black Sea, Sevastopol bays, morphodynamics, anthropogenic impact, coastline, salt lake, accumulative shore, abrasion shore

Acknowledgments: The work was carried out under state assignment no. FNNN-2021-0005.

For citation: Efremova, T.V. and Goryachkin, Yu.N., 2023. Morphodynamics of the Sevastopol Bays under Anthropogenic Impact. *Ecological Safety of Coastal and Shelf Zones of Sea*, (1), pp. 31. 47. doi:10.29039/2413-5577-2023-1-31-47

Морфодинамика севастопольских бухт под воздействием антропогенной деятельности

Т. В. Ефремова *, Ю. Н. Горячкин

Морской гидрофизический институт РАН, Севастополь, Россия
** e-mail: efremova@mhi-ras.ru*

Аннотация

Деградация берегов Крыма под влиянием антропогенного фактора стала серьезной проблемой, на преодоление которой затрачиваются значительные усилия и финансовые средства. Цель статьи – ретроспективно рассмотреть морфодинамику севастопольских бухт под воздействием хозяйственной деятельности. Использовались материалы наблюдений МГИ РАН, космические и аэрофотоснимки, литературные источники, а также массив карт и планов, главным образом XIX в. Показано, что в результате антропогенной деятельности природная среда севастопольских бухт существенно изменилась. Наибольшее воздействие на морфодинамику отмечается в районе Севастопольской бухты, где берега подверглись значительному антропогенному влиянию (срытие клифов, бетонирование береговой линии, строительство молов, пирсов и т. п.). Берега, которые можно отнести к непреобразованным, сохранились лишь на протяжении 1.1 км (3 % от первоначальной длины) береговой линии. Внешние берега бухт взморья в наибольшей степени сохранили природное состояние. Антропогенному воздействию, выразившемуся в срезке и планировании клифов, а также устройстве берегозащитных и пляжеудерживающих сооружений, подверглось только 1.3 км (17 %) береговой линии. Значительно большее воздействие испытали берега бухт взморья. Только в одной из них сохраняется средний уровень техногенной нагрузки, в трех он максимальный, а в трех – экстремальный. Из 33.5 км внутреннего периметра бухт относительно неизмененными остаются около 10 км (30 %). К настоящему времени в рассматриваемом регионе от ранее существовавших берегов с песчаными пляжами осталось только 0.3 км, или 10 %. Отмечается, что в результате антропогенной деятельности почти уничтожена Севастопольская группа соленых озер, ранее использовавшаяся в лечебных целях.

Ключевые слова: Черное море, севастопольские бухты, морфодинамика, антропогенное воздействие, береговая линия, соленые озера, аккумулятивные берега, абразионные берега

Благодарности : работа выполнена в рамках выполнения государственного задания FNNN-2021-0005.

Для цитирования: *Ефремова Т. В., Горячкин Ю. Н.* Морфодинамика севастопольских бухт под воздействием антропогенной деятельности // Экологическая безопасность прибрежной и шельфовой зон моря. 2023. № 1. С. 31-47. EDN THAAMX. doi:10.29039/2413-5577-2023-1-31-47

Introduction

Diverse and complex natural processes of various scales are constantly transforming the coast. At the same time, regional characteristics of the coastal zone determine various interactions and relative importance of individual natural processes. Human activity is another factor influencing coast transformation. It modifies natural environment and natural processes both directly and indirectly.

From the 20th century, the impact of the anthropogenic factor has increased so much that in some areas it significantly exceeded even the impact of natural processes. Urbanization, development of economy and communications, and the construction associated with them have changed natural landscapes of individual coasts beyond recognition, which, on the one hand, undoubtedly had a positive component, but on the other hand, led to a number of negative consequences. There are many such examples on the Black Sea coast [1–3].

Degradation of the coasts in the recreational areas of Crimea under the influence of the anthropogenic factor has become a serious problem, to overcome which significant efforts and financial resources are spent. Thus, the Southern coast of Crimea has almost completely lost its original coastal landscapes due to cost protection measures. In some parts of the coast, valuable accumulative beaches have disappeared either partially or completely (Evpatoria, Nikolaevka, Peschanoe village). The anthropogenic impact on the Crimean coast is considered in detail in [4].

A complete bibliography on the problems of studying the coastal zone of Crimea, available on the website of the library of the Federal Research Center "Marine Hydrophysical Institute of the Russian Academy of Sciences", contains almost no works devoted to the Sevastopol region. As a rule, it is mentioned among others, and there is not much information about it. This is quite understandable, since there was a base of the USSR Navy in the region for a long time, which limited publication possibilities. After the collapse of the USSR, hardly any research was carried out for a long time, and it was actually resumed 15 years ago. The purpose of the article is to retrospectively consider the morphodynamics of Sevastopol bays under the influence of anthropogenic activity.

Materials and methods of research

The materials of the MHI RAS observations, space and aerial photographs, literary sources, as well as a range of maps and plans (mainly of the 19th century) stored in the Sevastopol Maritime Library were used in the work.

Results and discussion

In the region under consideration, two areas can be distinguished.

The first one is Sevastopol Bay itself, currently with a total length of about 7.5 km and a perimeter length of 31.9 km from the entrance artificial piers (Fig. 1). The bay was formed due to flooding of the mouth of the Chernaya River during the post-glacial rise in sea level. The northern and southern shores of Sevastopol Bay, including Yuzhnaya Bay, were originally cliffs of Sarmatian limestone up to 30–80 feet (10–25 m) high [5]. The coastal relief is indented by gullies, which continue into smaller bays and concavities of the coastline. Before development, the coast could be attributed to the abrasion ingressive ria type. The ria type of shore, characteristic only for this region of the Black Sea, was indicated in the well-known monograph by V.P. Zenkovich [1)].

[1)] Zenkovich, V.P., 1960. [*Morphology and Dynamics of the Soviet Coasts of the Black Sea*]. Vol. 2. Moscow: Izd-vo AN SSSR, 216 p. (in Russian).

Fig. 1. Space image of the bays of Sevastopol, the numbers indicate the areas considered in the text (https://www.google.com/intl/ru/earth/)

Due to its configuration, the bay is only exposed to waves from the western direction. Before the construction of entrance piers in the 1970s the width of the entrance to the bay was 1.2 km; after construction, it decreased to 0.4 km. As a result, at present, significant waves hardly penetrate into the bay, and abrasion of the few surviving sections of the cliff is almost zero, which is also facilitated by blocky heaps on the shoreline. According to our calculations, by 2022 the coasts, which, with some reservations, can be classified as untransformed, have survived only 1.1 km (3 % of the original length) of the coastline. Almost all of them are located on the northern side of the bay.

The coasts of the region since the beginning of the 19th century were subjected to significant anthropogenic impact – concreting of the coastline, construction of piers, etc. In addition, significant parts of the cliffs were completely demolished. Thus, in Yuzhnaya Bay on the Korabelnaya Storona in 1830–1840 during the construction of the Lazarevsky Admiralty, a whole mountain of rock with a volume of 200,000 m^3 was manually demolished. During the construction of forts protecting the city from the sea, cliffs were also removed. First of all, these are the areas of the modern Primorsky Boulevard (on the site of the largest fort that has not survived – the Nikolaevsky), Konstantinovsky, Mikhailovsky and Pavlovsky forts.

At present, the coast of Sevastopol Bay can be confidently attributed to anthropogenic. The length of the modern coastline occupied by hydrotechnical facilities is 37,700 m; the coefficient 1.18 introduced in [6] testifies to the extreme technogenic load.

The second region stretches sublatitudinally to the west from the southern entrance pier to Cape Chersonesus. In a straight line, this distance is 10.5 km, and along the perimeter of the bays, it is 41.1 km. This section of the coast, together with the southern part of Sevastopol Bay, forms the northern coast of the Herakleian Peninsula. The flooded mouths of long and deep gullies form seven main bays. The ratio of the length of these bays to their width at the mouth varies from 0.8 (Pesochnaya) to 5.5 (Streletskaya) (Table 1).

Table 1. Morphometric characteristics of Sevastopol bays

Bay	Length (km)	Width (km)	Length/Width
Sevastopol	7.5	1.2	6.3
Karantinnaya	1.3	0.6	2.4
Pesochnaya	0.3	0.4	0.8
Streletskaya	2.2	0.4	5.5
Kruglaya	1.3	0.6	2.2
Abramova	0.8	0.6	1.3
Kamyshovaya	2.5	0.9	2.8
Kazachya	3.0	1.1	2.7

The shores between the bays are represented by an abrasion cliff composed of layered Sarmatian limestones, its height successively decreases from 25 m in the east to wedging out at Cape Chersonesus. Here on the shore, there is a shaft of large unrounded limestone fragments up to 1 m high. The foot of the cliff is bordered by a bench, on the edge there are heaps of blocks of large limestone fragments. In the concavities of the coast there are narrow (5–7 m wide) beaches made of boulders and large pebbles. The cliffs have wave-cut niches, which to the greatest extent intensify natural destruction of the coast (under the influence of precipitation, eolian and chemical processes, etc.) in the form of landslides. Therefore, the rate of cliff abrasion can only be estimated approximately, on large time scales. The average rate of coastal retreat, calculated from the data of repeated topographic surveys of the Chersonesus site over the past century, was 2.3–2.5 m [7]. The sector of active wave action on this region lies in a narrow range from west to north. Even with a relatively small acceleration of the waves, storm waves often develop here.

Recreational beaches on the open coast are artificial pebble beaches of the Pobedy Park, the Aquamarine Complex and the Cadet School on the watershed of Kruglaya and Streletskaya bays. The material of the beaches is quite successfully held with the help of the bun system. The outer shores of the second region have preserved their natural state to the greatest extent. Only 1.3 km (17 %) from the 7.6 km of the outer coast underwent anthropogenic transformation.

Table 2. Morphometric characteristics of Sevastopol bays and technogenic impact coefficients

Bay	Coast length (m)	Linear dimensions of hydrotechnical structures (m)	Technogenic impact coefficient (K)
Karantinnaya	3700	1775	0.47
Pesochnaya	1029	1087	1.05
Streletskaya	6007	3264	0.54
Kruglaya	3466	3312	0.95
Abramova	2370	1637	0.69
Kamyshovaya	7280	8640	1.18
Kazachya	9670	3577	0.37

Almost all of these sites are located between Kruglaya and Streletskaya bays. The anthropogenic impact here was expressed in the cutting and planning of cliffs, construction of coast-protection and beach-retaining structures.

The spaces of the bays themselves have undergone significantly greater anthropogenic impact, and this impact is constantly increasing. As can be seen from Table 2, only in Kazachya Bay the average level of technogenic load is preserved; in three bays it is extreme (Pesochnaya, Abramova and Kamyshovaya bays); in the rest – it is maximum. About 10 km (30 %) of the 33.5 km of the inner perimeter of the bays remain relatively unchanged.

In the mouths of the bays, the movement of sediments is directed towards the apex, most pronounced in relatively shallow bays with a wide mouth (see Table 1), in the apex of which accumulative forms were created. At the foot of the cliffs adjacent to the outer side of the bays, there are narrow (up to 5 m) beaches made of poorly rounded limestone fragments. Sandy fractions are characteristic mainly of the apex parts of the bays.

In the region under consideration, accumulative forms occupied insignificant sections of the coast, and almost nothing was said about them in scientific literature. Meanwhile, there were bay-bars that separated the sea from salt lakes. At present, it can be said that under the influence of man, the lakes and, accordingly, the bay-bars have disappeared as a landscape and landform.

In Crimea, there are four groups of salt lakes – Kerch, Tarkhankut, Evpatoria and Perekop [2)]. From time immemorial, salt was mined here and at the end of the 19th century Crimean lakes provided 40 % of Russia's total salt production. From the 20th century, the therapeutic mud of the Evpatoria group of lakes has been used for medical purposes and brine has been used as a raw material for the chemical industry (production of bromine, magnesium oxide, etc.). From the 1930s such production was also deployed at the Perekop group of lakes.

Salt lakes of Crimea, depending on the characteristics of alimentation (sea, surface or groundwater runoff), are usually divided into two groups: *continental*, with a predominance of surface or groundwater runoff, and *marine*, the alimentation of which, in addition to surface and groundwater runoff, includes the sea [2)]. In this group, two subgroups are distinguished, one of which includes estuaries and bays that have retained communication with the sea. The second group includes lakes separated from the sea by solid barriers through which relatively weak filtration of sea water takes place. In addition, sea water in stormy weather can break through bay-bars. This subgroup covers most of the Crimean lakes, as well as the salt lakes of the Sevastopol group considered below, which were not included in any classification. This is due to the fact that now there is only one lake left out of at least nine that existed before (Fig. 2). For comparison, there are 14 lakes in the Evpatoria group, and 10 in the Kerch group.

The salt lakes of the Sevastopol region are mentioned in [8], where the Chersonesus group of lakes is distinguished, but by the time this work was published, the lakes indicated in it had not existed for a long time, some of these lakes were briefly mentioned by V.P. Zenkovich in his work [1)].

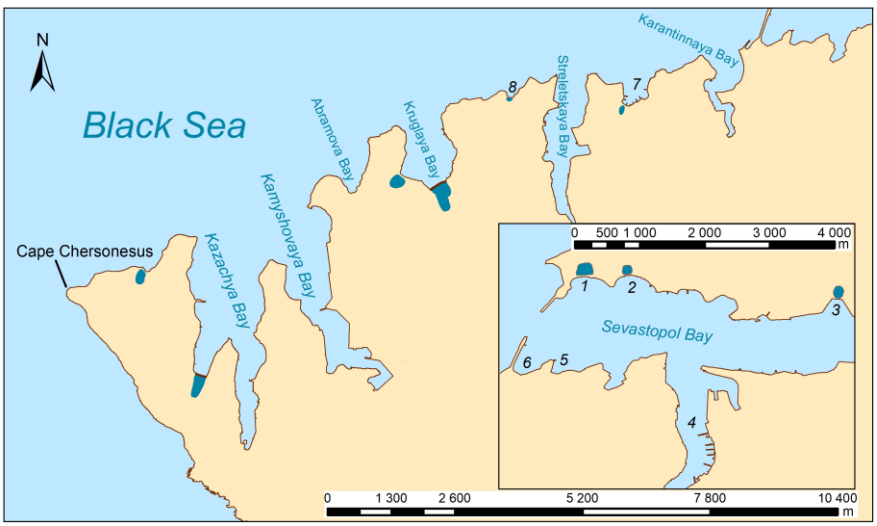

F i g . 2 . Locations of salt lakes in the bays of Sevastopol

[2)] Ponizovsky, A.M., 1965. [*Salt Resources of Crimea*]. Simferopol: Izd-vo "Krym", 162 p. (in Russian).

F i g . 3 . A fragment of a map of the coast of the northern side of Sevastopol: *above* – on the first map by navigator Baturin (1773); *below* – on the map by navigator Radionov (1840). The arrows show the lakes

There were three lakes in the first region: two in the lowlands on both sides of the watershed between the Konstantinovsky and the Mikhailovsky forts, Konstantinovskaya and Matyushenko bays (numbers *1* and *2* in Fig. 2); the third was located in the Panayotovaya Gully (number *3* in Fig. 2). These lakes are marked on the first map of Sevastopol by navigator Baturin, 1773 (Fig. 3).

For the first time, the contours of the lakes were shown in detail on the map of 1840. The area of each of them was 30–40 thousand m^2, they existed until the First World War.

On the site of the lake in the Panayotovaya (now Dokovaya) Gully in 1915, the largest dry dock in the city was built. At the same time, a seaplane base was deployed on the site of the lake in Matyushenko Bay, now there is a wasteland, partially overgrown with reeds. The lake near the Konstantinovsky Fort was liquidated in the 1930s, at present there is a residential development here.

Small fragments of sandy beaches have been preserved on the site of the former bay-bars. It is obvious that alimentation of accumulative forms (bay-bars) and their formation in this area is associated with the existence of a vast sandbar in the area of the Northern Spit, which Pallas wrote about based on the results of a survey in 1793: "... there is a small sandbank in front of the Northern Spit" [5, p. 37]. The author of [9], noting a swell-like elevation 1–2 m high elongated from north to south to the west of the entrance piers to Sevastopol Bay, makes an assumption that these are the remains of a bay-bar at the entrance to the bay, formed when the coast was lower than modern marks, when the estuary of the Chernaya River was a coastal salt lake.

On the first map of Sevastopol mentioned above, a continuous strip of sand is marked along the coast from the Northern Spit to Matyushenko Bay (Fig. 3). It is interesting that a comparison of maps for different years shows that at present the area of the sandbar has increased, while the depths in it have decreased, which can be associated with the construction in the 1970s of a 250 m long northern pier near the Konstantinovsky Fort, which interrupted the alongshore sediment flow. It is appropriate to note here that after construction of the southern pier 500 m long, the sediment inflow into Severnaya Bay completely stopped, and the water exchange, according to some estimates, decreased by a factor of three [10]. It can be seen from the analysis of old maps that earlier accumulative forms in the shape of sandbars were present in Yuzhnaya, Aleksandrovskaya, and Martynova bays (numbers *4*, *5*, *6* in Fig. 2). Now fragments of these forms have remained only in Aleksandrovskaya Bay.

In the second region, in the northern part of the Herakleian Peninsula, there were six lakes. One of them was located in Pesochnaya Bay (number *7* in Fig. 2). Its area was small – about 10,000 m^2. A mud bath was in operation on the basis of the silts of this lake in the late 19th – early 20th centuries. Like the bay-bars of the lakes of the Northern Side, the bay-bar in Pesochnaya Bay was composed of medium- and fine-grained sand, with the latter predominating. The bay-bar, unlike the lake, has survived to the present day in the form of Pesochny beach. However, its recreational properties are doubtful, because due to an erroneous design decision, crushed stone from a nearby artificial beach comes here. As a result, the beach contains both the original sandy material, which makes up the main body of the beach, and crushed stone, concentrated in the shoreline up to 15 m wide.

Two salt lakes were located in the southern and western parts of Kruglaya Bay; they were separated from the sea by two bay-bars [11]. Here is how they are described by Pallas: "Kruglaya Bay bears its name for a reason. It does not reach one verst in length and width and is no more than 6 sazhens (11 m) deep; it has a small islet inside with shallow depths of water around, and there are two salt lakes on the shore; one of them is separated from the bay in its depths only by a narrow bay-bar, and the other, on the western side, by a wider isthmus" [5, p. 41].

There was a mud bath that used the silt of the lake in the western part of the bay until the middle of the 19th century. According to an aerial photograph of 1942, the bay-bar in the southern part had a length of about 400 m, a width of up to 80 m, in the western part, respectively, 150 and 40 m. The area of the southern lake was about 80,000 m^2, and that of the western lake was 15,000 m^2. In the 1950s–1960s, the bay-bar of the southern lake was almost completely dismantled

into building sand, and the lake turned into a shallow (depth less than 0.5 m) apex part of the bay. Back in the middle of 1990s, a part of the bay-bar with the beach was preserved here. At the beginning of the 21st century, it was covered with soil where some apartments were built. As for the western lake, it is currently covered with construction debris, overgrown with reeds.

In place of the former bay-bar of the southern lake, the bottom topography now represents accumulative forms in the shape of underwater sandbars composed of sandy fractions. Starting from 2015, a new bay-bar has formed to the south of the pre-existing one; at present, its length is 45 m, and its width is about 25 m (Fig. 4).

The root part of the new spit is formed 400 m south of the previously existing one. This is due to the fact that a single alongshore sediment flow in the bay was interrupted due to the construction of three buns to the north, and the source of alimentation (sand poured onto the beach before the holiday season) is located to the south of them. The sand migrates to the inner part during storms. That is, we see the desire of the lithodynamic system of Kruglaya Bay (in the presence of alimentation sources) to return to its original equilibrium state. According to the sounding data, the depths are decreasing in the apex, where the base of a small fleet is located, i.e., the process of sediment accumulation continues. At the same time, the sediment flow in the bay itself is small, as evidenced by the apparent absence of sediment accumulation from the sea near the buns. The city authorities planned to fill up the apex of the bay. It was also planned to bury the remnants of the islet to improve navigation. These plans were based on an erroneous idea of the lithodynamics of the bay.

Fig. 4. The junction of the emerging sand spit on satellite images at the place of the former salt lake: *left* – 2009; *right* – 2020

F.i g . 5 . An islet in the center of Kruglaya Bay on the map of 1854 (*left*) [3] and 1856 [4] (*right*)

In the central part of the bay, there is an uplift of the bottom, which, during the period of the lowest stand of the level, protrudes above the water surface. Its length is about 150 m, its width is from 20 to 90 m. On ancient maps, this relief form was designated as a small islet (Fig. 5). By origin, it is, apparently, a remnant on which antique buildings were constructed. This was possible, since at that time the sea level was 2–3 m lower than today. This is indirectly confirmed by the presence of wave-cut niches in the western part of the bay at a depth of about 2 m, which we found during the survey of the bottom.

The underwater research in the bay was carried out by an expedition of the Department of Underwater Archeology of the Tauric Chersonesus Museum-Reserve [12, 13]. Some findings of artifacts made it possible to assume the existence of a public or religious building on the islet. On the southern side of the sandbar, using a diving survey and shooting from a quadrocopter, a rock fill about 60 m long and 20 m wide was revealed, the existence of which, presumably, was associated with the use of the bay water area as a harbor. Even 100 years ago, most of the bottom of the bay was covered with a sand layer and wide sandy beaches were formed

[3] Captain E. Lyons R.N., H.M.S, 1854. *Harbour of Sevastopol or Akhtiar, the antient Ctenus*. *From a Russian MS with additional soundings: map*. Scale: [circa 1:40,000]. G236:6/39. [London]: Hydrographic Office. 1 map; 57.5 × 34 cm.

[4] Lieut. Geo. R. Wilkinson, R.N. and Capt. T. Spratt, R.N.C.B., 1856. *Sevastopol, shewing the Russian defence works and the approaches of the allied armies*: *map*. Scale: 1 : 18,300. [London]: Hydrographic Office. 1 map: col.; 77 × 118 cm.

(survey by S. A. Zernov in 1912 [5]). To date, the amount of sand has significantly decreased due to its extraction, since the coast and the bottom are abraded under the influence of waves quite slowly due to the uplift in the center of the bay, which dampens the wave energy.

A significant salt lake existed in the apex of Kazachya Bay. According to [5], the length of the lake at the end of the 18th century was about 130 sazhens (238 m); a low bay-bar separating it was 60 sazhens long and 23 wide (110 and 49 m, respectively), of which 14 sazhens (26 m) was a flat white shore, apparently, flooded from time to time.

Further in [5, p. 41] it is noted: "In the salt lake, the bottom is as white as in the bay; the water level in it in the summer ... seemed much lower than in the bay." The area of the lake, apparently, was about 60,000 m^2. A dirt road ran along the bay-bar for many years. In the 1950s, most of the bay-bar, as in Kruglaya Bay, was dismantled for construction sand. At present, a small part of the spit in the eastern part of the bay has been preserved (Fig. 6). It is composed of sand with an admixture of rounded limestone fragments. Analysis of satellite images shows the current accumulation of sediments in the area of the former bay-bar.

Before the beginning of the 21st century, a small salt lake existed in the concavity of the coast at the site of the modern Aquamarine Complex (number *8* in Fig. 2). The area of the lake was about 1000 m^2, and the bay-bar was about 60 m long and 10 m wide. It was composed mainly of rounded limestone fragments. In 2010, the lake was filled in, and an embankment was built in its place.

Fig. 6. The remnant of the saline lake bay-bar in Kazachya Bay

[5] Zernov, S.A., 1913. [On Study of Life in the Black Sea]. *Zapiski Imperatorskoy Akademii Nauk po Fiziko-Matematicheskomu Otdeleniyu* [Transactions of the Imerial Academy of Sciences. Physical and Mathematical Department], 32(1), 280 p.

Finally, the only lake that has survived to this day is located near Cape Chersonesus. Here is how it is described in [5, p. 41]: "There is also a salt lake ... 60 sazhens (110 m – *Author's note*) in length on a shovel-shaped cape, which ends Crimea in the northwest. This lake also, apparently, was part of the bay, and its bay-bar was formed by the run-up of waves that carried silt and gravel into a dam of 60 sazhens in length and about 20 in width, one height with the shore; everything is surrounded by fragments of stones, like a small rampart, so that now salt settles in this lake, separated from the sea, which, however, does not happen every year. This salt, although of poor quality because [the lake] is saturated with bitter salt, is used and taken by the Tatars from neighboring mountain villages, who are forced to take the tenth load to the owner in Akhtiar for free; the same is done with regard to the lakes of Kruglaya Bay. Several salt flats, almost dry, visible on this cape at a distance of 60 sazhens from the lighthouse, apparently, are of the same origin and are separated from the sea by coastal, low drafts, like stone walls."

At present, the lake is double, in its southern, apex part there is one more bay-bar, both of them are composed of limestone fragments. The area of the lake is about 15,000 m^2, the bay-bar is 150 m long and up to 30 m wide. The landscape of the surrounding area is lacustrine-estuary with halophyte vegetation [14] (Fig. 7).

In 2016, the southern part of the lake was filled in during the road construction. Currently, the lake is in a regime zone and is not available for research. In general, it can be said that the bay-bars of the second region were formed in relatively wide and open bays with a shallow depth, where significant waves can reach their apex parts. In other bays, the movement of sediments either created spits or filled in the concavities of the coastline.

F i g . 7 . The last remaining salt lake in the Sevastopol region

Thus, in the upper reaches of Kamyshovaya Bay, on its eastern shore, there was a small fringing accumulative form – Marfa Spit. In the post-war period, the sand composing it was used as building material. Judging by the old maps, a short gully was covered with sand on the western shore of the central part of Streletskaya Bay within a fairly short period in the 20th century. In ancient times, the gully in the central part of Karantinnaya Bay, which was the inner harbor of ancient Chersonesus, was also "covered with sand as a result of the movement of marine sediments" [15, p. 8].

According to our calculations, the bay-bars of the lakes with sandy beaches previously occupied about 1.1 km of the coastline in the first region, 1.5 km in the second region, and 2.6 km in total. This is not much in relation to the total length of the coast, but by now only 0.3 km (10 %) of the coast with a sandy beach remains.

The estuary part of the Chernaya River, flowing into Sevastopol Bay, has undergone significant transformations under the influence of anthropogenic activity. In the post-glacial period, thick marine, firth-marine and alluvial deposits formed in the sea mouth of the river. In the middle of the 19th century, the mouth of the river was a swampy area – a river delta with numerous branches. It can be seen on old maps that there was a wide bar with depths of up to 1 m on the bank of the river. An even older inner river delta, the remains of which can still be traced, was located in the area of the modern bridge. Probably, the mouth section of the river and the Inkerman estuary were flooded by the sea during the next transgression, then, as a result of filling with sediments and regression of the sea, the marine stage of development of the mouth was replaced by the estuary, and later by the river development, and the mouth acquired modern relief [16]. At present, a deep water area is located on the site of the swampy delta. The configuration of the shores has been anthropogenically changed by the construction of piers, moorings, dams and other hydraulic structures on bulk soils. The main transformations of the mouth of the Chernaya River included construction of a bucket for the Sevastopol Seaport (in Inkerman), creation of an artificial reservoir with an area of about 0.4 km^2 at the mouth section of the river and the site of a floodplain swamp, and digging of a navigable canal (Fig. 8). Now the territory is a continuous industrial zone. In recent years, illegal sand mining has been carried out under the guise of leveling the coastline.

Significant swampy areas at the confluence of temporary watercourses were previously located in the apex parts of Yuzhnaya and Artilleriyskaya bays. Back in the 19th century, they were covered with soil excavated during cliff removal: in Yuzhnaya Bay during the construction of the Lazarevsky Admiralty (see above), in Artilleriyskaya Bay during the construction of the Nikolaevsky Fort. In place of the former swamp in Yuzhnaya Bay, there is now a railway station and a bus station. Small swampy areas at the mouths of temporary streams are now preserved only in Streletskaya and Kazachya bays.

Fig. 8. The mouth of the Chernaya River: on 1773 map (*left*), on 2021 space image (*right*) (https://www.google.com/intl/ru/earth/)

Conclusion

Based on the foregoing, the following main conclusions can be drawn:

1. as a result of anthropogenic activity, the natural environment of Sevastopol bays has changed significantly;

2. the greatest impact is noted in the area of Sevastopol Bay, where the shores have undergone significant anthropogenic changes: removal of cliffs, concreting of the coastline, construction of piers, etc. The shores, which can be classified as untransformed, have survived only for 1.1 km (or 3 % of the original length) of the coastline. The degree of technogenic load is extreme;

3. the outer shores of the coastal bays have preserved their natural state to the greatest extent. Only 1.3 km (17 %) of the 7.6 km of the coastline was subjected to anthropogenic impact, expressed in the cutting and planning of cliffs, installation of coast-protection and beach-retaining structures;

4. the shores of seaside bays have undergone significantly greater anthropogenic impact, and this impact is constantly increasing. Only in one of the bays an average level of technogenic load is preserved, in three bays it is extreme and in the remaining three it is maximum. About 10 km of the inner perimeter of the bays (30 %) of the 33.5 km remain relatively unchanged;

5. as a result of anthropogenic activity, the Sevastopol group of salt lakes, which were previously used for medicinal purposes, is almost destroyed. Only one lake of at least nine pre-existing lakes remains;

6. to date, in the region under consideration, only 0.3 km (10 %) of the previously existing coast with a sandy beach has remained;

7. significant transformations under the influence of anthropogenic activity are also noted in the estuary part of the Chernaya River and the swampy areas at the confluence of temporary watercourses, which were previously located in the apex of the bays, and in the 19th century were covered with soil excavated during cliff removal.

REFERENCES

1. Kuroki, K., Goda, Y., Panin, N., Stanica, A., Diaconeasa, D.I. and Babu, G., 2006. Beach Erosion and Coastal Protection Plan along the Southern Romanian Black Sea-shore. In: J. M. Smith, ed., 2006. *Coastal Engineering. Proceedings of the 30th International Conference, San Diego, California, USA, 3–8 September 2006*. World Scientific, pp. 3788–3799. doi:10.1142/9789812709554_0318
2. Nikolov, H., Trifonova, E., Cherneva, Zh., Ostrowski, R., Skaja, M. and Szmytkiewicz, M., 2006. Longshore Sediment Transport at Golden Sands (Bulgaria). *Oceanologia*, 48(3), pp. 413–432. Available at: https://www.iopan.gda.pl/oceanologia/483nikol.pdf [Accessed: 7 February 2023].
3. Stancheva, M., Marinski, J., Peychev, V., Palazov, A. and Stanchev, H., 2011. Long-Term Coastal Changes of Varna Bay Caused by Anthropogenic Influence. *Geo-Eco-Marina*, 17, pp. 33–40. doi:10.5281/zenodo.56892
4. Goryachkin, Yu.N. and Efremova, T.V., 2022. Anthropogenic Impact on the Lithodynamics of the Black Sea Coastal Zone of the Crimean Peninsula. *Ecological Safety of Coastal and Shelf Zones of Sea*, (1), pp. 6–30. doi:10.22449/2413-5577-2022-1-6-30
5. Pallas, P.S., 1999. [*Observations Made while Travelling along Southern Governorships of the Russian State in 1793-1794*]. Moscow: Nauka, 246 p. (in Russian).
6. Aibulatov, N.A. and Artyukhin, Yu.V., 1993. [*Geoecology of the Shelf and Coasts of the World Ocean*]. Saint Petersburg: Gidrometeoizdat, 304 p. (in Russian).
7. Lebedinski, V. and Pronina, J., 2014. Study of Ancient Coastline of Chersonesos and its Chora. *Khersonesskiy Sbornik*. Sevastopol. Issue 21, pp. 7–16 (in Russian).
8. Oliferov, A.N. and Timchenko, Z.V., 2005. [*Rivers and Lakes of Crimea*]. Simferopol: Dolya, 216 p. (in Russian).
9. Myslivets, V.I., 2017. Interrelationship of Man and Nature on the Coast of the South-Western Crimea. *Almanac Space and Time*, 14(1) (in Russian).
10. Ivanov, V.A., Ovsyany, E.I., Repetin, L.N., Romanov, A.S. and Ignatyeva, O.G., 2006. *Hydrological and Hydrochemical Regime of the Sebastopol Bay and its Changing under Influence of Climatic and Anthropogenic Factors*. Sevastopol: MHI NAS of Ukraine, 90 p. (in Russian).
11. Udovik, V.F., Kharitonova, L.V. and Goryachkin, Yu.N., 2017. Monitoring of the Urban Beaches of Sevastopol. *Ecological Safety of Coastal and Shelf Zones of Sea*, (4), pp. 86–94 (in Russian).
12. Bukatov, A.A., 2020. [Underwater Archaeological Studies in Kruglaya Bay]. *Problems of Underwater Archaeology*, (11), pp. 22–29 doi:10.24412/2220-0959-2020-11-22-29 (in Russian).
13. Bukatov, A.A., Bondarev, I.P. and Dyuzhenko, T.V., 2020. To the Question of the Existence of Chersonese Harbor in Round (Kruglaya) Bay. In: A. V. Zaikov, ed., 2020. *Khersonesskiy Sbornik*. Sevastopol. Issue 21, pp. 7–16 (in Russian).
14. Pankeeva, T.V. and Bondareva, L.V., 2014. Methodical Approaches to Landscape-Sozological Assessment of Coastal Systems. In: TNU, 2014. *Optimization and Protection of Ecosystems*. Simferopol: TNU. Iss. 11, pp. 57-67 (in Russian).
15. Bukatov, A.A., Bondarev, I.P. and Dyuzhenko, T.V., 2019. Tauric Chersonese Seaport in Quarantine Bay and Natural Processes. In: A. V. Zaikov, ed., 2019. *Khersonesskiy Sbornik*. Sevastopol: Albatros. Issue 20, pp. 7–20 (in Russian).
16. Minkovskaya, R.Ya. and Demidov, A.N., 2016. Evolution of Marine Mouth of the Chernaya River (Sevastopol Region). *Ecological Safety of Coastal and Shelf Zones of Sea*, (1), pp. 81–88 (in Russian).

Submitted 24.11.2022; accepted after review 23.01.2023;
revised 1.02.2023; published 24.03.2023

About the authors:

Tatiana V. Efremova, Engineer, Marine Hydrophysical Institute of RAS (2 Kapitanskaya St., Sevastopol, 299011, Russian Federation), *efremova@mhi-ras.ru*

Yuri N. Goryachkin, Chief Research Associate, Marine Hydrophysical Institute of RAS (2 Kapitanskaya St., Sevastopol, 299011, Russian Federation), Dr.Sci. (Geogr.), **ORCID ID: 0000-0002-2807-201X, ResearcherID: I-3062-2015**, *yngor@mhi-ras.ru*

Contribution of the authors:

Tatiana V. Efremova – problem statement, data processing and analysis, article text preparation

Yuri N. Goryachkin – problem statement, data processing and analysis, article text and map preparation

All the authors have read and approved the final manuscript.

Original article **DOI:** 10.29039/2413-5577-2023-1-48-64

Interannual Variability of Water Circulation Regimes in the Arctic Ocean

E. E. Lemeshko

Marine Hydrophysical Institute of RAS, Sevastopol, Russia
e-mail: e.lemeshko@mhi-ras.ru

Abstract
The article studies the interannual variability of the Arctic Ocean water circulation regimes according to altimetry data for the area from 65°N to 89.75°N including the ice-covered area of the ocean. The purpose of the work is to study the variability of the ocean level and the velocities of surface geostrophic currents depending on the value of the Arctic oscillation index, and to establish quantitative patterns between them. In addition, the paper considers the influence of different ocean circulation regimes and the value of the Arctic oscillation index on the steric level variability as an indicator of freshening/salinization processes in the polar region north of 81.5°N. The steric component of level was calculated as the difference between the dynamic topography from altimetry data and the GRACE data of the manometric level component. On an interannual time scale, the sea level response averaged over the Arctic Ocean is in antiphase with the Arctic Oscillation Index. Based on the method of multiple regression, quantitative estimates of the dependence of the sea level and geostrophic velocity components on the value of the Arctic oscillation index were obtained. The level difference between the shelf and the deeper part of the ocean was ~ 4 cm per unit of the Arctic oscillation index. The difference between the areas of positive and negative values of the sea level anomalies creates a pressure gradient, which leads to an increase in the anomalies of surface geostrophic velocities and enhances the inflow of Atlantic waters along the shelf edge in an easterly direction during the cyclonic regime (Arctic Oscillation Index is greater than 0). Under the anticyclonic regime of atmospheric circulation (the index is less than 0), the effect becomes opposite. This agrees with the estimates of the linear regression coefficients for the velocity anomalies of geostrophic currents, which amounted to ~ 0.5 cm/s per 1 index unit. On the basis of the obtained results, a conceptual scheme of the regimes of circulation and distribution of desalinated waters depending on the phase of the Arctic oscillation is proposed.

Keywords: Arctic Ocean, altimetry, steric level, arctic oscillation, ocean circulation regimes, altimetry, GRACE

Acknowledgements: The work was funded by the RFBR under research project no. 20-35-90061.

For citation: Lemeshko, E.E., 2023. Interannual Variability of Water Circulation Regimes in the Arctic Ocean. *Ecological Safety of Coastal and Shelf Zones of Sea*, (1), pp. 48–64. doi:10.29039/2413-5577-2023-1-48-64

Межгодовая изменчивость режимов циркуляции вод Северного Ледовитого океана

Е. Е. Лемешко

Морской гидрофизический институт РАН, Севастополь, Россия
e-mail: e.lemeshko@mhi-ras.ru

Аннотация

Статья посвящена изучению межгодовой изменчивости режимов циркуляции вод Северного Ледовитого океана по данным альтиметрии для области от 65° до 89.75° с. ш., включая область океана, покрытую льдом. Цель работы заключается в исследовании изменчивости уровня океана и скоростей поверхностных геострофических течений в зависимости от величины индекса арктической осцилляции, а также в установлении количественных закономерностей между ними. Дополнительно рассмотрено влияние различных режимов циркуляции океана и величины индекса арктической осцилляции на изменчивость стерического уровня как индикатора процессов распреснения/осолонения в полярной области севернее 81.5° с. ш. Стерическая компонента уровня рассчитывалась как разница между динамической топографией по данным альтиметрии и данными *GRACE* о манометрической компоненте уровня. На межгодовом масштабе временно́й изменчивости отклик уровня моря, осредненного по Северному Ледовитому океану, находится в противофазе с индексом арктической осцилляции. На основе метода множественной регрессии получены количественные оценки зависимости уровня моря и компонент геострофической скорости от величины индекса арктической осцилляции. Перепад уровня между шельфом и более глубоководной частью океана составил ~ 4 см на 1 единицу индекса арктической осцилляции. Разница между областями положительных и отрицательных значений аномалий уровня моря создает градиент давления, что приводит к увеличению аномалий поверхностных геострофических скоростей и усиливает поступление атлантических вод вдоль кромки шельфа в восточном направлении при циклоническом режиме (индекс арктической осцилляции больше нуля). При антициклоническом режиме циркуляции атмосферы (индекс меньше нуля) эффект становится противоположным. С этим согласуются оценки коэффициентов линейной регрессии для аномалий скорости геострофических течений, которые составили ~ 0.5 см/с на 1 единицу индекса. На основании полученных результатов предложена концептуальная схема режимов циркуляции и распространения распресненных вод в зависимости от фазы арктической осцилляции.

Ключевые слова: Северный Ледовитый океан, альтиметрия, стерический уровень, арктическая осцилляция, режимы циркуляции океана, *GRACE*

Благодарности: работа выполнена при финансовой поддержке РФФИ в рамках научного проекта № 20-35-90061.

Для цитирования: *Лемешко Е. Е.* Межгодовая изменчивость режимов циркуляции вод Северного Ледовитого океана // Экологическая безопасность прибрежной и шельфовой зон моря. 2023. № 1. С. 48–64. EDN TYGZLF. doi:10.29039/2413-5577- 2023-1-48-64

Introduction

The Arctic Ocean near-surface circulation is mainly characterized by the alternation of anticyclonic and cyclonic phases on interannual variability scales [1–3]. Such a description of the circulation was based on the analysis of the dynamic topography calculated from the data of hydrological observations, as well as on numerical modelling [1–3]. According to modern field studies, the most dramatic changes in the Arctic Ocean occurred in the 2010s [1].

The area around the North Pole (NP) north of 81.5°N, sometimes called a "blind" spot (NP area in Fig. 1) due to the lack of any altimetry data there until 2011, is important for understanding hydrophysical changes in the Arctic Ocean. Sea ice and desalinated surface waters are carried by the Transpolar Drift (TPD) through this region towards the North Atlantic and largely determine the thermohaline structure of its subpolar regions. Therefore, such parameters as ice thickness, bottom pressure, and steric level (reflecting the vertical hydrological structure of waters) are key indicators of the variability of the entire Arctic Ocean.

Independent assessments of the freshwater balance based on the analysis of hydrological data showed two independent trends in the variability of the Arctic Ocean freshwater balance [4]. On the one hand, freshening was observed in the Canadian basin with a rate of change in the freshwater layer thickness of 2.04 ± 0.64 m/10 years, and on the other hand, salinization was observed in the East Eurasian basin with a trend of 0.96 ± 0.86 m/10 years [4]. According to long-term hydrological observations, freshening was also noted in the North Pole region with a trend of 1.19 ± 0.02 m/10 years [4].

As a result of the analysis of complex data from field studies in the area of the Beaufort Gyre, it was concluded that the fresh water supply increased by 40 % from 2003 to 2018 compared to the long-term average for 1970–2000. Accumulation of fresh water due to the impact of anticyclonic atmospheric circulation was considered as the main mechanism of freshening [5].

Based on the results of sea level analysis according to altimetry data for the area of the Beaufort Gyre and the North Sea, opposite level trends of 2009–2011 were identified. [6]. As a result, it was concluded that the shift in sea level variability in these areas took place due to changes in large-scale atmospheric circulation associated with the Arctic Oscillation (AO) Index [5, 6].

The Arctic Oscillation (AO) is a climate index that characterizes the distribution of atmospheric pressure and peculiarities of the wind field over the Arctic. When most of the Arctic is occupied by a cyclone, the AO Index is positive. It becomes negative during the anticyclonic circulation of the atmosphere. During the positive phase of the AO Index, the inflow of warm Atlantic waters increases and the distribution of the Pacific waters weakens. In addition, the transport of sea ice and near-surface desalinated waters to the Atlantic increases, and the distribution routes of the runoff of the Eurasian rivers change. During the negative phase of the AO Index, an anticyclonic pressure area is located over the Arctic,

and the sign of the current discharge anomaly changes to the opposite one [2]. The ocean circulation cyclonic mode lags behind the AO Index by about 1 year [7–9].

The article studies the variability of the ocean level and the velocities of surface geostrophic currents depending on the value of the AO Index, as well as the establishment of quantitative patterns between them. In addition, the paper considers the influence of different ocean circulation regimes and the value of the AO Index on the steric level variability as an indicator of freshening/salinization processes in the area of the Beaufort Gyre and in the polar region north of 81.5°N. The reconstructed steric component of level was calculated as the difference between the dynamic topography from altimetry data and the GRACE data of the manometric level component. Then, the reconstructed steric level was averaged over the area of the Beaufort Gyre and over the blind polar area north of 81.5°N, which was inaccessible to satellite altimetry until 2011 (Fig. 1).

Data and Methods

After 2011, new Envisat and CryoSat-2 satellites were launched in high-altitude orbits, which receive altimetry data in the "blind" spot area up to 89.75°N and improve the accuracy of anomalous sea level measurements [9].

Methodological work was carried out to compare altimetry data with sea level measurements using coastal tide gauges. The results showed a fairly high degree of correlation between them for periods of open water: in the Norwegian Sea, the average values were 0.86 [9, 10], and in the Barents Sea, 0.89 [2].

The obtained new altimetry data were used to estimate the dynamic topography of the entire Arctic Ocean, including the area north of 81.5°N, according to the following formula:

$$H_{DT} = H_{SSH} - H_G, \quad (1)$$

where H_{DT} – dynamic ocean topography; H_{SSH} – sea surface height; H_G – geoid surface height [9, 10]. Surface geostrophic velocities were calculated from the H_{DT} dynamic topography values obtained by formula (1) [10, 11].

Two arrays of satellite altimetry data in the form of monthly average data of dynamic ocean topography and surface geostrophic velocities provided by the Centre for Polar Observation and Modelling, University College London (www.cpom.ucl.ac.uk/dynamic_topography), were used in the paper. The first array consists of the data for 2003–2014 covering from 65° to 81.5°N on a grid of 0.75° × 0.25° [11], and the second array includes the data for 2011–2020 with a higher resolution (20 × 20 km) on a polar stereographic grid covering from 65° to 89.75°N. Both arrays include data concerning ocean areas covered with ice. The description of the method for calculating sea level is given in [10].

In addition, gravimetry data (Gravity Recovery And Climate Experiment (GRACE)), version RL06, grid 1° × 1°, monthly averages, 2002–2017, and GRACE-FO, 2018–2021, covering the entire ocean up to 89.9°N, were used (https://podaac.jpl.nasa.gov/datasetlist?search=tellus).

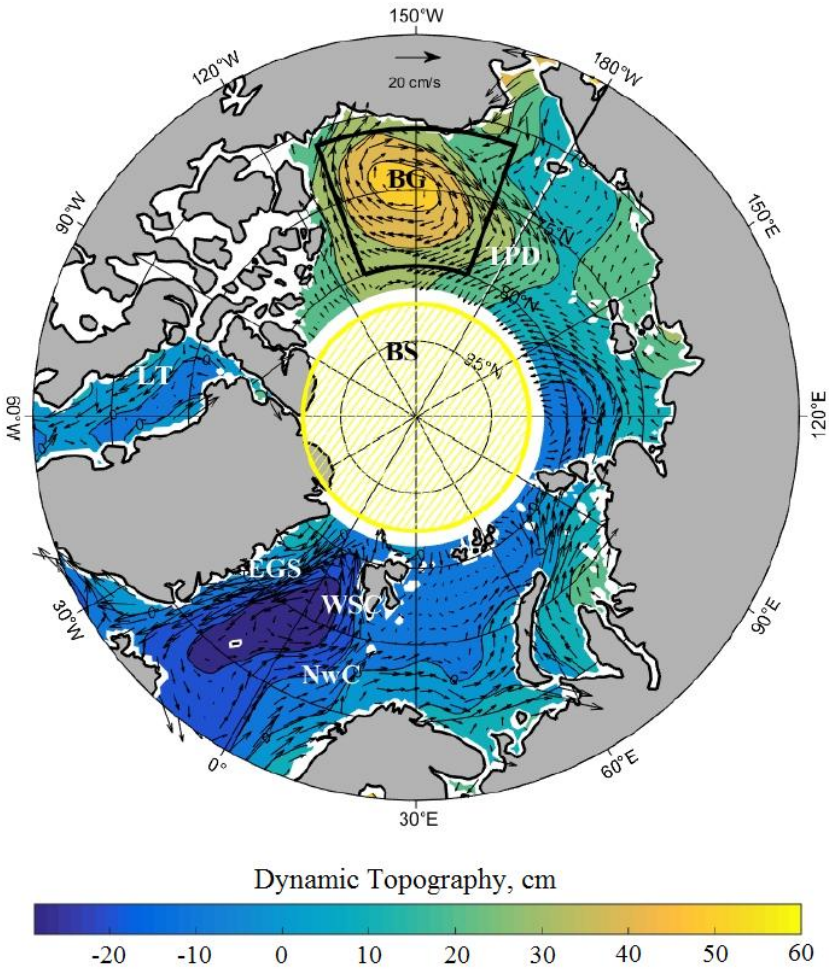

Fig. 1. Scheme of the surface currents of the Arctic Ocean: dynamic topography and geostrophic currents averaged from altimetry data for 2003–2014. BS – "blind" spot – the region north of 81.5°N; NwC – Norwegian Current; LT – Labrador Current; WSC – West Spitsbergen Current; EGC – East Greenland Current; TPD – Transpolar Drift; BG – Beaufort Gyre

Results

For the Arctic Ocean, the mean values of dynamic topography and surface geostrophic velocities for 2003–2014 were calculated (Fig. 1). Figure 1 illustrates the following main currents and large-scale elements of the ocean circulation marked with white symbols: the Norwegian Current, the Labrador Current, the West Spitsbergen Current, the East Greenland Current, the Transpolar Drift, and the Beaufort

Gyre (Fig. 1), which correspond to the known pattern of currents [1)] and to the estimates of geostrophic velocities obtained for these regions from earlier altimetry products [10].

The average current velocities calculated by us for the period 2003–2014 are ~ 10 and ~ 15 cm/s in the area west of Spitsbergen and near Novaya Zemlya, respec-tively. The level difference between the shelf and the deep part of the basin reaches 30 cm (Fig. 1).

In addition, when compared with the data of current meters at ten mooring buoys for 2011–2018, the correlation value for the Laptev Sea and the Beaufort Sea was 0.7, and for the Fram Strait it was 0.34. At the same time, the root-mean-square (RMS) deviations between the modules of geostrophic current velocities according to altimetry data and contact measurements by ADCP at mooring buoys amounted to 1–2 cm/s, and the RMS deviations of the difference in angle values were about 60° for 2005–2008 [10].

To analyze the interannual sea level variability, intraseasonal fluctuations were removed using a moving average filter with a window width of 12 months, then series of sea level anomalies were formed as deviations from their long-term average values. Figure 2 shows the obtained sea level anomalies averaged over the entire Arctic Ocean.

Both altimetry arrays are in good agreement with each other in the 2011–2014 data overlap interval (Fig. 2).

Anticyclonic regimes in the Arctic Ocean identified by positive sea level anomalies H_{DT} were observed in 2006–2007, 2009–2013, and 2016–2017 (Fig. 2).

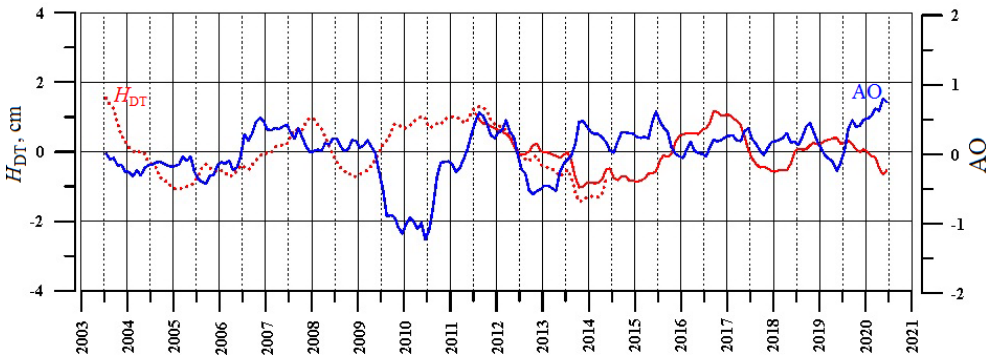

Fig. 2. Plots of dynamic topography averaged over the Arctic Ocean (cm) according to altimetry data (H_{DT}) for the period 2003–2014 (red dashed line), for the period 2011–2020 (red solid line) and the Arctic Oscillation (AO) Index (blue line) after filtering by a moving average with a window width of 12 months

[1)] Treshnikov, A.F., 1985. [*Arctic Atlas*]. Moscow: Glavnoe Upravlenie Geodezii i Kartografii, 204 p. (in Russian).

Cyclonic regimes (negative level anomalies) were observed in 2005, 2008, and 2014 (Fig. 2). For the entire period of altimetry observations for 2003–2020, the maximum duration of the anticyclonic regime of the ocean was ~ 3.5 years in 2009–2013, and this corresponded to the negative phase of the AO Index (Fig. 2). Conversely, during the positive phase of the AO Index (2013–2016), when the cyclonic regime is identified in the surface atmospheric pressure field, negative values of sea level anomalies are observed with a maximum duration of ~ 2.5 years (Fig. 2).

The AO Index data provided by NOAA/NWS Climate Prediction Center (USA)[2)], were used in the paper. Long periods of the AO Index negative phase can be observed in 2003–2006, 2009–2011, 2012–2013, and 2016–2017. This corresponds to the anticyclonic circulation in the Arctic Ocean: average values of dynamic topography over the water area are positive (Fig. 2). For the AO Index positive phase, negative values of the dynamic topography averaged over the Arctic Ocean are observed, most pronounced in 2013–2016 (Fig. 2). During the period when the cyclonic regime prevailed in the atmosphere during the AO positive phase, the cyclonic circulation of the ocean manifested itself in a decrease in the mean sea level with a time delay of about 1 year relative to the AO Index phase (Fig. 2).

Sea level H consists of the sum of steric level component H_{Sth} stipulated by seawater density changes, and manometric level component H_{man} stipulated by variations in the water mass of the liquid column, with their different characteristic time scales of variability [12, 13]:

$$H = H_{\text{Sth}} + H_{\text{man}}. \qquad (2)$$

The variability of the manometric level in the Norwegian and Barents Seas is mainly intraseasonal in nature, and its contribution reaches 80 % of the total dispersion. Therefore, the barotropic response of sea level to wind forcing has a scale of several months and can be masked by longer-term steric level variability.

In papers [12, 13], based on the analysis of GRACE data and numerical modelling, it was found that on the intraseasonal scales, the variations in the manometric sea level had a high correlation with the anomalies of the wind field for the sector under consideration.

To analyze the interannual variability of dynamic topography data and surface geostrophic velocities, a linear trend was removed from the data at each grid point after filtering by the moving average with the window width of 12 months. The resulting ocean level anomalies were averaged over the periods of the positive (AO > 0) and negative (AO < 0) phases of the AO Index [14]. First, such an approach was tested for the ocean sector (65°–81.5°N, 0°–70°E) that includes

[2)] NWs. *Artctic Ocsillations*. 202. [onine] Available at: http://www.cpc.ncep.noaa.gov/products/precip/CWlink/daily_ao_index/ao.shtml [Accessed: 30 March 2023].

the North, Norwegian, and Barents Seas for 2003–2014 [9]. During the periods when the AO Index is in its positive phase, the central part of the Arctic Ocean is occupied by a cyclonic area with negative values of level anomalies up to –3 cm, the zero level isoline corresponds approximately to the isobath of 300 m. In the southern part of the Barents Sea and in the Kara Sea, positive level anomalies up to 3 cm are distinguished; the vectors of velocity anomalies (~1 cm/s) correspond to the cyclonic circulation regime. For the periods when the AO Index was in its negative phase, the anomalies of the ocean level and velocities corresponded to the anticyclonic circulation regime. Similarly, for the entire water area of the Arctic Ocean for 2011–2020, the cyclonic circulation regime of the ocean during the positive phase of the AO Index > 0 and the anticyclonic circulation regime during the negative phase of the AO Index < 0 were distinguished.

To estimate quantitatively the effect of the AO Index on the variability of sea level anomalies H_{DT} and surface geostrophic velocities U, V, linear regression analysis [15] was used:

$$\begin{aligned} H^i_{\mathrm{DT}} &= \alpha^i_{\mathrm{DT}} \cdot \mathrm{AO} + \varepsilon^i_{\mathrm{DT}}, \\ U^i &= \alpha^i_U \cdot \mathrm{AO} + \varepsilon^i_U, \\ V^i &= \alpha^i_V \cdot \mathrm{AO} + \varepsilon^i_V, \end{aligned} \tag{3}$$

where regression coefficients for level α^i_{DT}, cm, and velocity component α^i_U, α^i_V, cm/s, were estimated at each i-th node of the grid, and $\varepsilon^i_{\mathrm{DT}}$, ε^i_U, ε^i_V are uncorrelated white noise. Figure 3 shows the sea level regression coefficients in the form of isolines and the corresponding coefficients of the current velocity modulus in the form of vectors $\alpha^i_{\mathrm{mod}V}$:

$$\alpha^i_{\mathrm{mod}V} = [(\alpha^i_U)^2 + (\alpha^i_V)^2]^{1\backslash 2}. \tag{4}$$

The spatial distribution of the coefficients of linear regression of the sea level and surface geostrophic velocities corresponds to the cyclonic circulation regime in the Arctic Ocean at positive values of the AO Index according to expression (3) (Fig. 3) and, thus, is consistent with the distribution of the sea level and velocities averaged for the positive phase of the AO Index. Similarly, for the negative phase of the AO Index, the distribution of the linear regression coefficients of the sea level and surface velocities changes sign to minus according to (3), which gives an anticyclonic pattern of circulation and is consistent with the map of sea level values and current velocities averaged over periods of the negative phase of the AO Index. To increase the robustness of the regression estimates, the linear trend was eliminated from the data of the AO Index, dynamic topography, and velocities after filtering by the moving average with the window width of 12 months. The anomalies obtained in this way were processed according to regression formula (3), and the results are shown in Figs. 3, 4.

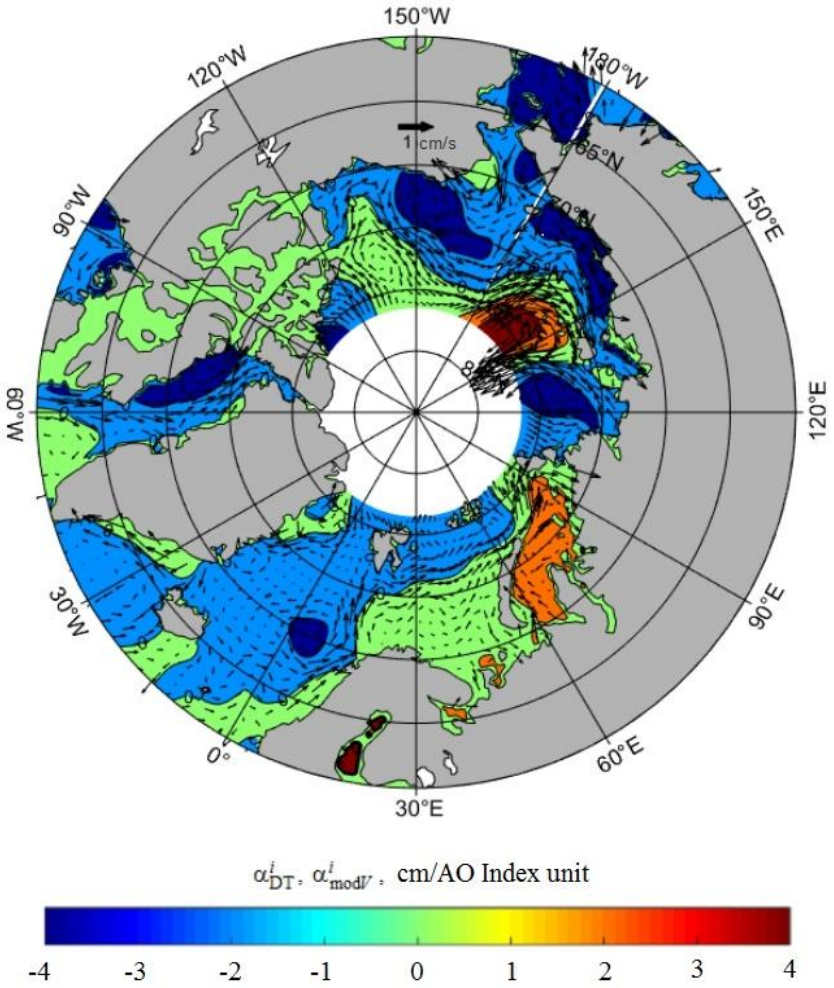

Fig. 3. Spatial distribution of linear regression coefficients for sea level anomalies α^i_{DT} (cm/AO Index unit) and for current velocity anomalies ((cm/s)/AO Index unit) as vectors for 2003–2014

As a result, regression relations for the sea level and geostrophic velocity components depending on the value of the AO Index were obtained. Calculated linear regression coefficients α^i_{DT} for sea level anomalies are more than ~2 cm in the shelf zone and about –2 cm in the deep part of the ocean (Fig. 3).

For the Norwegian Sea, the northern part of the Barents and Kara Seas, for the shelf of the Laptev Sea and the East Siberian Sea, the coefficients of linear regression of the modulus of current velocity anomalies α^i_{modV} have values of ~0.5 cm/s per AO Index unit concerning altimetry data for 2003–2014 and 0.6÷0.8 cm/s per AO Index unit concerning data for 2011–2020 (Fig. 3).

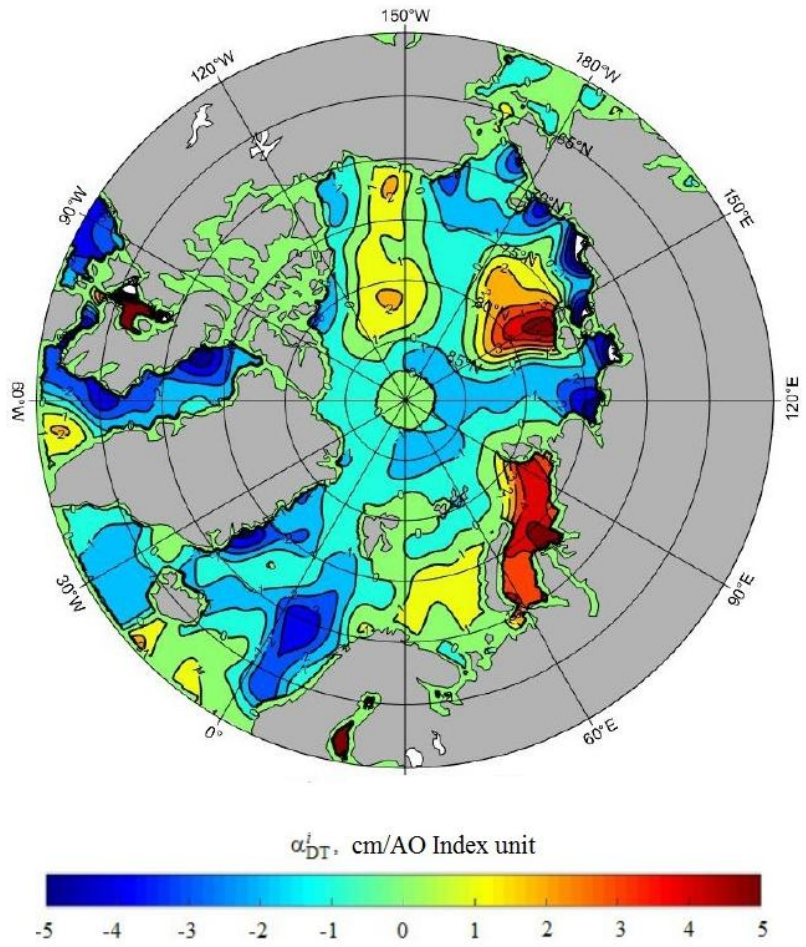

Fig. 4. Spatial distribution of linear regression coefficients for sea level anomalies (cm/AO Index unit) for 2011–2020

For the "blind" spot 81.5°–89°N in the sector 30°–80°E and 130°–180°E, high values of the coefficients were also noted (0.6–0.8 cm/s per AO Index unit), and in the sector 120° W – 30°E, on the contrary, low values (0.1–0.2 cm/s per AO Index unit) were observed (Fig. 4).

The sea level difference between the shelf and the deeper part is ~ 4 cm/AO Index unit (Fig. 4). This difference intensifies in the Kara Sea to ~ 5 cm, and in the Laptev and East Siberian Seas to ~ 8 cm/AO Index unit in the 150°–180°E sector (Fig. 4).

An increase in sea level gradients leads to an increase in pressure gradients between the shelf and the deeper part of the ocean and, as a result, to an increase

in geostrophic velocities up to ~1.5 cm/s per AO Index unit (Fig. 4). Consequently, during the positive AO phase, there is an increase in the transport of fresh water from the shelf of the Laptev Sea and the East Siberian Sea to the central part of the ocean.

Thus, during the positive phase of the AO Index, when the central part of the Arctic is occupied by a cyclone, there is an increase in the magnitude of current velocity anomalies, which contributes to the inflow of warm Atlantic waters into the Barents Sea and the central part of the ocean, and a decrease in the inflow of waters through the Bering Strait is also observed. During the negative AO phase, when an anticyclonic pressure area is located over the Arctic, the signs of the current velocity anomaly reverse, which reduces the inflow of warm Atlantic waters into the Arctic Ocean and increases the inflow of Pacific waters through the Bering Strait.

Altimetry and GRACE data were used to estimate the manometric component of the Arctic Ocean level. Manometric level H_{man} is stipulated by the variations of the water column mass. Ocean level H is determined by altimetry data. Thus, the reconstructed steric component of sea level H_{Sth} is equal to sea level H minus the manometric component of the level. Using relation (2), the steric level fields were reconstructed in accordance with altimetry and GRACE data. The reconstructed steric level was compared with the steric level calculated from the hydrological data (Unified Database for Arctic and Subarctic Hydrography, UDASH, Available at` https://doi.pangaea.de/10.1594/PANGAEA.872931). It was shown in [4, 5] that the contribution of the halosteric component prevails over the thermosteric component in the steric level of the Arctic Ocean. Thus, the variability of the Arctic Ocean steric level is an indicator of the ocean upper layer freshening [4]. The method for calculating the steric level from altimetry and GRACE data and its validation is described in [9]. Altimetry data for 2011–2020 in the polar re-gion north of 81.5°N made it possible to obtain estimates of the steric level for the "blind" spot area (Fig. 2). Figure 5 shows the reconstructed steric level av-eraged over this area.

The steric level in the "blind" spot area can be considered as an indicator of the freshening/salinization process, since the main contribution to the steric level is made by its halosteric component in the subpolar regions of the ocean. The trend of the steric level in this area is positive and amounts to 0.3–0.4 cm/year (Fig. 5), which indicates an increase in the fresh water supply in 2011–2020.

The reconstructed steric level experiences significant interannual fluctuations and reaches maxima during the negative AO phase, for example, in 2012–2013 and 2015–2017, which indicates an increase in the freshening of water masses (Fig. 5). Accordingly, during the periods of the positive AO phase in 2010–2012 and 2014–2015 minima of the steric level were observed, which indicates an increase in salinity during these periods (Fig. 5). The peculiarity of the steric level variability during the negative AO phase in 2018–2020 should be noted. Thus, the amplitude of fluctuations fell by 3–4 times while keeping a positive trend. This conclusion is confirmed by comparing the content of fresh water in the polar region, calculated from the data of hydrological surveys [4, 5]. Thus, the trend of fresh water content in the upper 100-meter layer for 1994–2008 was 11.19 cm/year [4].

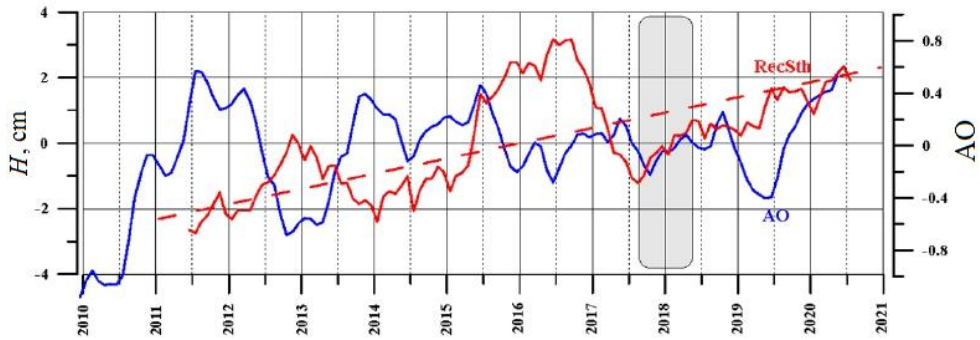

Fig. 5. Plots of the reconstructed steric level (cm) averaged over the area of the "blind" spot (Fig. 1) for 2011–2020 (red solid line), trend (red dashed line), and the AO Index (blue line) after being filtered by a moving average with a window width of 12 months. GRACE data for 07.2017–05.2018 were interpolated (grey area)

The conversion to the steric level was carried out using the constant 35.5 [5], which gives the steric level trend value of 0.34 cm/year and corresponds to the reconstructed steric level trend of 0.3–0.4 cm/year obtained by us.

Similarly, for the area of the Beaufort Gyre (Fig. 1), a positive trend of the reconstructed steric level was obtained (Fig. 6). The value of the trend of the steric level reconstructed from the altimetry and GRACE data was 0.45 cm/year, and the recalculation of the trend of fresh water content in the upper 100-meter layer of the Beaufort Gyre from hydrological data for 1994–2008 gives 0.57 cm/year, which agrees with our estimate with consideration to the error in determining the freshwater content trend [4]. It is interesting to note that the accumulation of fresh water during the positive AO phase was observed in the Beaufort Gyre in 2010–2013, while in 2013–2015, on the contrary, a decrease in the steric level was observed due to the removal of desalinated water from the Beaufort Gyre. After 2015, the accumulation of fresh water had occurred during the negative AO phase, which led to an increase in the steric level (Fig. 6).

The analysis of the atmospheric circulation variability identified by the phases of the AO Index, spatial and temporal variability of the dynamic topography, and reconstructed steric level makes it possible to propose a conceptual scheme of the Arctic Ocean circulation, which is given in Fig. 7. During the negative AO phase, high surface pressure over the Arctic causes anticyclonic circulation over most of the Arctic Ocean (Fig. 7, *a*). Desalinated waters from the runoff of the Eurasian rivers spread through the Eurasian basin and are carried out of the Arctic Ocean in the region of the Transpolar Drift (Fig. 1), which is shown in Fig. 7, *a*

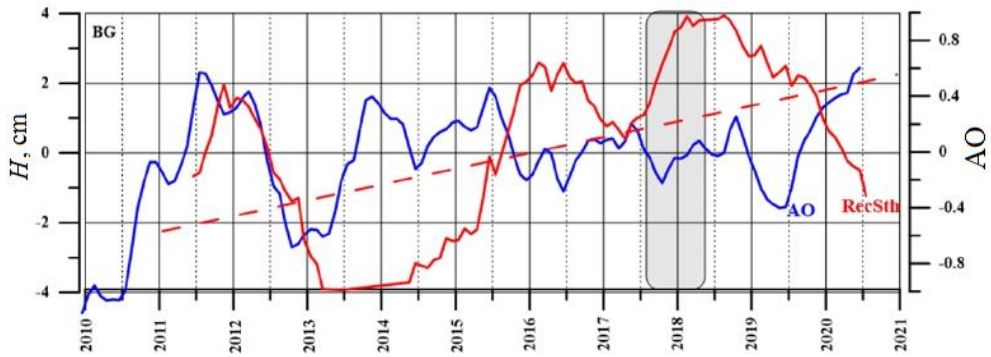

Fig. 6. Plots of the Beaufort gyre area-averaged (Fig. 1) reconstructed steric level (cm) for 2011–2020 (red solid line), its trend (red dashed line) and AO Index after filtering by a moving average with a window width of 12 months. GRACE data for 07.2017–05.2018 were interpolated (grey area)

with dark blue arrows. The analysis of the variability of the reconstructed steric level averaged over the area of the "blind" spot (Fig. 1) shows that it reaches its maximum during the negative AO phase, for example, in 2012–2013 and 2015–2017, which indicates an increase in the freshening of water masses (Fig. 5) and is compliant with the scheme in Fig. 7, *a*. On the other hand, for the area of the Beaufort Gyre, the accumulation of fresh water was also observed during the negative AO phase after 2015 (Fig. 6), which is stipulated by the convergence of the Ekman transport of fresh water on the shelf and is shown by green arrows in Fig. 7, *a* for the Beaufort Gyre, which corresponds to positive values of dynamic topography according to the altimetry data (Fig. 1).

During the positive AO phase, low surface pressure over the Arctic causes cyclonic circulation in the Eurasian basin of the Arctic Ocean (Fig. 7, *b*). Desalinated waters from the flow of the Eurasian rivers spread along the Arctic shelf of Russia by geostrophic currents and the secondary circulation of the ocean and are captured by the Beaufort Gyre, which is shown in Fig. 7, *b* with dark blue and purple arrows. The analysis of the variability of the reconstructed steric level averaged over the area of the "blind" spot shows that during the positive AO phase in 2010–2012 and 2014–2015 minima of the steric level were observed, which indicates an increase in salinity during these periods (Fig. 5) and is compliant with the circulation scheme in Fig. 7, *b*. For the area of the Beaufort Gyre, the accumulation of fresh water was observed during the positive AO phase only in 2011–2013, while in 2013–2015, on the contrary, a decrease in the steric level was observed (Fig. 6). However, for the entire period of 2011–2020, the accumulation of fresh water

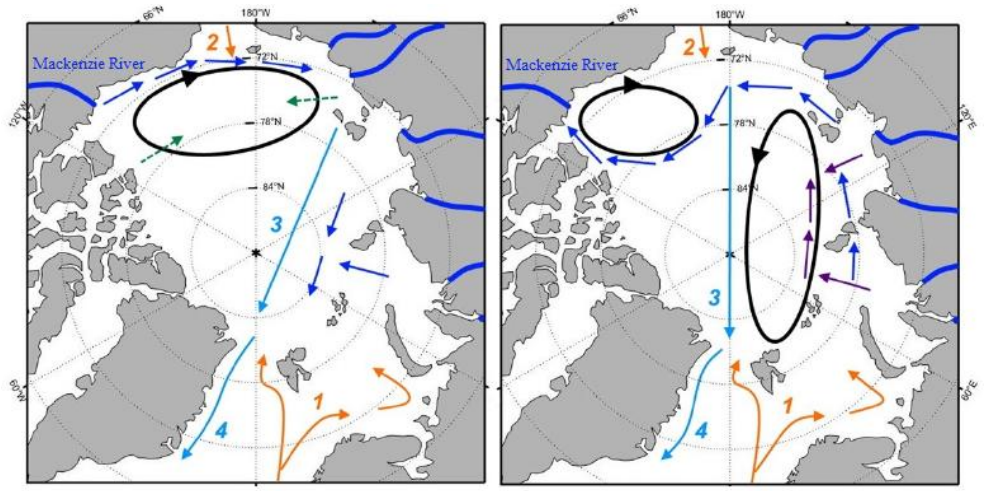

a ***b***

Fig. 7. Conceptual scheme of the Arctic Ocean circulation: (a) during the negative AO phase (anticyclonic, AO < 0); b) during the positive AO phase (cyclonic, AO > 0). The black arrows indicate surface geostrophic circulation, the orange arrows indicate the inflow of Atlantic (1) and Pacific waters (2); the light blue arrows – Transpolar Drift (3) and East Greenland Current (4). The dark blue and purple arrows show the distribution of fresh water from the Mackenzie River and from the Eurasian Rivers. Green arrows show Ekman transfer of fresh water. The bold dark blue lines are for the rivers flowing into the Arctic Ocean

increased in the Beaufort Gyre as the trend in the steric level was positive (0.45 cm/year), which is also confirmed by the positive trend in freshwater content in the upper 100 m layer of the Beaufort Gyre according to the hydrological data for 1994–2008 [4, 5].

As a result, the proposed conceptual scheme shown in Fig. 7 integrates the results of the analysis of dynamic topography, surface geostrophic currents according to the altimetry data, and reconstructed steric level and AO Index in the context of the influence of atmospheric circulation regimes on the way of fresh water distribution in the Arctic Ocean.

Conclusion

The change in the level of the Arctic Ocean is an important indicator of climate variability in the Arctic and of the Earth's climate system as a whole due to the integral nature of sea level formation. For the Arctic, progress has been made in the last decade in processing altimetry information and improving its accuracy,

and the launch of the Envisat and CryoSat-2 satellites made it possible to increase the coverage area at high latitudes up to 89.75°N. Therefore, the use of new altimetry data both for the Arctic Ocean regions covered with ice and for the open water area made it possible to obtain the estimates of dynamic topography and surface geostrophic velocities, including the area of the "blind" spot north of 81.5°N, for which altimetry data had not been available until 2011. Using the GRACE gravity data, it was possible to obtain the estimates of the variability of the ocean level manometric and steric components. These estimates are in good agreement with the calculations based on the available instrumental observations. The effect of atmospheric circulation regimes on the spatiotemporal variability of the ocean level and surface currents was studied based on the analysis of the AO Index.

On the basis of the obtained results, a conceptual scheme of the regimes of circulation and distribution of desalinated waters depending on the phase of the Arctic oscillation is proposed. The scheme is compliant with the interannual variability of the reconstructed steric level component for the polar region of the ocean for 2011–2020.

Thus, the main results can be summarized as follows.

1. The spatiotemporal variability of the steric and manometric components of the sea level is specified, and estimates of their trends are obtained from the altimetry, GRACE, and archival hydrological data. Estimates of the steric level variability are obtained for the regions of the Arctic Ocean where the availability of hydrological measurements has been low or almost absent, including the altimetry "blind" spot north of 81.5°N after 2011.

2. The peculiarities of the response of the sea level and surface geostrophic currents of the Arctic Ocean to the cyclonic/anticyclonic circulation of the atmosphere described by the AO Index are characterized.

3. Quantitative estimates of the dependence of the interannual variability of sea level anomalies and surface geostrophic currents are obtained based on regression relationships depending on the value of the AO Index: the level difference between the shelf and the deeper part is ~ 4 cm per AO Index unit, and for current velocity anomalies it is ~ 0.6–0.8 cm/s per AO Index unit for 2003–2014. This difference increases in the Kara Sea up to ~ 5 cm and to ~ 8 cm per AO Index unit in the 150–180°E sector (in the Laptev Sea and the East Siberian Sea) in 2011–2020. An increase in level gradients leads to an increase in pressure gradients between the shelf and the deeper part of the ocean and, as a result, to an increase in geostrophic velocities up to ~ 1.5 cm/s per AO Index unit.

Thus, during the positive phase of the AO Index, when the central part of the Arctic is occupied by a cyclone, an increase in the anomalies of current velocities is observed, which contributes to the inflow of warm Atlantic waters. During the negative AO phase, the anomalies of the current velocities reverse.

4. Estimates of trends and interannual variability of the steric component of the level for the area of the "blind" spot north of 81.5°N are obtained for the first time owing to the altimetry and GRACE reconstruction.

5. According to the obtained quantitative patterns, during the negative AO phase, there is an increase in the transport of fresh water from the shelf of the Laptev Sea and the East Siberian Sea to the central part of the ocean. This is confirmed by the interannual variability of the reconstructed steric component of the level averaged over the "blind" spot region north of 81.5°N. As shown, the steric level is an indicator of an increase in freshening/salinization of water masses for the Arctic Ocean. Correspondingly, during the periods of the positive AO phase, minima of the steric level are observed, which indicates an increase in salinity during these periods of time.

6. On the basis of the obtained results, a conceptual scheme of the regimes of circulation and distribution of desalinated waters depending on the phase of the Arctic oscillation is proposed. The scheme is compliant with the ocean circulation regimes based on the analysis of surface geostrophic currents according to the altimetry data and the interannual variability of the reconstructed level steric component for the polar region of the ocean for 2011–2020.

REFERENCES

1. Ivanov, V.V., Frolov, I.E. and Filchuk, K.V., 2020. Transformation of Atlantic Water in the North-Eastern Barents Sea in Winter. *Arctic and Antarctic Research*, 66(3), pp. 246–266. doi:10.30758/0555-2648-2020-66-3-246-266
2. Armitage, T.W.K., Bacon, S. and Kwok, R., 2018. Arctic Sea Level and Surface Circulation Response to the Arctic Oscillation. *Geophysical Research Letters*, 45(13), pp. 6576–6584. doi:10.1029/2018GL078386
3. Proshutinsky, A.Y. and Johnson, M.A., 1997. Two Circulation Regimes of the Wind-Driven Arctic Ocean. *Journal of Geophysical Research: Oceans*, 102(C6), pp. 12493–12514. doi:10.1029/97JC00738
4. Pnyushkov, A.V., Alekseev, G.V. and Smirnov, A.V., 2022. On the Interplay between Freshwater Content and Hydrographic Conditions in the Arctic Ocean in the 1990s–2010s. *Journal of Marine Science and Engineering*, 10(3), 401. doi:10.3390/jmse10030401
5. Proshutinsky, A., Krishfield, R., Toole, J.M., Timmermans, M.-L., Williams, W., Zimmermann, S., Yamamoto-Kawai, M., Armitage, T.W.K., Dukhovskoy, D. [et al.], 2019. Analysis of the Beaufort Gyre Freshwater Content in 2003–2018. *Journal of Geophysical Research: Oceans*, 124(12), pp. 9658–9689. doi:10.1029/2019JC015281
6. Raj, R.P., Andersen, O.B., Johannessen, J.A., Gutknecht, B.D., Chatterjee, S., Rose, S.K., Bonaduce, A., Horwath, M., Ranndal, H. [et al.], 2020. Arctic Sea Level Budget Assessment during the GRACE/Argo Time Period. *Remote Sensing*, 12(17), 2837. doi:10.3390/rs12172837
7. Proshutinsky, A., Dukhovskoy, D., Timmermans, M.-L., Krishfield, R. and Bamber, J.L., 2015. Arctic Circulation Regimes. *Philosophical Transactions of the Royal Society A: Mathematical, Physical and Engineering Sciences*, 373(2052), 20140160. doi:10.1098/rsta.2014.0160
8. Belokopytov, V.N., 2017. Factors Reducing Efficiency of the Operational Oceanographic Forecast Systems in the Arctic Basin. *Physical Oceanography*, (2), pp. 19–24. doi:10.22449/1573-160X-2017-2-19-24
9. Lemeshko, E.E., Lemeshko, E.M. and Novitskaya, V.P., 2021. Influence of the Arctic Oscillation on the Formation of Water Circulation Regimes in the Sector of the North, Norwegian and Barents Seas. *Ecological Safety of Coastal and Shelf Zones of Sea*, (2), pp. 47–64. doi:10.22449/2413-5577-2021-2-47-64 (in Russian).

10. Doglioni, F., Ricker, R., Rabe, B., Barth, A., Troupin, C. and Kanzow, T., 2023. Sea Surface Height Anomaly and Geostrophic Current Velocity from Altimetry Measurements over the Arctic Ocean (2011–2020). *Earth System Science Data*, 15(1), pp. 225–263. https://doi.org/10.5194/essd-15-225-2023
11. Armitage, T.W.K., Bacon, S., Ridout, A.L., Petty, A.A., Wolbach, S. and Tsamados, M., 2017. Arctic Ocean Surface Geostrophic Circulation 2003–2014. *The Cryosphere*, 11(4), pp. 1767–1780. doi:10.5194/tc-11-1767-2017
12. Volkov, D.L. and Landerer, F.W., 2013. Nonseasonal Fluctuations of the Arctic Ocean Mass Observed by the GRACE Satellites. *Journal of Geophysical Research: Oceans*, 118(12), pp. 6451–6460. doi:10.1002/2013JC009341
13. Peralta-Ferriz, C., Morison, J.H., Wallace, J.M., Bonin, J.A. and Zhang, J., 2014. Arctic Ocean Circulation Patterns Revealed by GRACE. *Journal of Climate*, 27(4), pp. 1445–1468. doi:10.1175/JCLI-D-13-00013.1
14. Morison, J., Kwok, R., Dickinson, S., Andersen, R., Peralta-Ferriz, C., Morison, D., Rigor, I., Dewey, S. and Guthrie, J., 2021. The Cyclonic Mode of Arctic Ocean Circulation. *Journal of Physical Oceanography*, 51(4), pp. 1053–1075. doi:10.1175/JPO-D-20-0190.1
15. Seber, G.A.F., 1980. *Linear Regression Analysis*. New York: Wiley, 465 p.

Submitted 16.12.2022; accepted after review 21.01.2023;
revised 1.02.2023; published 24.03.2023

About the author:

Egor E. Lemeshko, Junior Research Associate, Marine Hydrophysical Institute of RAS (2 Kapitanskaya St., Sevastopol, 299011, Russian Federation), **SPIN-код: 7313-4819; ResearcherID: C-5691-2016; Scopus Author ID: 57205681264**, *e.lemeshko@mhi-ras.ru*

The author has read and approved the final manuscript.

Original article **DOI**: 10.29039/2413-5577-2023-1-65-76

Influence of Organic Matter Content in Bottom Sediments in Crimean Water Areas with Intensive Water Exchange on Zinc, Chromium, and Nickel Accumulation

E. E. Sovga, E. A. Kotelyanets *

Marine Hydrophysical Institute of RAS, Sevastopol, Russia
* *e-mail: plistus@mail.ru*

Abstract
The paper analyzes the data obtained during field studies in water areas with intensive water exchange: Kalamita Bay (2011, 2012), Feodosiya Bay (2006), and the Kerch Strait (2007, 2008). The content of heavy metals (Zn, Ni, Cr) in the bottom sediments of the studied water areas was determined using X-ray fluorescent spectroscan MAKS-G. Spatial heterogeneities in the distribution of Zn, Ni, Cr in the bottom sediments of Kalamita Bay, Feodosiya Bay, and the Kerch Strait were assessed, with the organic matter content taken into account. A comparative analysis was carried out of the organic matter content in the bottom sediments of the studied water areas. The organic matter not only forms the type of sediments, but also determines their ability to accumulate various substances, including macro- and micronutrients. It is shown that the bottom sediments of Feodosiya Bay and the Kerch Strait contain increased levels of organic carbon. Correlation relations between the contents of heavy metals and organic carbon as one of the main sediment-forming components of the bottom sediments were calculated using the method of constructing matrices of pair correlations. A high level of correlations between Zn, Ni, Cr and organic carbon contents (0.7–0.8) was determined in the bottom sediments of Kalamita Bay and the Kerch Strait. In the bottom sediments of Feodosiya Bay, high correlation coefficient with C_{org} content (0.9) was observed only for Zn. The hydrodynamic regime of water areas with intensive water exchange (especially in the Kerch Strait) determines the spatial heterogeneity of the particle size distribution of bottom sediments, especially the fine fraction and the organic matter associated with it, which also affects the behaviour of the studied metals.

Keywords: Kalamita Bay, Feodosiya Bay, Kerch Strait, bottom sediments, organic carbon, heavy metals

Acknowledgements: The work was performed under state assignement no. FNNN-2022-0005 “Coastal studies”.

For citation: Sovga, E.E. and Kotelyanets, E.A., 2023. Influence of Organic Matter Content in Bottom Sediments in Crimean Water Areas with Intensive Water Exchange on Zinc, Chromium, and Nickel Accumulation. *Ecological Safety of Coastal and Shelf Zones of Sea*, (1), pp. 65–76. doi:10.29039/2413-5577-2023-1-65-76

Влияние содержания органического вещества в донных отложениях акваторий Крыма с интенсивным водообменом на накопление цинка, хрома и никеля

Е. Е. Совга, Е. А. Котельянец *

Морской гидрофизический институт РАН, Севастополь, Россия
* *e-mail: plistus@mail.ru*

Аннотация

Проанализированы данные, полученные в ходе экспедиционных исследований в прибрежных акваториях Крыма с интенсивным водообменом: Каламитском (2011, 2012 гг.), Феодосийском (2006 г.) заливах и Керченском проливе (2007, 2008 гг.). Содержание тяжелых металлов (Zn, Ni, Cr) в донных отложениях исследуемых акваторий определяли рентгенофлуоресцентным методом с использованием прибора «Спектроскан МАКС-*G*». Оценены пространственные неоднородности в распределении Zn, Ni, Cr в донных отложениях Каламитского и Феодосийского заливов, Керченского пролива с учетом содержания органического вещества. Осуществлен сравнительный анализ содержания органического вещества в донных отложениях исследуемых акваторий, которое не только формирует тип осадков, но и определяет их способность к накоплению различных веществ, в том числе макро- и микроэлементов. Показано, что в донных отложениях Феодосийского залива и Керченского пролива повышено содержание органического углерода, цинка и хрома. Выполнен расчет коэффициентов корреляции между содержанием тяжелых металлов и органического углерода как одного из основных осадкообразующих компонентов донных отложений с применением методики построения матриц парных корреляций. Высокий уровень корреляционных связей содержания Zn, Ni, Cr с содержанием органического углерода (0.7–0.8) определен для донных отложений Каламитского залива и Керченского пролива. В донных отложениях Феодосийского залива высокое значение коэффициентов корреляции с содержанием $C_{орг}$ (0.9) наблюдается только для Zn. Гидродинамический режим акваторий с интенсивным водообменом (особенно в Керченском проливе) определяет пространственную неоднородность распределения мелкодисперсной фракции донных отложений и связанного с ней органического вещества, что также влияет на особенности поведения исследуемых металлов.

Ключевые слова: Каламитский залив, Феодосийский залив, Керченский пролив, донные отложения, органический углерод, тяжелые металлы

Благодарности: работа выполнена в рамках государственного задания по теме № FNNN-2022-0005 «Прибрежные исследования».

Для цитирования: *Совга Е. Е., Котельянец Е. А.* Влияние содержания органического вещества в донных отложениях акваторий Крыма с интенсивным водообменом на накопление цинка, хрома и никеля // Экологическая безопасность прибрежной и шельфовой зон моря. 2023. № 1. С. 65–76. EDN TZBTZD. doi:10.29039/2413-5577-2023-1-65-76

Introduction

The Crimean coastal water areas are subject to a complex impact as a result of the effluence of the organic matter of anthropogenic and natural origin into the coastal areas. Regardless of its genesis, the organic matter specifically plays an important role in the formation of the type of sediments and their ability to accumulate various substances coming with sedimentary material, including macro- and microelements. The spatial distribution of microelements and heavy metals in bottom sediments is determined by their content of organic and inorganic carbon and their granulometric composition [1]. In previous works, individual features of the spatial distribution of microelements and heavy metals in the surface layer of bottom sediments of the studied water areas of Kalamita Bay [2], Feodosiya Bay [3], and the Kerch Strait [4] were considered.

The aim of this work is to evaluate the effect of organic carbon content in bottom sediments of the Crimean coastal water areas with intensive water exchange on the peculiarities of the spatial distribution of zinc, nickel, and chromium.

Materials and Methods

We analyzed the data obtained during field studies in the water areas of Kalamita Bay (2011, 2012), Feodosiya Bay (2006), and the Kerch Strait (2007, 2008) (Fig. 1).

Figure 1 shows the location of bottom sediment sampling stations in the areas under study. Sampling was carried out using Peterson samplers according to state standards GOST 17.1.5.01-80 and DSTU ISO 5667-19:2007 [1)]. The upper layer of sediments (0–5 cm) was studied. The studied metals (total forms) were determined by the X-ray fluorescence method of analysis using spectroscan MAKS-G [2)]. To assess the reproducibility and accuracy of measurements of the content of zinc, nickel, and chromium, the analysis of certified bottom sediment state standard DSZU 163.1-98 was used in eight replicates [1)].

The organic carbon concentration in the sample was determined by the spectrophotometric method after the oxidation of the organic matter with a sulfochromic mixture (state standards DSTU ISO 14235-2005 [3)]; DSTU 4289:2004 [4)]. The error estimate of the organic matter content for the as-deposited sediments is up to 3 % with its content not exceeding 2.5 % [3), 4)].

[1)] State Standard, 1980. *General Requirements for Sampling of Bottom Sediments of Water Objects for their Pollution Analysis*. Available at: https://docs.cntd.ru/document/1200012787 [Accessed: 25 May 2020] (in Russian).

[2)] [*Methods for the Measurement of the Mass Fraction of Metals and Metal Oxides in Powder Soil Samples by X-ray Fluorescence Analysis. M049-П/02*]. Saint Petersburg: OOO "Spektron", 2002, 16 p. (in Russian).

[3)] State Standard, 2007. *Soil Quality. Determination of Organic Carbon by Sulfochromic Oxidation* (*ISO* 14235-1998, *IDT*). Kiev: Derzhspozhivstandart Ukrainy, 10 p. (in Ukrainian).

[4)] State Standard, 2005. *Soil Quality. Methods for Determination of Organic Matter*. Kiev: Derzhspozhivstandart Ukrainy, 14 p. (in Ukrainian).

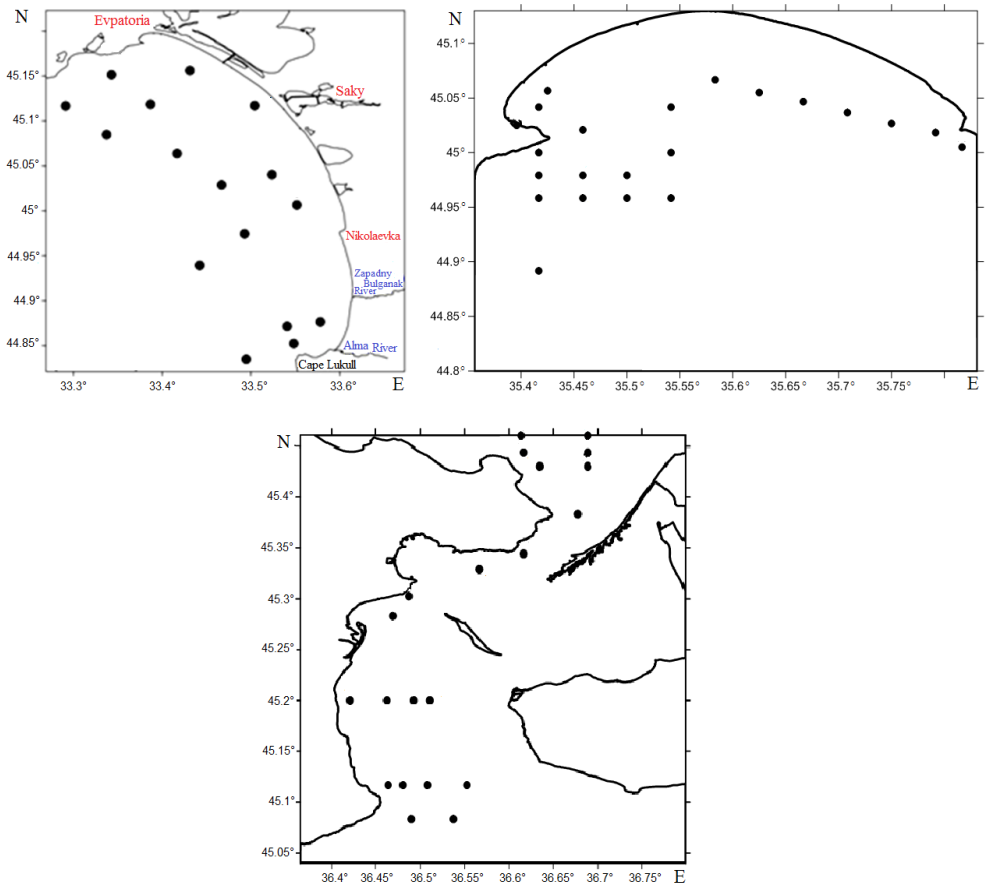

Fig. 1. Bottom sediment sampling areas in the coastal water areas of Crimea: *a* – Kalamita Bay (August 2011; September 2012); *b* – Feodosiya Bay (2006, 22 stations); *c* – the Kerch Strait (December 2007; March 2008). The points denote stations

The absence or presence of a correlation between the content of heavy metals and the content of organic carbon was determined by the method of constructing matrices of pair correlations (Table 1) in the program *Statistika* 6.0 [5].

Results and Discussion

Kalamita and Feodosiya Bays as well as the Kerch Strait, as coastal water areas of Crimea with intensive water exchange, are subject to the influence of natural, climatic, and anthropogenic factors.

Due to its geographical location, **Kalamita Bay** is influenced by the deep-water part of the Black Sea. It is a transitional link from the open part of the sea to the northwestern shelf and successfully avoids such phenomena as bottom hypoxia and

Table 1. Coefficients of correlation between C_{org} and studied metals

Element, mg/kg	C_{org}		
	Kalamita Bay	Feodosiya Bay	Kerch Strait
Zn	0.8	0.9	0.7
Ni	0.8	0.5	0.7
Cr	0.7	0.3	0.8

subsequent fish kills. The absence of abundant freshwater runoff and significant industrial infrastructure on the shores of West Crimea, as well as undisturbed water exchange with the deep part of the sea, make the waters of the bay more similar to the waters of the open sea.

Feodosiya Bay is one of the least studied areas of the Black Sea coast in terms of the structure and dynamics of waters and their hydrochemical composition under the conditions of modern anthropogenic impact. This region had been used for a long time as a training area for the USSR naval forces, which excluded the possibility to obtain any field data in the field studies of civil ships. At the same time, the Feodosiya region is of great recreational importance. The arc of Feodosiya Bay coast is framed by a beach strip [3].

The Kerch Strait is a heavy shipping area. The work of ports significantly affects the ecological situation in the region. Offshore cargo transshipment points in the southwestern part of the strait also make their negative contribution [6].

According to previously published data [7], the geochemical background of the abovementioned metals is increased in bottom sediments, regardless of the hydrodynamic situation in coastal waters. And in accordance with [7] and[5)], these metals are able to form stable compounds with various organic ligands. This is also confirmed by the value of the positive correlation coefficients between the content of these metals and the content of the organic matter in bottom sediments, calculated in this work (Table 1).

Zinc. The content of zinc in sea water and bottom sediments very often exceeds the maximum allowable concentration (MAC). The element maximum concentrations are often determined on the shelf of the Crimean Peninsula and in the waters of the Kerch Strait. The sources of this element are mainly anthropogenic in nature [4].

Nickel. For the water area of the Crimean Peninsula shelf zone, the main source of Ni is the river runoff. Increased nickel concentrations are often found in water areas with active shipping lanes. In our work, it is the water area of

[5)] Mitropolskiy, A.Yu., Bezborodov, A.A. and Ovsyany, E.I., 1982. [*Geochemistry of the Black Sea*]. Kiev: Naukova Dumka, 144 p. (in Russian).

the Kerch Strait. Due to active adsorption processes and insignificant geochemical mobility, Ni accumulates in bottom sediments in the immediate vicinity of the main sources [4].

Chromium. High content of chromium in the bottom sediments of the Black Sea shelf zone is determined by the proximity of the sources of this element. In [2–4], it is said that Cr can also enter the water area with river waters. Increased chromium concentrations in bottom sediments are often associated with anthropogenic sources [2–4].

Table 2 shows the content of organic carbon in the bottom sediments of the studied water areas.

As a result of studies carried out in the water area of Kalamita Bay, data were obtained on the peculiarities of the spatial distribution of heavy metals, which repeated the distribution of organic carbon in the bottom sediments of the bay. Figure 2 shows the distribution of C_{org}, Zn, Ni, and Cr. Significant concentrations of the elements were observed in the seaward part of the bay water area, while their minimum concentrations were observed in the coastal part, which coincided with the distribution of the organic matter in the sediments of the bay (Table 3).

Increased Cr content (Fig. 2, *d*) was noted in the bottom sediments of the central and northern parts of the bay. The average content of chromium was 64 mg/kg, and the maximum one was 90 mg/kg. The maximum zinc content was 36 mg/kg, which did not exceed its concentration in the bottom sediments of the shelf [7] and corresponded to its content in the earth's crust according to A.P. Vinogradov [6]. The maximum nickel content was 31 mg/kg, which did not exceed the background values typical for this water area [8]. The excess of the geochemical background was noted only for chromium.

Table 2. Organic carbon content (%) in the bottom sediments of the studied water areas

Water area	C_{org}			
	Content range	Average content	Coastal part	Seaward part
Kalamita Bay	0.07–0.6	0.07–0.11	0.23–0.4	0.24–0.6
Feodosiya Bay	0.2–3.3	1.2	1.8–3.2	0.8–1.1
Kerch Strait [9]	0.12–3.35	1.25	2.0–3.0	0.12–1.0

[6] Vinogradov, A.P., 1962. [Average Content of Chemical Elements in Rocks]. *Geokhimiya*, (7), pp. 555–571 (in Russian).

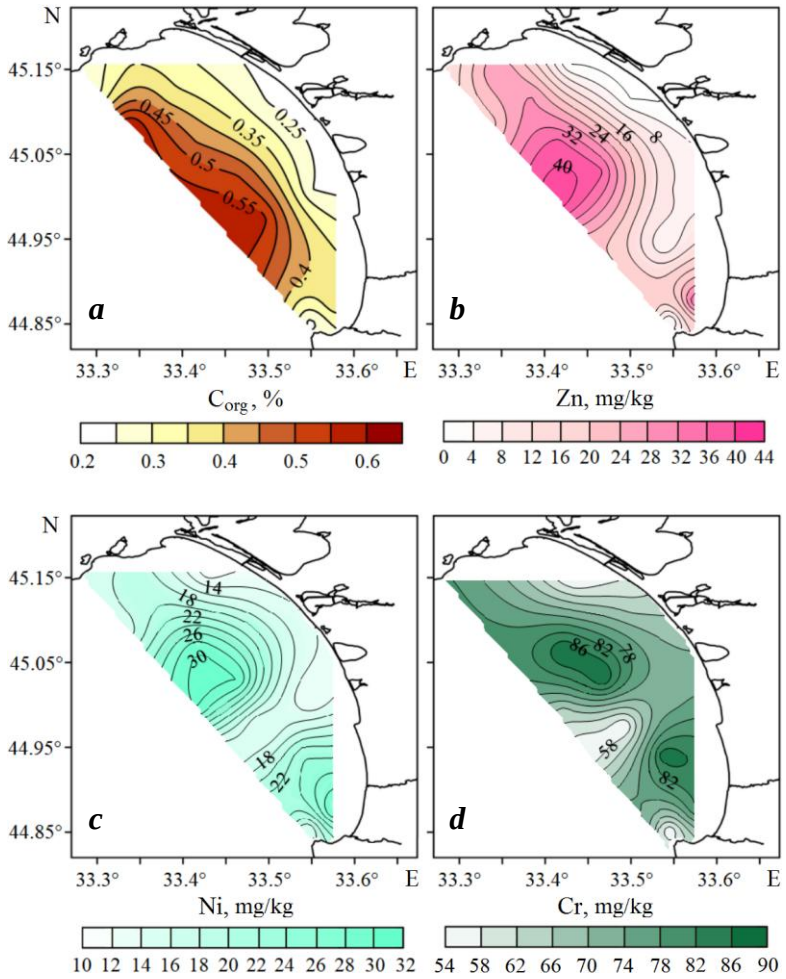

Fig. 2. Spatial distribution of organic carbon (*a*), zinc (*b*), nickel (*c*), and chrome (*d*) in the bottom sediments of Kalamita Bay

The content of organic carbon in the bottom sediments of the bay varies within 0.07–0.11 %. The C_{org} concentration in the coastal part of the bay is 0.23–0.40 %, and in the seaward part it is 0.24–0.60 %. The maximum positive values of the correlation between the content of the element and the content of organic carbon were recorded for Zn ($r = 0.8$), Ni ($r = 0.8$), and Cr ($r = 0.7$) (Table 2).

Feodosiya Bay. According to [2], the content of C_{org} in the bottom sediments of Feodosiya Bay did not exceed 1.2% of the dry weight. According to the results of studies carried out in the waters of Feodosiya Bay, areas of increased zinc and chromium content were identified. It is shown that the average values of the total concentration of the studied metals in the bottom sediments of Feodosiya Bay do not exceed the value of the geochemical background (Table 3).

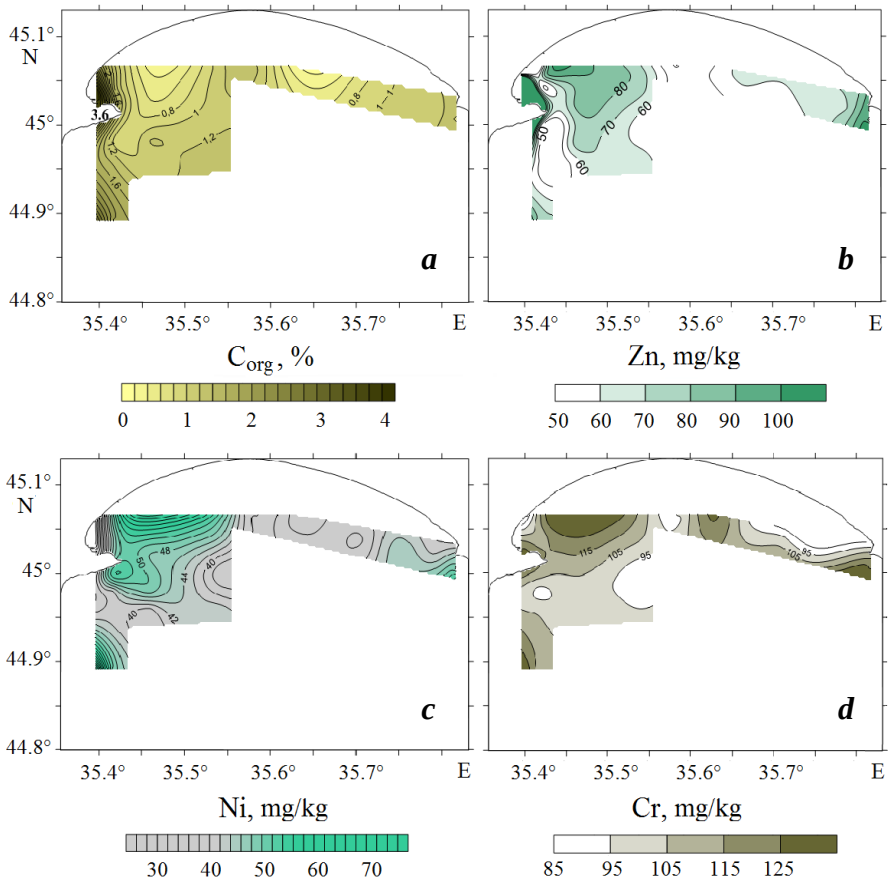

F i g . 3 . Spatial distribution of organic carbon (*a*), zinc (*b*), nickel (*c*), and chrome (*d*) in the bottom sediments of Feodosiya Bay

According to the calculations, the maximum correlation coefficient was noted for zinc ($r = 0.9$) (Table 1).

Figure 3 shows that the areas of increased content of zinc, chromium and nickel, as well as C_{org}, are observed in the water area of the city and port of Feodosiya located in the bay. In the seaward part of the bay, lower content of the studied metals is observed.

The Kerch Strait is subject to a significant influence of both natural and climatic and anthropogenic factors (intense traffic flows, bottom dredging). At the same time, the strait is characterized by along-strait currents, the direction of which changes up to the opposite, depending on the prevailing wind direction and speed. The specific features of the studied water area were reflected in the general nature of the spatial distribution of the studied heavy metals in the strait bottom sediments.

In the modern period, the content of C_{org} in the bottom sediments of the part of the strait adjacent to the Kerch Peninsula varies from 0.12 to 3.35 wt % with the average value of 1.25 wt. % (see Table 2) [9].

Figure 4 shows the spatial distribution of nickel, zinc and chromium depending on the content of organic carbon in the bottom sediments of the Kerch Strait.

It follows from Figure 4 that the spatial distribution of Zn, Ni, Cr in the water area of the strait corresponds to the distribution of the organic matter with the formation of maxima in the pre-strait area of the Sea of Azov and in the coastal part of

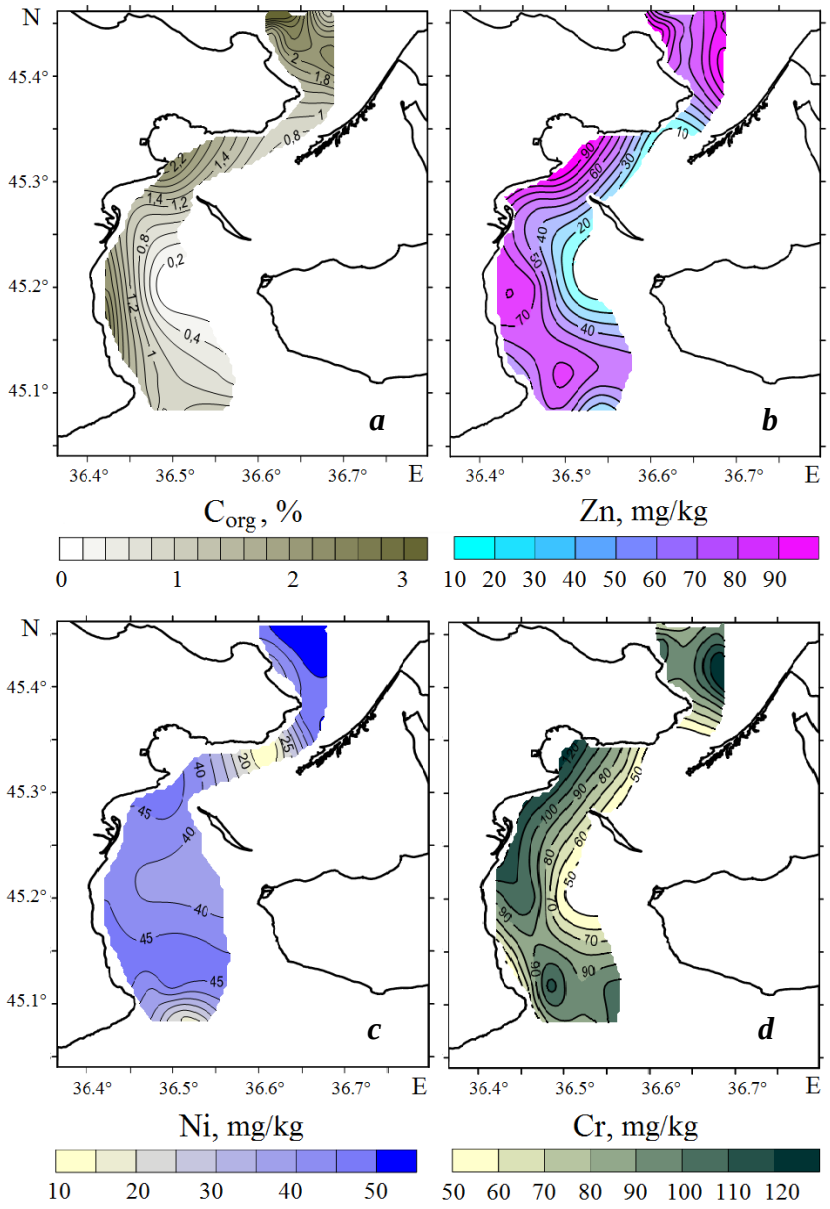

F i g . 4 . Spatial distribution of organic carbon (*a*), zinc (*b*), nickel (*c*) and chrome (*d*) in the bottom sediments of the Kerch Strait

Table 3. Microelement accumulation level (mg/kg) in the bottom sediments of Kalamita Bay, Feodosiya Bay and the Kerch Strait against the geochemical background

Elements	Content			Clarkes according to A.P. Vinogradov [6]	Average content in shelf bottom sediments [8]
	Kalamita Bay (2011, 2012)	Feodosiya Bay (2006)	Kerch Strait (2007, 2008)		
Zn	4–48	50–412	25–78	83	60
Ni	10–32	34–54	10–50	58	34
Cr	48–90	87–124	43–147	83	45

the strait. At the same time, high values of the coefficients of correlation between the content of metals and the content of the organic matter in bottom sediments suggest that these pollutants accumulate in the bottom sediments of the Kerch Strait.

The accumulation levels of heavy metals Zn, Ni, Cr in the bottom sediments of water areas with intensive water exchange against the geochemical background are shown in Table 3.

From the data presented in Table 3, it can be seen that Zn and Ni concentrations in the bottom sediments of Kalamita Bay are lower than in the sediments of Feodosiya Bay, the Kerch Strait, and the background areas of the Black Sea shelf [7]. At the same time, in Kalamita Bay, as in a water area with low content of the organic matter in bottom sediments, an excess of the geochemical background is observed only for chromium due to the noticeable correlation between the metal content and the C_{org} content (0.7) (see Table 1).

It is shown that in the bottom sediments of areas with high content of organic carbon (Feodosiya Bay and the Kerch Strait), the excess of the geochemical background of such metals as zinc and chromium is characteristic.

It was noted that the geochemical background for nickel was not exceeded in any of the studied water areas (Table 3). At the same time, despite the excess of the geochemical background for chromium in Feodosiya Bay, the correlation coefficient between the content of this metal and the content of the organic matter is rather low ($r = 0.3$) (Table 1).

It is possible that in addition to the organic matter, other components of bottom sediments, which are not considered in this work, contribute to the accumulation of the studied metals.

Conclusion

Analysis of the array of field data made it possible to evaluate the spatial heterogeneity of the Zn, Ni, Cr distribution in the bottom sediments of Kalamita Bay, Feodosiya Bay, and the Kerch Strait, taking into account the levels of the organic matter content and the calculated correlation coefficients between metal content and C_{org} content.

The high values of these correlation coefficients for water areas with intensive water exchange are explained by the ability of the studied metals to form stable compounds with organic ligands.

The spatial heterogeneity of the organic matter distribution is determined by the hydrodynamic regime of the considered water areas and its intensity. This distribution heterogeneity also influences the behavior of the metals under study.

REFERENCES

1. Orekhova, N.A., Ovsyany, E.I., Gurov, K.I. and Popov, M.A., 2018. Organic Matter and Grain-Size Distribution of the Modern Bottom Sediments in the Balaklava Bay (the Black Sea). *Physical Oceanography*, 25(6), pp. 479–488. doi:10.22449/1573-160X-2018-6-479-488
2. Gurov, K.I., Ovsyany E.I., Kotelyanets E.A. and Konovalov S.K., 2014. [Geochemical Characteristics of Bottom Sediments in the Kalamita Bay Water Area of the Black Sea]. *Morskoy Gidrofizicheskiy Zhurnal*, (5), pp. 69–80 (in Russian).
3. Kotelyanets, E.A. and Konovalov, S.K., 2008. Distribution of Heavy Metals in Bottom Sediments of Feodosiya Bay. In: MHI, 2008. *Ekologicheskaya Bezopasnost' Pribrezhnoi i Shel'fovoi Zon i Kompleksnoe Ispol'zovanie Resursov Shel'fa* [Ecological Safety of Coastal and Shelf Zones and Comprehensive Use of Shelf Resources]. Sevastopol: ECOSI-Gidrofizika. Iss. 17, pp. 171–175 (in Russian).
4. Kotelyanets, E.A. and Konovalov, S.K., 2012. [Heavy Metals in Bottom Sediments of the Kerch Strait]. *Morskoy Gidrofizicheskiy Zhurnal*, (4), pp. 50–60 (in Russian).
5. Shigabaeva, G.N. and Akhtyrskaya, E.O., 2014. Correlation Analysis of Heavy Metals in Sediments. *Izvestiya MGTU "MAMI"*, 3(2), pp. 55–59 (in Russian).
6. Zavialov, P.O., Zavialov, I.B., Izhitskiy, A.S., Izhitskaya, E.S., Konovalov, B.V., Krementskiy, V.V., Nemirovskaya, I.A. and Chasovnikov, V.K., 2022. Assessment of Pollution of the Kerch Strait and the Adjacent Black Sea Area Based on Field Measurements of 2019–2020. *Okeanologiya*, 62(2), pp. 194–203. doi:10.31857/S0030157422020174 (in Russian).
7. Kotelyanets, E.A., 2021. Peculiarities of Macro- and Microelement Accumulation in Bottom Sediments of the Crimean Coastal Water Areas (the Black Sea) with Different Water Exchange Intensity based on XRF Data. *Ecological Safety of Coastal and Shelf Zones of Sea*, (2), pp. 106–120. doi:10.22449/2413-5577-2021-2-106-120 (in Russian).
8. Emelyanov, V.A., Mitropolskiy, A.Yu., Nasedkin, E.I., Pasynkov, A.A., Stepanyak, Yu.D. and Shnyukova, E.E., 2004. [*Geoecology of the Ukrainian Black Sea Shelf*]. Kyiv: Akademperiodika, 293 p. (in Russian).
9. Ovsyanyi, E.I., Konovalov, S.K., Kotel'yanets, E.A. and Mitropolskii, A.Y., 2015. Organic Carbon and Carbonates in the Recent Bottom Sediments of the Kerch Strait. *Geochemistry International*, 53(12), pp. 1123–1133. doi:10.1134/S0016702915120071

Submitted 16.12.2022; accepted after review 21.01.2023;
revised 1.02.2023; published 24.03.2023

About the authors:

Elena E. Sovga, Leading Research Associate, Marine Hydrophysical Institute of RAS (2 Kapitanskaya St., Sevastopol, 299011, Russian Federation), Dr.Sci. (Geogr.), **ORCID ID: 0000-0002-0670-4573, SPIN-code: 8675-2443, ResearcherID: A-9774-2018**, *esovga@mhi-ras.ru*

Ekaterina A. Kotelyanets, Junior Research Associate, Marine Hydrophysical Institute of RAS (2 Kapitanskaya St., Sevastopol, 299011, Russian Federation), **ResearcherID: AAA-8699-2019**, *plistus@mail.ru*

Contribution of the authors:

Elena E. Sovga – goal statement, critical analysis of the text and its revision

Ekaterina A. Kotelyanets – sampling, identification of studied microelements, quantitative and qualitative analysis of the results, preparation of graphic materials, goal statement

All the authors have read and approved the final manuscript.

Original article **DOI**: 10.29039/2413-5577-2023-1-77-90

Atmospheric Input of Silica in Crimea and Factors Affecting it

A. V. Varenik, M. A. Myslina *, D. V. Tarasevich

Marine Hydrophysical Institute of RAS, Sevastopol, Russia
**e-mail: myslina@mhi-ras.ru*

Abstract

Silica is one of the main nutrients (N, P, Si) and is a part of a large number of natural minerals, so it is constantly present in natural waters. It is mainly present as salts of silicic acid (silica). Atmospheric precipitation can be an important additional source of silica in the ecosystem. The purpose of this work is to estimate the silica content in the atmospheric precipitation based on long-term data, analyze the spatial and temporal variability of this content, and identify possible factors influencing the atmospheric silica input. The paper presents the results of continuous monitoring of silica input with the atmospheric precipitation in the Crimean coastal region in 2015–2021. Precipitation samples were collected in Sevastopol and Katsiveli in two types of samplers: a permanently open one to collect total (dry + wet) atmospheric precipitation and a wet-only one. It is shown that in the inter-annual dynamics of silica flux with the atmospheric precipitation in the both sampling points, the maximum input amount of this nutrient was determined in 2017–2018. The main factors influencing the amount of silica input with the atmospheric precipitation were determined. One of the main factors influencing the silica concentration in precipitation is the intensity of dust transport.

Keywords: silica, sampling, atmospheric precipitation, Crimea, dust atmospheric precipitation, long-term changes

Acknowledgements: The work was carried out under state assignment of FSBSI FRC MHI of RAS on the subject FNNN-2021-0005 “Coastal research”. The authors are grateful to the staff of the Sevastopol Marine Hydrometeorological Station and the Black Sea hydrophysical sub-satellite test site FSBSI FRC MHI of RAS for collecting the atmospheric precipitation samples and preparing them for transportation to the Marine Biogeochemistry Department of the FSBSI FRC MHI of RAS for chemical analysis.

For citation: Varenik, A.V., Myslina, M.A. and Tarasevich, D.V., 2023. Atmospheric Input of Silica in Crimea and Factors Affecting it. *Ecological Safety of Coastal and Shelf Zones of Sea*, (1), pp. 77–90. doi:10.29039/2413-5577-2023-1-77-90

Атмосферное поступление силикатов в Крыму и факторы, влияющие на него

А. В. Вареник, М. А. Мыслина *, Д. В. Тарасевич

Морской гидрофизический институт, Севастополь, Россия
**e-mail: myslina@mhi-ras.ru*

Аннотация

Кремний относится к основным биогенным элементам (N, P, Si) и входит в состав большого числа природных минералов, вследствие чего постоянно присутствует в природных водах. В природе он в основном присутствует в виде солей кремниевой кислоты (силикатов). Атмосферные осадки могут быть важным дополнительным источником поступления силикатов в экосистему. Целью данной работы является оценка содержания силикатов в атмосферных выпадениях на основе многолетних данных, анализ пространственно-временно́й изменчивости этого содержания, а также выявление возможных факторов, влияющих на атмосферное поступление силикатов. Представлены результаты непрерывного мониторинга поступления силикатов с атмосферными осадками в районе крымского побережья в 2015–2021 гг. Пробы осадков отбирались в г. Севастополе и п. Кацивели в два типа осадкосборников – постоянно открытый для отбора суммарных (сухие + влажные) атмосферных выпадений и для сбора только влажных атмосферных осадков. Показано, что в межгодовой динамике потока силикатов с атмосферными осадками в обоих пунктах отбора проб максимальная величина поступления этого биогенного элемента была определена в 2017–2018 гг. Выявлены основные факторы, влияющие на величину поступления силикатов с атмосферными осадками. Одним из основных факторов, влияющих на величину концентрации силикатов в осадках, является интенсивность пылевого переноса.

Ключевые слова: силикаты, отбор проб, атмосферные осадки, Крым, пылевые атмосферные выпадения, многолетнее изменение

Благодарности: работа выполнена в рамках государственного задания ФГБУН ФИЦ МГИ по теме FNNN-2021-0005 «Прибрежные исследования». Авторы выражают благодарность сотрудникам Морской гидрометеорологической станции г. Севастополя и Черноморского гидрофизического подспутникового полигона ФГБУН ФИЦ МГИ РАН за отбор проб атмосферных осадков и подготовке их к транспортировке в отдел биогеохимии моря ФГБУН ФИЦ МГИ для выполнения химического анализа.

Для цитирования: *Вареник А. В., Мыслина М. А., Тарасевич Д. В.* Атмосферное поступление силикатов в Крыму и факторы, влияющие на него // Экологическая безопасность прибрежной и шельфовой зон моря. 2023. № 1. С. 77–90. EDN VYBJPN. doi:10.29039/2413-5577-2023-1-77-90

Introduction

Silica (Si) is the second most abundant (after oxygen) chemical element in the Earth's crust, where its content is about 29 % [1]. In nature, it is mainly present in the form of silicic acid salts (silica). Silica is one of the main elements in biogeochemical cycles in the biosphere and plays an important role in the life of many living organisms.

There are natural and anthropogenic sources of Si entering the environment. During weathering, silica compounds enter the ecosystem in the form of dissolved orthosilicic acid (H_4SiO_4), which is facilitated by chemical, physical, and biological factors [2]. Dust transport can also be a natural source of atmospheric Si input [3]. For example, it was shown in [4] that the rise of a large amount of dust aerosol by strong updrafts promotes migration of microbiota and minerals, including high concentrations of silica, over tens of thousands of kilometers.

The anthropogenic sources of silica entering the atmosphere are local in nature. For example, when burning brown and black coal [5], some ash containing silica is produced, and its particles are found in large quantities in areas with developed industry. However, there are no global estimates of industrial silica emissions [6]. Another source of atmospheric silica input can be grain handling companies. When unloading and transporting grain, a significant amount of grain dust is released, containing fertilizer elements, which also include silica [1)]. For example, there is AVAL Stevedoring Company in Sevastopol, which handles grain, container, bulk, oversized and heavy cargo. The total volume of grain transshipment by this company in 2017 reached 583.7 thousand tons, which is 2.5 times more than in 2016 [2)].

Silica belongs to the main nutrients (N, P, Si) and is part of a large number of natural minerals, that is why it is constantly present in natural waters [3)]. Si is mainly involved in the formation of the exoskeleton of the simplest hydrobionts, such as diatoms and silicoflagellates, corals, sponges, and radiolarians. Silica can potentially limit production of phytoplankton and affect the production cycle of diatoms [7].

In [8], using Gelendzhik Bay as an example, the dependence of the development of the large diatom *Rhizosolenia calcaravis* on the concentration of silica was considered. It is shown that with a decrease in the content of silica in water, the intensity of its development and the amount of biomass decrease. As a result, the natural balance of Black Sea phytoplankton species can be restored (*Sceletonema costatum* and *Talassionema nitzschioides*) with a high content of mineral compounds of nitrogen and phosphorus [8].

According to the document [4)], the decrease in the abundance of silicoflagellates, which are sensitive to the content of silica, coincides with a decrease

---

[1)] *Purification of Atmospheric Discharge (Pollutants) in Manufacturing of Products (Goods), as well as Performing Works and Providing Services at Large Enterprises*. Information and Technical Reference Book for Best Available Techniques: ITS 22-2016 (in Russian).

[2)] TASS, 2017. *Novorossiysk Port is the Leader of 2017 among Cargo Terminals in Russia.* [online] Available at: https://www.korabel.ru/news/comments/novorossiyskiy_port_-_lider_2017_goda_sredi_gruzovyh_terminalov_rossii.html [Accessed: 2 April 2023] (in Russian).

[3)] Arkhipova, I.V., Ktitorova, E.N., Lukyanov, Yu.S. and Alyukaeva, A.F., 2020. [*РД 52.10.744-2020. Mass Concentration of Silicium in Seawater. Methods of Measurement by Photometric Method as Blue Form of Silicomolybdic Acid*]. Moscow: Rosgidromet, 9 p. (in Russian).

[4)] Mikaelyan, A.S., 2018. [*Temporal Dynamics of Phytoplankton in the Deep Basin of the Black Sea. Extended Abstract of Doctoral Thesis*]. Moscow, 51 p. (in Russian).

in the Si concentration in the pycnocline and the cold intermediate layer (CIL). The author of this work suggests that, in contrast to diatoms, a long-term decrease in the content of silica in the pycnocline and CIL and, as a result, in the photic zone could well lead to a limitation in the growth of silicoflagellates in the deep-water basin.

There are additional sources of silica entering the ecosystem (see Regulatory Document [3)] and [9]):

– domestic sewage formed as a result of the use of synthetic detergents containing silica;

– wastewater from industrial enterprises producing silicate materials;

– underground waters and rivers, which wash the land and take away huge amounts of silica in the form of suspensions of clay particles, fragments of aluminosilicates and solutions;

– mainland runoff.

The contribution of large rivers to the balance of nutrients flowing into the Black Sea, according to scientists [10], is from 2 to 6 %, however, the work [10] does not take into account the contribution of medium and small rivers.

The work [5)] shows that in the near mouth area of the Danube, as a result of the rise of bottom waters to the surface (upwelling), a significant increase in the content of nutrients in surface waters was recorded. At the same time, in the bottom waters, the concentrations that exceeded the content of silica in the surface estuarine waters were noted under hypoxic conditions.

One of the sources of Si entering water bodies is also bottom sediments, which are formed as a result of the death and decomposition of the remains of terrestrial (coniferous, cereal, sedge) and aquatic (diatom) plants capable of concentrating silica [9]. Diatoms extract 70–80 % of silica from water. After death, they dissolve, silica is released and passes into a soluble form. Insoluble parts settle to the bottom, forming extensive deposits of diatomaceous ooze. This is how the biogeochemical cycle of silica is formed [6)].

Human activity in the 20th century has significantly changed the cycle of nutrients, including silica [11]. At the same time, the more conservative properties of silica, in contrast to, for example, phosphorus and nitrogen, contribute to a lower intensity of changes in the silica cycle. However, disproportionate changes in the cycling and abundance of phosphate and inorganic nitrogen in marine ecosystems can lead to a relative decline in silica content. In turn, this limitation can affect the development of diatoms and shift the balance in ecosystems.

[5)] Eremchenko, O.Z., 2010. [*Theory of Bioshpere. Organized Nature of Biosphere and Biogeochemical Cycles. Tutorial*]. Perm: Izdatelstvo PGU, 104 p. (in Russian).

[6)] Zavaltseva, O.A., 2012. [*Biogeochemistry Basics: Tutorial for Bachelor Progamme Students in Disciplines "Soil Sciences", "Ecology", "Enbironmental Management", "Chemistry"*]. Ulyanovsk: UlGU, 71 p. (in Russian).

The input of silica into marine ecosystems also occurs as a result of dry and wet sedimentation processes [12], where they are in a soluble form and in the form of mineral particles suspended in water [3)]. The chemical composition of atmospheric precipitation is characterized by temporal and spatial variability, and is also a sensitive indicator of atmospheric pollution and, to a certain extent, can reflect the general regional load on a given territory [13]. According to estimates in [5)], from 600 million to 1.6 billion tons of aeolian dust enter the ocean from the continents. The atmospheric precipitation containing nutrients can change the classical Redfield ratio [14], which can affect the general state of the ecosystem and lead to eutrophication.

It was previously mentioned [15] that silica does not belong to polluting elements, however, the Si distribution analysis makes it possible to assess the influence of natural processes and anthropogenic factors on the formation of the hydrochemical structure of waters.

The purpose of this article is to estimate the content of silica in atmospheric precipitation based on long-term data obtained at the MHI, to analyze the spatial and temporal variability of this content, and to identify possible factors affecting the atmospheric silica input.

Methods and materials

Sampling area

Atmospheric precipitation samples were collected at two points on the Crimean coast – the city of Sevastopol and the settlement of Katsiveli (Fig. 1). For each case of precipitations, the meteorological conditions (wind speed and direction, air temperature and humidity, atmospheric pressure) at the start of precipitations, as well as the amount of precipitations, were recorded.

Fig. 1. The location of the precipitation sampling point (the source of the inset map: https://gidcrima.ru/sevastopol/dostoprimechatel-nosti/buhty-sevastopolya/)

In Sevastopol, the samples were collected into two types of samplers – permanently open for sampling total (wet + dry) precipitations and wet-only. An automatic sampler was installed at a height of 1.5 m above the underlying surface at a weather station operating around the clock. Until the middle of 2016, the Tretyakov rain gauge was used as a sampler in Katsiveli, which made it possible to select only total (dry + wet) atmospheric precipitations. In the middle of 2016, we purchased and installed an automatic sampler in Katsiveli. As a result, it became possible to receive both total

and wet-only precipitations, without the influence of dry precipitations. At both sampling points, samplers were installed in open areas away from buildings and trees.

Sampling method

Precipitation samples were taken for each rain or snow event. If the break in precipitations was more than 1 hour and the cloudiness changed, then the next precipitation was taken as a separate sample. All samples were poured into prewashed nalgen jars and frozen to exclude the possibility of chemical and microbiological transformation of the samples. Then, the samples were delivered to the Marine Biogeochemistry Department of Marine Hydrophysical Institute for chemical analysis.

Chemical method of analysis

Only the precipitation samples whose volume allowed chemical analysis were analyzed for the silica content. The spectrophotometric method for silica determination is based on the formation of a blue silicomolybdenum complex. The range of determined concentrations is 0.05–20 μmol/L. According to the work [7], the error of the method is 20 % when determining concentrations up to 0.36 μmol/L, ±10 % when determining concentrations up to 0.71 μmol/L and ±3…5 % when determining higher concentrations.

Results

During the study period, more than 500 samples were analyzed for each sampler in Sevastopol, more than 200 samples were collected in an open sampler, and more than 350 samples were collected in a wet-only sampler in Katsiveli. The content of silica in the atmospheric precipitations of Sevastopol exceeded the content in the precipitations of Katsiveli. The maximum concentration in the open sampler in Sevastopol was determined in November, in the wet-only one – in September. At the same time, in Katsiveli, for both types of samplers, the maximum concentrations of silica were more typical for the warm period (June – July), which corresponds to previously published data [2].

Some statistical characteristics of silica concentrations are presented in the Table.

In the inter-annual dynamics of the silica flux with atmospheric precipitations, a similar quasiperiodic change is observed at both monitoring points (Fig. 2).

The data for the wet-only sampler in Katsiveli is not enough to draw a trend line, but the same quasiperiodic change in the flux of silica is visible. The maximum silica flux with atmospheric precipitation was determined in 2017–2018 at both sampling points. At the same time, it can be seen that the silica input with precipitations in Katsiveli, according to the concentration data determined in the samples of the wet-only sampler, is much less than the input in Sevastopol. However, estimating the silica flux according to the data for the open sampler, we see that the flux is less only in 2017–2018, while in other years it even exceeds

[7] Bordovsky, O.K. and Ivanenkov, V.N., 1978. [*Ocean Hydrochemical Research Methods*]. Moscow: Nauka, 271 p. (in Russian).

Statistical characteristics of silica content in precipitation samples

Characteristic	Sevastopol		Katsiveli	
	Wet-only sampler	Open sampler	Wet-only sampler	Open sampler
Maximum concentration, μmol/L	34.46	36.79	4.96	13.58
Minimum concentration, μmol/L	0	0	0	0
Volume-weighted mean concentration, μmol/L	0.78	1.78	0.23	1.14
Standard deviation, μmol/L	2.69	4.56	0.63	1.69

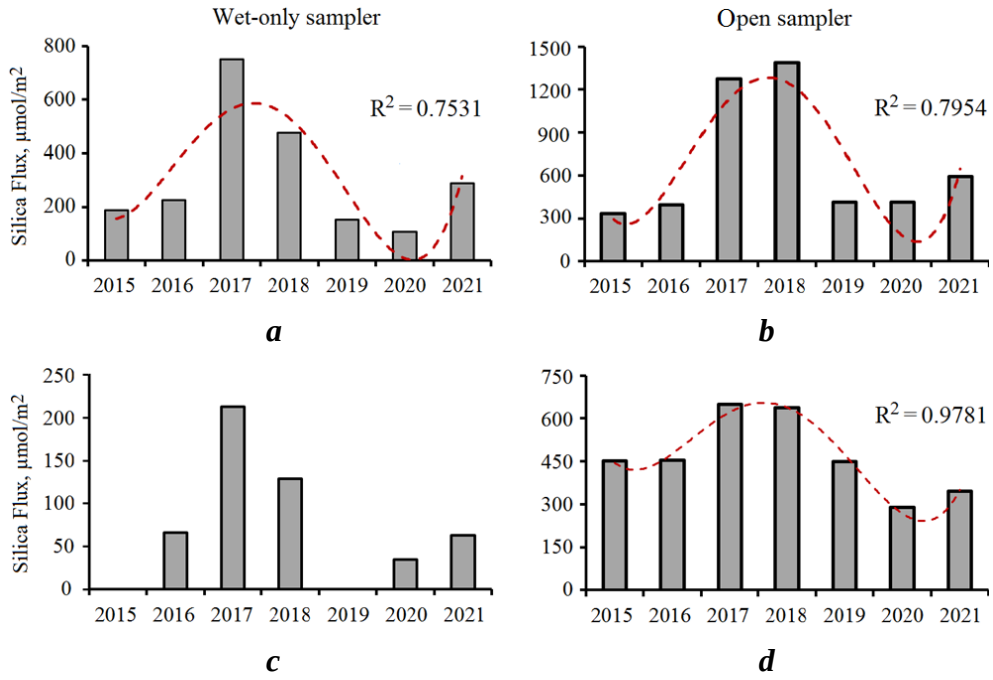

Fig. 2. Inter-annual variation in silica flux with the precipitation in Sevastopol (*a*, *b*) and Katsiveli (*c*, *d*)

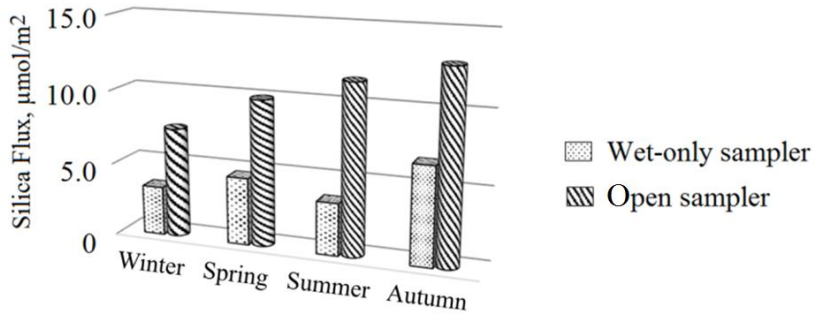

F i g . 3 . Seasonal variation in silica flux with the atmospheric precipitation in Sevastopol

the flux in Sevastopol. A possible reason for this may be an active development of the territory of the southern coast of Crimea, including Katsiveli. And if in Sevastopol the main contribution to the silica input can be made by atmospheric dust transport, then in Katsiveli, due to the geographical location, the contribution of dust transport is approximately equal to the contribution of the anthropogenic component, for example, construction work and the associated emission of silica into the atmosphere.

When considering the intra-annual change in the flux of silica with precipitation in Sevastopol, it was found that the maximum flux was observed in the period from September to November for both wet-only and open samplers (Fig. 3).

The open sampler was characterized by a gradual flux increase from winter to autumn. For samples from a wet-only sampler, a periodic change in the silica flux was observed with a gradual increase in spring and autumn, and a decrease in winter and summer.

Discussion of the results

Factors affecting the flux of silica with atmospheric precipitations

One of the factors determining the content of various pollutants in atmospheric precipitations is the content of these substances in the atmosphere [8)]. At the same time, under certain conditions, such as: temperature inversions, calm weather, a break between precipitations, accumulation of pollutants in the air can occur. Therefore, we estimated the change in silica concentration in precipitation samples at each monitoring point depending on the number of "dry" days between precipitation events (Fig. 4).

[8)] Morozov, A.E. and Starodubtseva, N.I., 2020. [*Meteorological Conditions and Atmospheric Pollution: Tutorial*]. Yekaterinburg: UGLTU, 128 p. (in Russian).

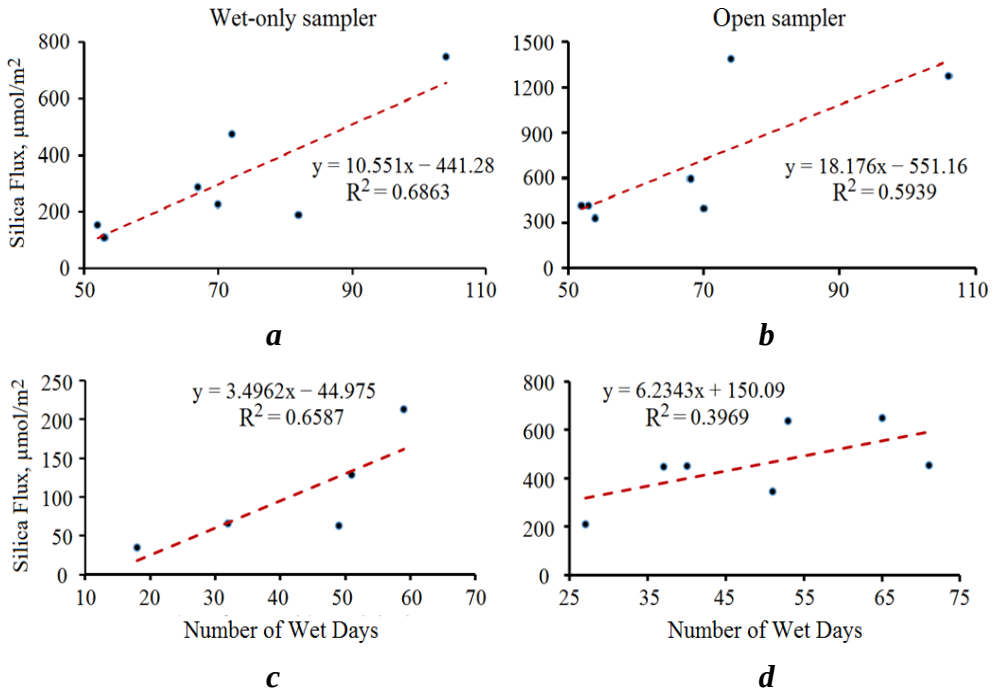

Fig. 4. Silica concentration in precipitation in Sevastopol (*a*, *b*) and Katsiveli (*c*, *d*) depending on the number of "dry" days between precipitation events

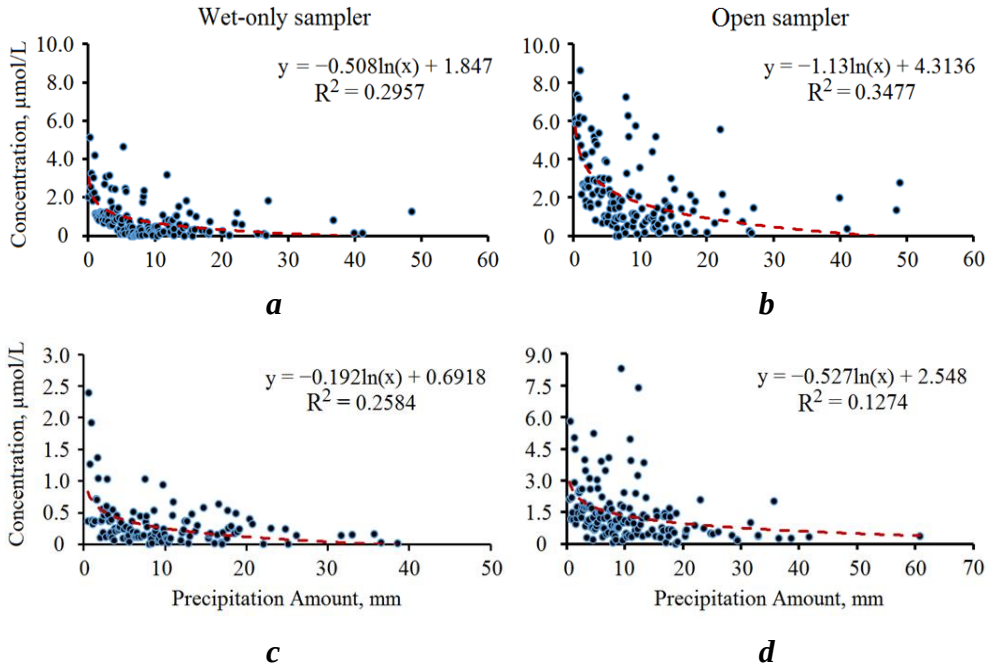

Fig. 5. Silica concentration in precipitation in Sevastopol (*a*, *b*) and Katsiveli (*c*, *d*) depending on changes in precipitation amount

With an increase in the duration of the interval between precipitations, an increase in the silica concentration in the precipitation samples is observed. This is a consequence of the silica accumulation in the atmosphere.

Atmospheric precipitations wash away the impurities contained in the atmosphere. Fig. 5 shows the change in the silica concentration in the samples for open and wet-only samplers at each observation point depending on the amount of precipitations.

As can be seen from the graphs in Fig. 5, the silica concentration decreases with increasing the amount of precipitations, since some dilution occurs. These data are consistent with the previously published results [16, 17] for other substances contained in atmospheric precipitation.

Previously [18], it was shown for inorganic nitrogen that changes in the flux of this nutrient element in atmospheric precipitation are determined primarily by changes in the amount of precipitations: the more precipitation falls, the greater the flux of inorganic nitrogen that comes with it. Therefore, we analyzed the change in precipitation amount for each year of the study period. Fig. 6 shows histograms of changes in the total amount of precipitations for each year of observation (for analyzed samples).

As can be seen from the graphs, there is a similar periodicity in the change in both the amount of precipitations (Fig. 6) and the silica flow (Fig. 2) in Sevastopol. The maximum annual precipitation amount was in 2017–2018 and 2021. At the same time, for Katsiveli, there is some difference in the frequency of change in the silica flux (Fig. 2) and the total annual amount of precipitations (Fig. 6): in 2016, the amount of precipitations during the year was at its maximum, while the silica flux remained at the level of 2015. At the same time, in Sevastopol, the change in the amount of precipitations (Fig. 6) occurs more smoothly compared to the change in the silica flux during the same years (Fig. 2). Taking into account that silica is a terrigenous nutrient element and does not have such solubility as, for example, inorganic nitrogen, both wind erosion of the soil cover near the sampling area and the dust transboundary transport can influence the change in its content to a greater extent.

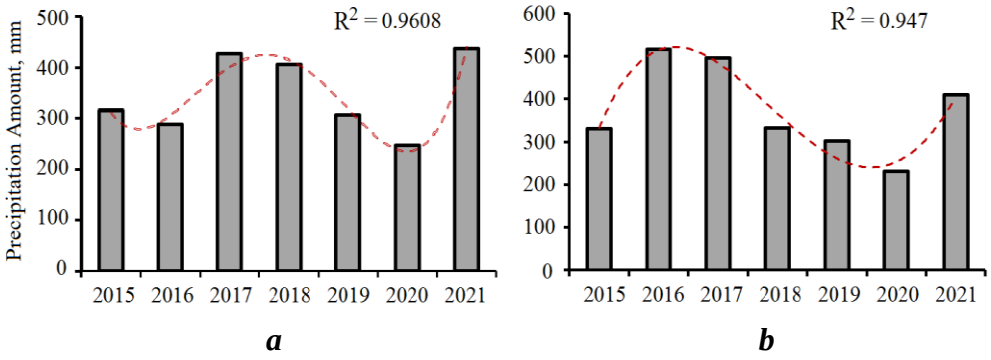

Fig. 6. Inter-annual variation in precipitation amount in Sevastopol (*a*) and Katsiveli (*b*)

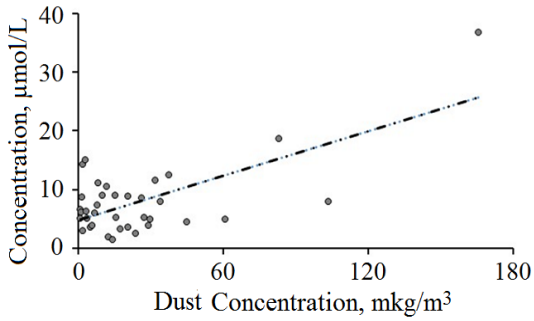

Fig. 7. Silica flux with the atmospheric precipitation in Sevastopol depending on the dust transport intensity

An analysis was made of the data on silica concentration in atmospheric precipitations and mass concentration of dust in the atmospheric air of Sevastopol, which were obtained from satellite monitoring data [9] in September – November for the entire study period. As a result, it was found that the more intense the dust transport was, the higher the silica concentration was in the samples of atmospheric precipitations (Fig. 7). Based on the obtained intra-annual distribution of the silica flux with atmospheric precipitations (see Fig. 3), we assumed that dust transport can have the maximum effect on the silica content in the atmospheric air of the study area during this period.

After analyzing the correlation of two data sets using the Data Analysis package in Excel, we found that the correlation coefficient was 0.61. The correlation coefficient evaluation using Student's t-test showed the statistical significance of the obtained dependence.

Potential impact of atmospheric silica precipitations on marine ecosystems

The possible effect of atmospheric silica precipitations on the value of primary production can be calculated based on the C:N:P:Si ratio, which is 106:16:1:15 [19]. Marine primary production depends on many external (atmospheric, riverine and industrial nutrient input) and internal (upwelling nutrient input) factors.

During the study period, the average silica flux with atmospheric precipitations in Sevastopol was 0.75 $\mu mol \cdot m^{-2} \cdot yr^{-1}$. At the C:Si = 106:15 ratio, the additional amount of produced organic carbon will be 5.30 $\mu mol \cdot m^{-2} \cdot yr^{-1}$. According to [20], the average annual primary production in coastal areas is 140 $gC \cdot m^{-2} \cdot yr^{-1}$ (11,667 $\mu mol \cdot m^{-2} \cdot yr^{-1}$). Based on the data obtained, the average annual silica input with atmospheric precipitations in Sevastopol can lead to an insignificant change in the content of organic carbon in the seawater – less than 0.1 %. At the same time, according to the analysis of the main nutrients input with atmospheric precipitations, the N:P:Si ratio in the atmospheric precipitations of Sevastopol is 79:1:1.9, which is very different from the classical Redfield ratio. This may

[9] Available at: https://giovanni.gsfc.nasa.gov/giovanni/ [Accessed: 05 April 2023].

contribute to the fact that, under conditions of high input of inorganic nitrogen with atmospheric precipitations, silica can become a limiting nutrient element in the coastal waters of the Black Sea.

Conclusion

The paper considers the silica input with atmospheric precipitation at two points on the Crimean coast – the city of Sevastopol and the Katsiveli settlement. It is shown that in the interannual dynamics of the silica flux with precipitations at both monitoring points, a similar quasiperiodic change is observed – the maximum flux of this nutrient element was determined in 2017–2018. The main factors influencing the amount of the silica input with atmospheric precipitations are revealed. With an increase in the duration of the interval between precipitations, an increase in the silica concentration in the precipitation samples was observed, which is a consequence of the silica accumulation in the atmosphere. As a result of the analysis of the data on silica concentration in precipitations and mass concentration of dust in the atmospheric air of Sevastopol, it was found that the more intense the dust transport was, the higher the silica concentration was in the atmospheric precipitations samples. When assessing the possible impact of silica influx with atmospheric precipitations on the value of primary production of coastal areas of the Crimea, it was found that the direct contribution of the silica flux can be insignificant. However, under conditions of varying input of inorganic nitrogen and phosphates with atmospheric precipitations, further studies are needed to assess silica contribution to the state of marine coastal ecosystems.

REFERENCES

1. Wedepohl, K.H., 1995. The Composition of the Continental Crust. *Geochimica et Cosmochimica Acta*, 59(7), pp. 1217–1232. https://doi.org/10.1016/0016-7037(95)00038-2
2. Xi, Y., Wang, Q., Zhu, J., Zhang, Q., Chen, Y., He, N. and Yu, G., 2022. Atmospheric Silicon Wet Deposition and Its Influencing Factors in China. *Environmental Research*, 214, 114084. doi:10.1016/j.envres.2022.114084
3. Kalinskaya, D. and Varenik, A., 2019. The Research of the Dust Transport Impact on the Biogeochemical Characteristics of the Black Sea Surface Layer. In: SPIE, 2019. *Proceedings of SPIE*. Vol. 11208: 25th International Symposium on Atmospheric and Ocean Optics: Atmospheric Physics, 1120845. doi:10.1117/12.2540432
4. Kalinskaya, D.V., Varenik, A.V. and Papkova, A.S., 2018. Phosphorus and Silicon as Markers of Dust Aerosol Transfer over the Black Sea Region. *Sovremennye Problemy Distantsionnogo Zondirovaniya Zemli iz Kosmosa*, 15(3), pp. 217–225. doi:10.21046/2070-7401-2018-15-3-217-225 (in Russian).
5. Leonova, M. and Potapova, E., 2012. Quartz Raw Material for Silicon Production in Ore-Smelting Furnaces. *Young Researchers' Journal of ISTU*, (4), pp. 49 (in Russian).
6. Tegen, I. and Kohfeld, K., 2006. Atmospheric Transport of Silicon. In: V. Ittekkot, D. Unger, C. Humborg and N. Tan An, eds., 2006. *The Silicon Cycle: Human Perturbations and Impacts on Aquatic Systems*. Washington, DC: Island Press, pp. 81–91.

7. Matveev, V.I., Tikhomirova, E.A. and Luchin, V.A., 2015. Primary Production of the Sea of Okhotsk in Years with Different Temperature Conditions. *Russian Journal of Marine Biology*, 41(3), pp. 176–185. https://doi.org/10.1134/S1063074015030062
8. Polyakova, T.V. and Polyakova, A.V., 2017. The Impact of Variability of Biogenous Base on Phytoplankton of Gelendzhik Bay of the Black Sea. *Issues of Modern Algology*, (1). Available at: http://algology.ru/1148 [Accessed: 05 March 2023] (in Russian).
9. Mokienko, A.V., 2020. Silicon in Water: from Toxicity to Essence. *Bulletin of Marine Medicine*, (4), pp. 136–142. doi:10.5281/zenodo.4430795 (in Russian).
10. Makkaveev, P.N. and Zavyalov, P.O., 2018. Runoff of Small and Medium Rivers of the Russian Black Sea Coast and Its Influence on Water Characteristics. In: A. P. Lisitsyn, ed., 2018. *The Black Sea System*. Moscow: Nauchny Mir, pp. 287–322. doi:10.29006/978-5-91522-473-4.2018.287-322 (in Russian).
11. Zotkin, G.A. and Karavaev, D.A., 2013. [Impact of Anthropogenic Activity on Biochemical Cycles]. *Modern High Technologies*, (8-2), pp. 330 (in Russian).
12. Spokes, L.J. and Jickells, T.D., 2005. Is the Atmosphere Really an Important Source of Reactive Nitrogen to Coastal Waters? *Continental Shelf Research*, 25(16), pp. 2022–2035. doi:10.1016/j.csr.2005.07.004
13. Baranov, D.Y., Moiseenko, T.I. and Dinu, M.I., 2020. Geochemical Trends in the Formation of Atmospheric Precipitation in the Conditionally Background Area of the Valdai National Park. *Geochemistry International*, 58(10), pp. 1159–1173. https://doi.org/10.1134/S0016702920100031
14. Redfield, A.C., 1934. On the Proportions of Organic Derivatives in Sea Water and Their Relation to the Composition of Plankton. In: J. Johnstone, R. J. Daniel, 1934. *James Johnstone Memorial Volume*. Liverpool: University Press of Liverpool, pp. 176–192.
15. Khoruzhii, D.S. and Konovalov, S.K., 2010. Silicon in Waters of the Sevastopol Bay in Spring 2008. *Physical Oceanography*, 20(3), pp. 196–206. https://doi.org/10.1007/s11110-010-9078-y
16. Varenik, A.V., Kozlovskaya, O.N. and Simonova, Yu.V., 2016. Estimation of Nutrient Flux Input to the Crimean Southern Coast (Katsiveli) Supplied by the Atmospheric Precipitation in 2010–2015. *Physical Oceanography*, (5), pp. 61–70. doi:10.22449/1573-160X-2016-5-61-70
17. Iavorivska, L., Boyer, E.W. and DeWalle, D.R., 2016. Atmospheric Deposition of Organic Carbon via Precipitation. *Atmospheric Environment*, 146, pp. 153–163. https://doi.org/10.1016/j.atmosenv.2016.06.006
18. Varenik, A.V., 2019. Applying the Brandon Method to Estimate the Concentration of Inorganic Nitrogen in Precipitation. *Russian Meteorology and Hydrology*, 44(5), pp. 326–330. https://doi.org/10.3103/S1068373919050030
19. Brzezinski, M.A., 1985. The Si:C:N Ratio of Marine Diatoms: Interspecific Variability and the Effect of Some Environmental Variables. *Journal of Phycology*, 21(3), pp. 347–357. https://doi.org/10.1111/j.0022-3646.1985.00347.x
20. Demidov, A.B., 2008. Seasonal Dynamics and Estimation of the Annual Primary Production of Phytoplankton in the Black Sea. *Oceanology*, 48(5), pp. 664–678. https://doi.org/10.1134/S0001437008050068

Submitted 20.12.2022; accepted after review 25.01.2023;
revised 1.02.2023; published 24.03.2023

About the authors:

Alla V. Varenik, Senior Research Associate, Marine Hydrophysical Institute of RAS (2 Kapitanskaya St., Sevastopol, 299011, Russian Federation), Ph.D. (Geogr.), **ResearcherID: H-1880-2014**, *alla.varenik@mhi-ras.ru*

Maria A. Myslina, Junior Research Associate, Marine Hydrophysical Institute of RAS (2 Kapitanskaya St., Sevastopol, 299011, Russian Federation), **ORCID ID: 0000-0002-0054-0379**, *myslina@mhi-ras.ru*

Diana V. Tarasevich, Research Engineer, Marine Hydrophysical Institute of RAS (2 Kapitanskaya St., Sevastopol, 299011, Russian Federation), **ORCID ID: 0000-0003-4893-9685**, *ledi_di2020@bk.ru*

Contribution of the authors:

Alla V. Varenik – general scientific supervision of the study, statement of study goals and objectives, qualitative and quantitative analysis of the results and their interpretation, discussion of the results, preparation of graphic materials, drawing conclusions

Maria A. Myslina – review of the related literature, qualitative and quantitative analysis of the results and their interpretation

Diana V. Tarasevich – review of the related literature, qualitative and quantitative analysis of the results and their interpretation

All the authors have read and approved the final manuscript.

Original article **DOI**: 10.29039/2413-5577-2023-1-91-103

Hydrological, Hydrochemical Conditions of Lake Donuzlav (Western Crimea, Black Sea) Based on the Results of Expeditions in 2019

V. I. Ryabushko [1]*, S. V. Shchurov [1], N. P. Kovrigina [1], A. I. Chepyzhenko [2]

[1] *A.O. Kovalevsky Institute of Biology of the Southern Seas of RAS, Sevastopol, Russia*

[2] *Marine Hydrophysical Institute of RAS, Sevastopol, Russia*

* *e-mail: rabushko2006@yandex.ru*

Abstract

Industrial sand extraction and wastewater discharge are among the main anthropogenic factors affecting the state of the ecosystem of Lake Donuzlav (Crimea, Black Sea). Sand mining primarily significantly changes the seabed and can cause the formation of an oxygen-deficient zone. In this regard, it is necessary to continue the up-to-date hydrochemical and hydrobiological monitoring in the areas of mussel-and-oyster farms, sand mining zones, cargo port, and in the area affected by the release of the Donuzlav sewerage treatment plant. The purpose of this work is to study the hydrological and hydrochemical structure of the southwestern region of Lake Donuzlav, which is subject to anthropogenic influence and includes a zone of industrial sand mining. In April, May and September 2019, studies of the hydrological and hydrochemical structure of lake waters were carried out, including measurements of temperature, salinity, content of dissolved oxygen, five-day biochemical oxygen demand (BOD_5), alkaline permanganate oxidizability, content of silicate, mineral and organic nitrogen and phosphorus. It is shown that the spatial distribution of water temperature and salinity is characterized by great heterogeneity and temporal variability. The hydrochemical studies indicate high oxygen supply in the lake; no cases of oxygen deficiency were detected during the research period. The minimum concentrations of dissolved oxygen did not drop to the minimum allowable levels. All BOD_5 values were below the maximum allowable levels. Local anthropogenic impact on the lake waters was registered in the increased concentrations of nutrients and oxidizability values in the sand mining areas, near the sewerage outlet, in the port area and in the area affected by the domestic wastewater release.

Keywords: hydrological and hydrochemical structure, biogenic elements, Lake Donuzlav, Crimea, Black Sea

Acknowledgements: The work was performed under state assignment of IBSS of RAS "Research of control mechanisms for production processes in biotechnological complexes with the aim of developing scientific foundations for obtaining biologically active substances and technical products of marine genesis", state registration no. 121030300149-0; and of MHI RAS "Complex interdisciplinary research of oceanologic processes, which determine functioning and evolution of the Black and Azov Sea coastal ecosystems", state registration no. 08272019-0005.

For citation: Ryabushko, V.I., Shchurov, S.V., Kovrigina, N.P. and Chepyzhenko, A.I., 2023. Hydrological, Hydrochemical Conditions of Lake Donuzlav (Western Crimea, Black Sea) based on the Results of Expeditions in 2019. *Ecological Safety of Coastal and Shelf Zones of Sea,* (1), pp. 91–103.doi:10.29039/2413-5577-2023-1-91-103

Гидролого-гидрохимический режим вод озера Донузлав (Западный Крым, Черное море) по результатам экспедиций 2019 года

В. И. Рябушко [1]*, С. В. Щуров [1], Н. П. Ковригина [1], А. И. Чепыженко [2]

[1] *Институт биологии южных морей им. А. О. Ковалевского РАН, Севастополь, Россия*
[2] *Морской гидрофизический институт РАН, Севастополь, Россия*
*****e-mail: rabushko2006@yandex.ru*

Аннотация

Промышленная добыча песка и сброс сточных вод относятся к основным антропогенным факторам, влияющим на состояние экосистемы озера Донузлав (Крым, Черное море). Добыча песка, прежде всего, существенно меняет рельеф дна и может стать причиной возникновения зон с дефицитом кислорода. В связи с этим в районах мидийно-устричных ферм, зонах добычи песка, грузового порта, а также в районе влияния выпуска КОС «Донузлав» необходимо продолжение мониторинговых гидрохимических и гидробиологических работ в современных условиях. Цель настоящей работы – исследование гидролого-гидрохимической структуры юго-западного района озера Донузлав, подверженного антропогенному влиянию и включающего зону промышленной добычи песка. В апреле, мае и сентябре 2019 г. проведены исследования гидролого-гидрохимической структуры вод озера, включающие измерения температуры, солености, а также определения содержания растворенного кислорода, биохимического потребления кислорода за пять суток ($БПК_5$), перманганатной окисляемости в щелочной среде, содержания кремния, минеральных и органических форм азота и фосфора. Показано, что распределение температуры и солености воды отличается большой пространственной неоднородностью. Материалы гидрохимических исследований свидетельствуют о высокой концентрации кислорода в воде; случаев дефицита кислорода за период исследований не обнаружено. Минимальные концентрации растворенного кислорода не снижались до значений предельно допустимых концентраций (ПДК). Все значения $БПК_5$ не превышали ПДК. Локальное антропогенное воздействие на воды озера заключается в повышении концентраций биогенных веществ, органического азота и фосфора, а также значений окисляемости в районе добычи песка, вблизи выпуска сточных вод КОС «Донузлав» и в районе порта.

Ключевые слова: гидролого-гидрохимическая структура, биогенные элементы, озеро Донузлав, Крым, Черное море

Благодарности: работа выполнена по темам государственных заданий: ФИЦ ИнБЮМ «Исследование механизмов управления продукционными процессами в биотехнологических комплексах с целью разработки научных основ получения биологически активных веществ и технических продуктов морского генезиса» (номер гос. регистрации 121030300149-0) и ФГБУН ФИЦ МГИ «Комплексные междисциплинарные исследования океанологических процессов, определяющих функционирование и эволюцию экосистем прибрежных зон Черного и Азовского морей» (номер гос. регистрации 0555-2021-0005).

Для цитирования: Гидролого-гидрохимический режим озера Донузлав (Западный Крым, Черное море) по результатам экспедиций 2019 года / В. И. Рябушко [и др.] // Экологическая безопасность прибрежной и шельфовой зон моря. 2023. № 1. С. 91–103. EDN WWDOFG. doi:10. 29039/2413-5577-2023-1-91-103

Introduction

Lake Donuzlav is a unique semi-enclosed man-made sea bay located on the western coast of Crimea. Until 1961, the lake had no connection with the sea and was the second largest saline lake in Crimea with high salinity values (90–95 PSU); however, its traditional denomination as “lake” has still been preserved. The earliest detailed information about the hydrochemical structure of Lake Donuzlav and the field of currents in it are given in [1, 2]. Industrial sand mining in the lake began in 1962 and continues in the present. Papers [3–6] were focused on various aspects of the impact of this activity on the ecosystem of the bay. First of all, sand mining significantly alters the seabed and can cause the formation of oxygen-deficient zones.

The results of the studies carried out in Lake Donuzlav in recent years (2015–2021) are included in the monograph *Modern Hydrometeorological and Hydrochemical Regimes of the Donuzlav Bay*, 2021, where the main focus is on the thermohaline and hydrochemical conditions and water dynamics [7]. The analysis of the materials obtained from the results of expeditions in 2018 [8] gives an idea of the current state of the thermohaline and hydrochemical structure of the bay. These works show the need for regular monitoring of the environmental state of the lake in order to prevent possible negative effects of economic activity on the industrial and recreational potential of the lake.

The purpose of this work is to study the thermohaline and hydrochemical structure of the southwestern area of Lake Donuzlav, which is subject to anthropogenic influence and includes an area of modern industrial sand mining. The main focus is on the results of the 2019 expeditions obtained in the areas of sand mining, cargo port, mussel-and-oyster farm, as well as in the area affected by the domestic wastewater discharge of the Donuzlav sewage treatment plant.

Material and Methods

Studies of the southwestern part of Lake Donuzlav were carried out in April, May, and September 2019. A total of three surveys were performed; samples were taken at 51 stations (Fig. 1) in the surface layer and near the bottom using a type of the Nansen bottle BM-48M. The water temperature in April was measured using a deep-sea reversing thermometer *TG* and, in May and September,

Fig. 1. Sampling scheme in Lake Donuzlav in 2019: April (green squares), May (blue squares), September (red squares); I – mussel-and-oyster farm; II – discharge of domestic water; III – sand production site; IC – input channel

using an optical biophysical sounding probe *Condor* (available at: http://ecodevice.com.ru/ecodevice-catalogue/multit). In total, 79 water samples were taken, in which salinity (using an electric salinometer GM-65), pH value, dissolved oxygen, five-day biochemical oxygen demand (BOD_5), alkaline permanganate oxidizability and concentrations of silicate, mineral and organic nitrogen and phosphorus were determined.

Sample analysis was carried out in accordance with the Russian regulatory documents (RD) [1)]. The dissolved oxygen concentration was determined by the standard Winkler method. The quantitation range is from 0.1 mL/dm^3 to oversaturation. The measurement error (ME) is 3.4 %. The determination of the concentration of dissolved inorganic phosphorus was carried out according to the Murphy–Riley method. The quantitation range is 5÷1000 μg/dm^3, and the ME is 4.6 %.

[1)] RD 52.24.420-2019, RD 52.24.383-2018, RD 52.24.380-2017, RD 52.24.381-2017, RD 52.24.382-2019, RD 52.24.432-2018, RD 52.10.805-2013, RD 52.24.387-2019.

The dissolved inorganic silicon was determined by Koroleff's colorimetric method. The quantitation range is 10÷2000 μg/dm^3, and the ME is 5.8÷4.7 %. Nitrite nitrogen was determined using the method based on the azo dye formation by reacting nitrite with hydrochloric sulfanilamide and α-naphthylethylenediamine. The quantitation range is 0.5÷100 μg/dm^3, and the ME is 18.0÷1.5 %. Nitrate nitrogen was determined after its reduction to nitrite nitrogen on cadmium columns. The range is 5÷500 μg/dm^3, and the ME is 7÷2.7 %. Ammonium nitrogen was determined using the modified Sagi–Solórzano method. The quantifiable ammonium nitrogen con-centration range is 15÷1500 μg/dm^3, and the ME is 11.4÷1.7 %.

Results and Discussion

Survey dated April 08, 2019. No sand mining took place during the survey. According to the data of Yevpatoria marine hydrometeorological station (available at: https://rp5.ru/Архив_погоды_в_Евпатории), in the first decade of April. The air temperature dropped to 6 °C in the morning and rose to 21 °C in the afternoon. During the survey period, the easterly and northeasterly winds with the speed of 2–5 m/s prevailed.

Temperature and Salinity. The water temperature in the surface layer was characterized by insignificant spatial variation in the range of 10.6–10.8 °C, and only by 15:00 in the shallow area of the sand mining site, the water warmed up to 12.6 °C. The water temperature decreased slightly with depth. For example, at the stations along the fairway, at depths greater than 10 m, the water temperature was 9.6–10.0 °C. The salinity in the surface water layer varied from 17.85 PSU in the farm area to 18.05 PSU in the areas of the sand mining site and lake entrance channel. The salinity varied slightly with depth.

Hydrochemical Parameters. The studies showed high oxygen concentration in the entire water column (saturation above 100 %) and its fairly even horizontal distribution. The minimum oxygen content (100.4 %) observed in the bottom layer, was more than 2.5 times above the minimum allowable level (40 %) according to the water quality standards for water bodies of fishery importance [2)]. *BOD_5 and oxidizability* in the surface layer demonstrated low values, which varied within 0.91–1.36 mgO_2/dm^3 and 2.56–3.53 mgO_2/dm^3 and were below the maximum allowable levels (2.0 mgO_2/dm^3 and 4.0 mgO_2/dm^3, respectively). From the BOD_5 and oxidizability values, the water area under study can be characterized as unpolluted.

In the sand mining area in the near-bottom water layer, the lowest oxygen concentration and the highest concentrations of organic phosphorus and silicate were observed. The concentrations of *mineral nitrogen and phosphorus* in the surface water were as follows: the nitrite nitrogen and mineral phosphorus concentrations in the layer (0.3–1.1 μg/dm^3 and 0.6–2.5 μg/dm^3) did not exceed the maximum

[2)] *On the Approval of Water Quality Standards for Water Bodies of Commercial Fishing Importance, Including Standards for Maximum Permissible Concentrations of Harmful Substances in the Waters of Water Bodies of Commercial Fishing Importance*: Order of the Ministry of Agriculture of Russia dated December 13, 2016, No. 552. URL: http://publication.pravo.gov.ru/Document/View/0001201701160006 [Accessed: 11 March 2023).]

allowable levels. The concentrations of nitrate nitrogen varied from 9.2 to 19.1 μg/dm^3 and those of ammonium nitrogen from 0.6 to 191.8 μg/dm^3. In the mussel-and-oyster farm area, the decrease in the nitrate and increase in the ammonium concentrations with depth were observed.

The distribution of the silicate and ammonium nitrogen concentrations in the surface and bottom layers was uneven (Fig. 2). The ranges of the silicate fluctuations were 49.7–137.4 μg/dm^3 in the surface layer and 38.4–130 μg/dm^3 in the bottom layer. The highest concentration of silicon in the bottom layer coincided with the maximum concentration of ammonium nitrogen (Station *4*), and the highest concentration of silicon (137.4 μg/dm^3) in the surface layer was observed in the sand mining site area.

Organic nitrogen and phosphorus were determined only in the surface water layer, and their concentrations varied from 6.1 to 9.5 μg/dm^3 and from 875 to 1104 μg/dm^3, respectively. In the farm area and in the areas adjacent to it, increased organic nitrogen concentrations were observed, and in the sand mining site area, the highest concentration of organic phosphorus was noted.

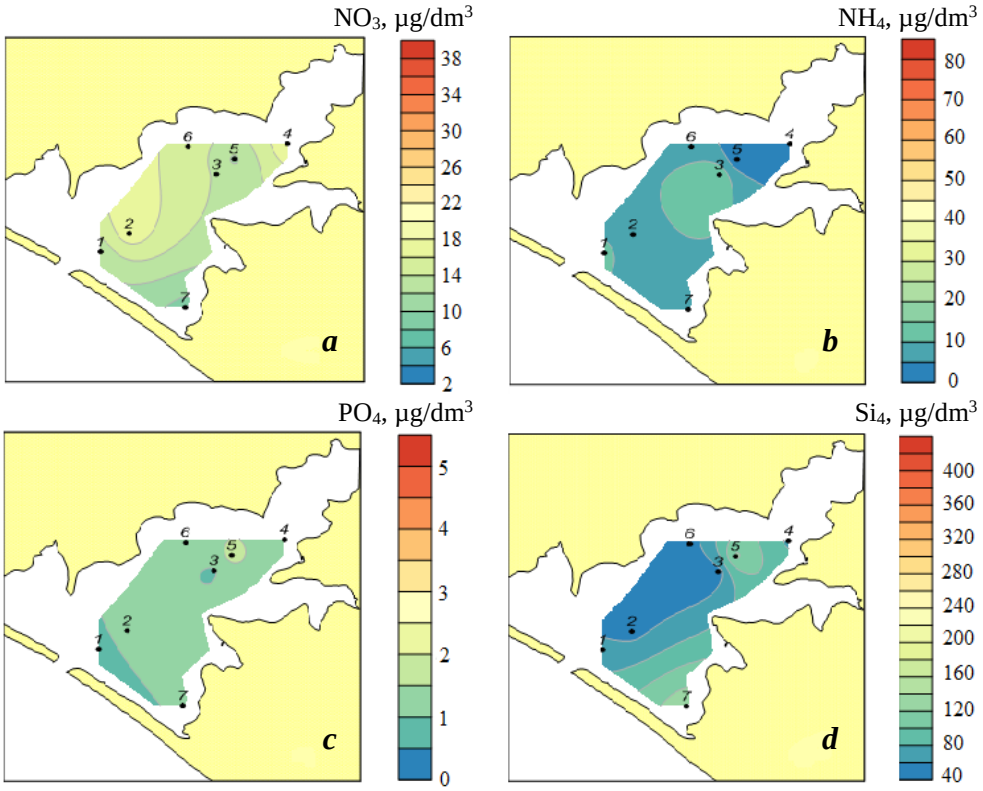

Fig. 2. Distribution of nutrient concentrations in the surface layer: nitrates (*a*), ammonium nitrogen (*b*), phosphates (*c*), silicon (*d*); April 2019. Numbers denote stations

Survey dated May 27, 2019 was conducted during the sand mining. The survey was preceded (on May 26) by blowing of a westerly wind of 5–8 m/s (and blasts up to 10 m/s). Simultaneously with the water sampling, a scheme of frequent station locations was worked out using the multi-parameter probe *Condor*. The survey yielded data on the water temperature and parameters related to pollution in the area. This made it possible to choose the location of water sampling stations. In the sand mining site area with the depths of less than 2 m, the suspended matter pollution area was stretched downwind, with its horizontal spread about 600 m [9].

Temperature and Salinity. At the end of the spring period, intense warming of the waters and formation of a thermocline took place in the lake. There was no temperature stratification in areas shallower than 4 m (including the sand mining site area) (Fig. 3). The water column was homogeneous and warmed up to 22.9–23.3 °C. At stations with depths greater than 8 m, the temperature distribution was characterized by a presence of a 4–8-m-thick upper quasi-homogeneous layer with a temperature of 22.3–22.7 °C and a 3–5-m-thick transient layer with the vertical gradient of no greater than 0.6°C/m. Under the transient layer at a depth of 12–16 m, the temperature was the lowest, 18.8–19.5 °C (Fig. 4).

The salinity of the surface layer varied in the range of 18.29–18.45 PSU, increasing to the northeast and reaching its maximum in the shallow Shchelkunov Bay. At depths over 10 m, along the channel fairway transect, the vertical salinity gradient was insignificant and the maximum salinity values did not exceed 18.32 PSU.

Hydrochemical Parameters. The *dissolved oxygen* saturation was high. In the surface layer, the saturation reached as much as 121.7 % with the average value of 109.7 %. In the bottom layer, the oxygen saturation was slightly lower: the average value was 103.2 % and the lowest one was 95.7 % (near the lake

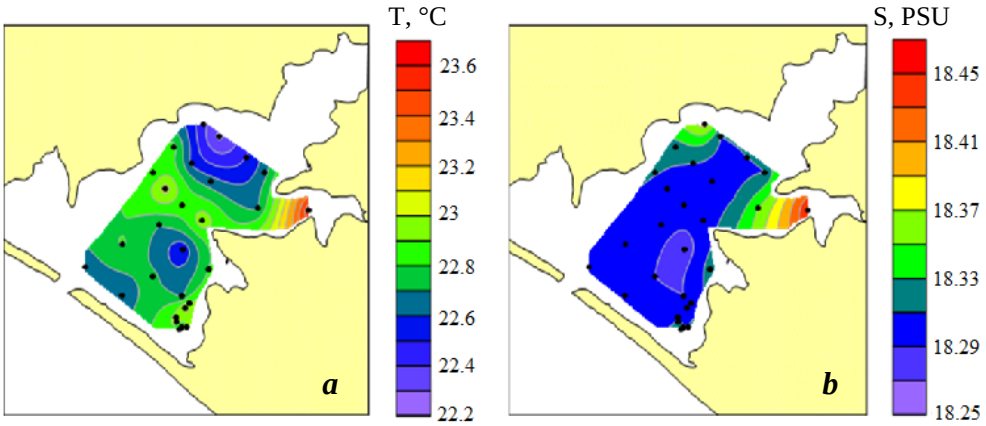

F i g . 3 . Distribution of temperature (*a*) and salinity (*b*) in the surface layer, May 2019. Points are station locations

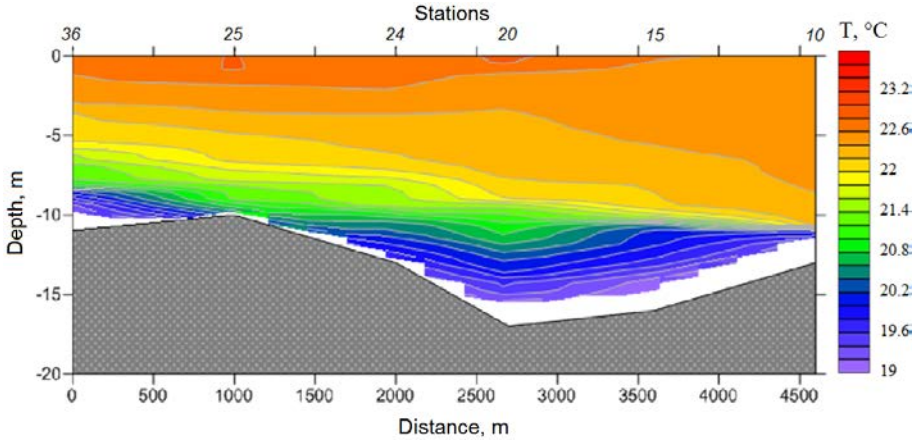

Fig. 4. Temperature distribution at the channel transect; May 2019

entrance channel). In addition, at Stations *10* and *15* along the channel fairway transect, the oxygen saturation in the near-bottom layer was 97.8 % and 97.5 %.

BOD_5 demonstrated low values with insignificant spatial variability: they did not exceed the maximum allowable levels (MAL) according to fishery standards and varied from 1.12 to 1.97 mgO_2/dm^3 with the average equal to 1.54 mgO_2/dm^3. The *oxidizability* values, like BOD_5, did not exceed MAL. The only exception was the measurement in the sand mining site area, where the value of oxidizability was 4.24 mgO_2/dm^3 and exceeded the corresponding MAL by 0.24 mgO_2/dm^3. In general, the low BOD_5 and oxidizability values registered in the May survey indicate that the area under study was not polluted.

The concentrations of *mineral nitrogen and phosphorus* were low and evenly distributed over the water area under study. The concentrations of nitrate nitrogen in the surface layer varied from 2.7 to 20.0 $\mu g/dm^3$ and those of ammonium nitrogen from 8.9 to 48.4 $\mu g/dm^3$, with the average values equal to 8.1 and 26.2 $\mu g/dm^3$, respectively. The highest concentrations of nitrate and ammonium nitrogen were observed in the sand mining site area. The concentrations of mineral phosphorus and mineral nitrogen were low (from 0.1 to 5.4 $\mu g/dm^3$) with the average value of 2.2 $\mu g/dm^3$ for the surface layer. The maximum values were observed in the areas of the mussel-and-oyster farm and the sand mining site.

Figure 5 shows the distribution of concentrations of mineral nitrogen, phosphorus, and silicon in the surface layer of the lake. The phosphate concentrations in May were almost twice as high as in April. The concentrations of mineral forms of nitrogen in the surface layer of Lake Donuzlav in 2019 and 2018 did not differ. The silicate concentration distribution in the survey was uneven; the fluctuation range in the surface layer was 44.1–409.8 $\mu g/dm^3$ with the average value of 111.3 $\mu g/dm^3$. The highest silicate concentration was found in the area affected by the domestic wastewater discharge. The average silicate concentrations in May were almost 1.5-fold higher than in April. The concentrations of organic nitrogen

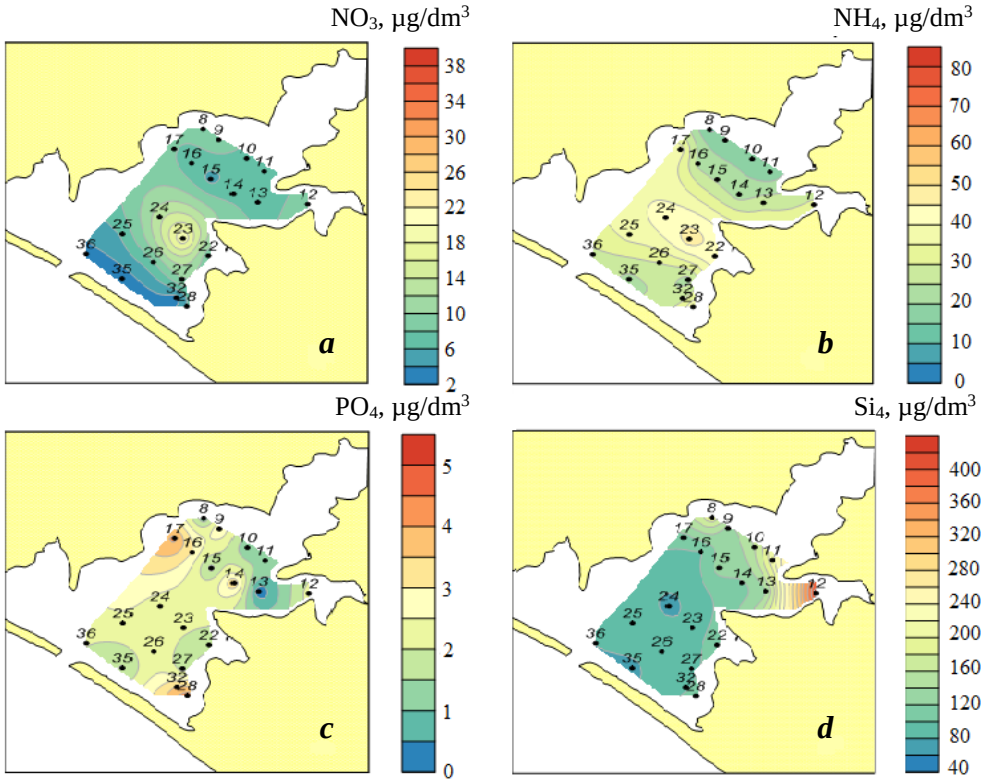

Fig. 5. Distribution of concentrations of biogenic elements in the surface layer: nitrates (*a*), ammonium nitrogen (*b*), phosphates (*c*), silicon (*d*); May 2019. Numbers denote stations

and phosphorus varied in the surface layer from 643 to 1426 µg/dm^3 and from 11.4 to 20.1 µg/dm^3, respectively. In the sand mining site area, an increase in the contents of both organic nitrogen and phosphorus was observed.

The permanganate oxidizability method allows indirectly obtaining an approximate estimate of dissolved organic carbon content in water. According to Skopintsev [3)], the value 0.34 is the mean ratio of the oxidizability oxygen in the 0–50 m layer (1.22 mg/dm^3) to organic carbon (3.6 mg/dm^3). Using the permanganate oxidizability values measured by us and the coefficient 0.34, we calculated the content of dissolved organic carbon (C_{DOC}) in the surface layer. The range of the C_{DOC} variations was 8.09–12.47 mgC/dm^3. The maximum was recorded in the sand mining site area (Station *28*) and the minimum was in the mussel-and-oyster farm area.

[3)] Skopintsev, B.A., 1975. [*Formation of the Modern Chemical Composition of the Black Sea Waters*]. Leningrad: Gidrometeoizdat, 335 p. (in Russian).

Survey dated September 16, 2019. According to the data of Yevpatoria marine hydrometeorological station, the air temperature on September 15–16 varied from 13 to 23.8 °C. On September 15, northeasterly winds at a speed of 3–6 m/s prevailed, and within one day they changed to westerly and southwesterly winds with the speed of 3–5 m/s. The amounts of sand mining were reduced that day, the wastewater discharge occurred intermittently and with different intensities. Therefore, the size of the area of increased concentration of suspended solids was smaller than on May 27, 2019. The suspension patch was elongated along the coast to the northeast.

Temperature and Salinity. In September, the autumn cooling of the waters begins and the temperature is equalized throughout the entire water column. On September 15–16, the air temperature dropped to 13 °C at night and rose to 24 °C in the daytime. The local temperature minimum (19 °C) was observed in the sand mining site area, while in most of the area under study the temperature was about 21 °C (Fig. 6). Up to the depth of 17 m, the water temperature was almost uniform. The salinity varied in the range of 18.4–18.8 PSU, increasing from the lake entrance channel to the middle part of the lake. The maximum salinity values (18.8 PSU) were recorded in the shallow area of the sand mining site.

Hydrochemical Parameters. The oxygen distribution in the water area in the late summer was quite uniform. In terms of saturation, its content varied from 89.9 to 108.7 % in the surface water layer and from 89.9 to 108.7 % in the near-bottom layer. The lowest values were recorded on the border of the sand mining site area and the adjacent water area; the highest values were recorded in the area along the channel fairway transect.

The values of BOD_5 varied in the surface layer from 0.73 to 1.95 mg/dm^3 and did not exceed MAL. The highest BOD_5 value was observed in the sand mining site area. The *oxidizability* varied from 3.29 to 5.37 mgO/dm^3. The lowest value was observed in the port area at a depth of 9 m, and the highest value, exceeding MAL by 1.37 mgO/dm^3, was observed in the surface layer of the same station. In the sand mining site area, the oxidizability values exceeded MAL due to the return water discharge.

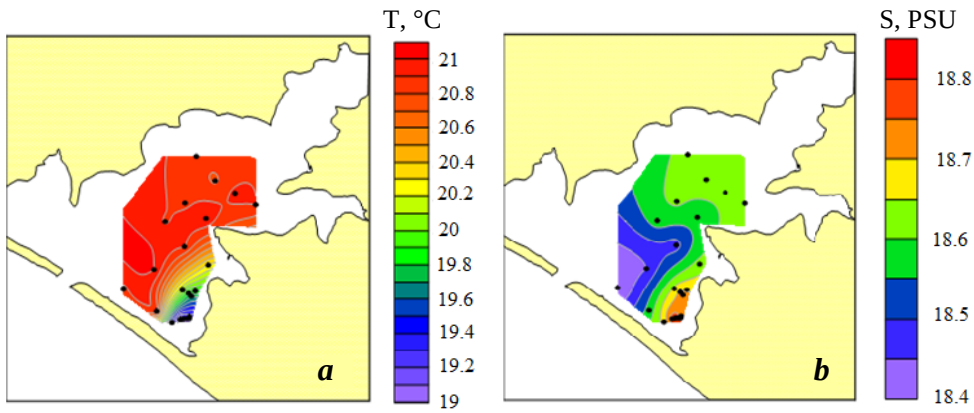

Fig. 6. Distribution of temperature (*a*) and salinity (*b*) in the surface layer September 2019. Points are station locations

The dissolved organic carbon concentration C_{DOC} calculated from oxidizability changed during the survey from 9.68 to 15.79 mgC/dm^3 and approached the ranges of C_{DOC} obtained in May (8.09–12.47 mgC/dm^3) in Lake Donuzlav.

Similarly to the previous survey, the concentrations of *nitrite nitrogen and mineral phosphorus* demonstrated low values and uniform distribution over the area (Fig. 7). The concentrations of nitrite nitrogen in the surface and bottom layers varied from 0.2 to 1.2 μg/dm^3 and those of mineral phosphorus from 1.5 to 4.6 μg/dm^3. The distribution of the nitrate nitrogen, ammonium nitrogen, and silicon concentrations was uneven both horizontally and vertically. The highest concentrations of nitrate in the surface (38.0 μg/dm^3) and bottom layers (42.4 μg/dm^3) were recorded in the port and sand mining site areas. The concentrations of nitrate nitrogen at other stations were fairly even, with their average values being 13.4 μg/dm^3 in the surface layer and 12.6 μg/dm^3 in the bottom layer. The concentrations of ammonium nitrogen in the surface layer varied from 3.2 to 78.8 μg/dm^3 with the average of 24.5 μg/dm^3. The highest ammonium nitrogen concentration was noted in the surface layer at the sand mining site.

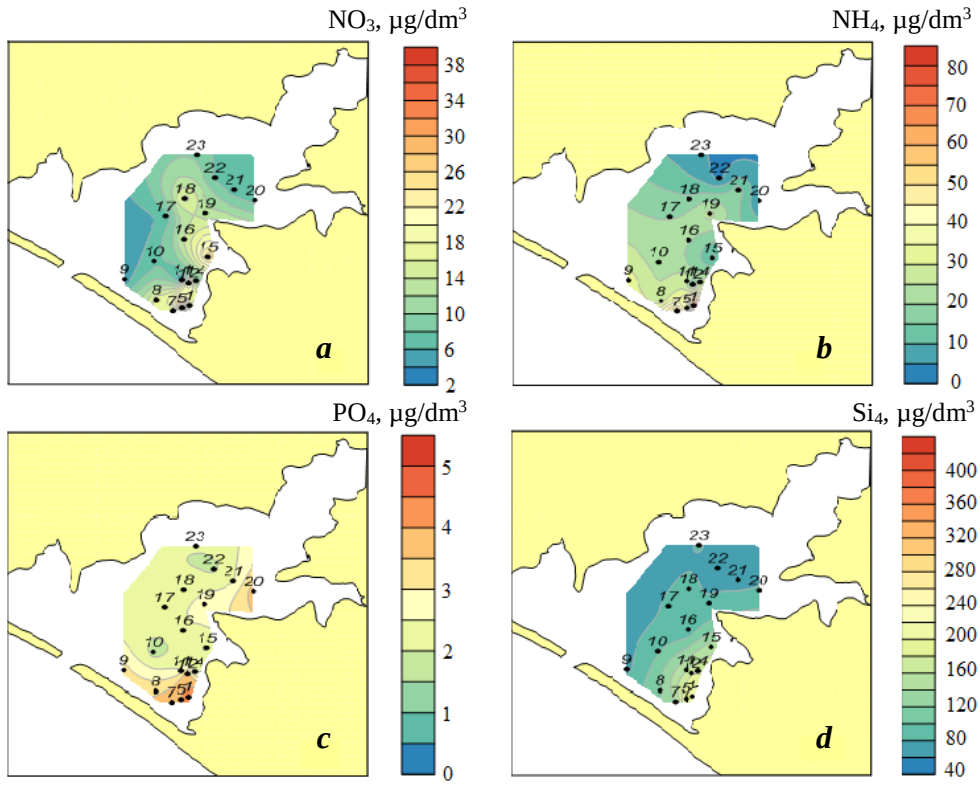

Fig. 7. Distribution of concentrations of biogenic elements in the surface layer: nitrates (*a*), ammonium nitrogen (*b*), phosphates (*c*), silicon (*d*); September 2019. Numbers denote stations

The distribution of *silicon* concentrations in the surface layer varied from 73.3 to 211.5 μg/dm^3 with the average of 119.7 μg/dm^3. Increased values were observed both in the sand mining site area (Stations *1*, *5–8*) and in the suspension patch, which was observed up to Stations *11–15*. In the rest of the water area, the concentration of silicon was low.

The concentrations of *organic nitrogen and organic phosphorus* were distributed as follows: in the areas affected by the domestic wastewater discharge and sand mining, increased organic nitrogen concentrations (from 1033 to 1297 μg/dm^3) were noted. In the rest of the water area, the respective values were significantly lower and varied from 703 to 885 μg/dm^3. The organic phosphorus distribution was similar to the distribution of organic nitrogen: the increased values (from 18.6 to 30.9 μg/dm^3) were observed in the areas where the organic nitrogen increase was observed, and lower values (from 17.6 to 26.9 μg/dm^3) were in the areas of the organic nitrogen decrease.

Conclusion

The spatial distribution of the thermohaline characteristics in waters of Lake Donuzlav is highly heterogeneous. In spring, there is intensive warming of water and formation of thermal stratification in the lake. In the second half of September, the autumn cooling of waters begins and the vertical distribution of temperature is uniform throughout the entire water column. The hydrochemical studies performed indicate high oxygen concentration in waters of the lake. The lowest concentrations of dissolved oxygen never reached the minimum allowable values. No cases of oxygen deficiency were found over the period under study. All BOD_5 values were lower than MAL. The anthropogenic impact on Lake Donuzlav in the areas of sand mining, port and domestic wastewater discharge results in the local increase in oxidizability and concentration of nutrients, as well as organic phosphorus and nitrogen. The highest values of the mineral and organic nitrogen and phosphorus concentrations were observed in the sand mining site area.

References

1. Nemirovsky, M.S. and Kovrigina, N.P., 2000. Dynamics of the Lake Donuzlav Waters. *Ekologiya Morya*, 51, pp. 10–13 (in Russian).
2. Kovrigina, N.P. and Nemirovsky, M.S., 1999. Hyrochemical Characteristic of the Lake Donuzlav Waters Based on Data of 1990–1997. *Ekologiya Morya*, 48, pp. 10–14 (in Russian).
3. Zuev, G.V. and Boltachev, A.R., 1999. Influence of Underwater Quarrying of Sand on the Donuzlav Estuary Ecosystem. *Ekologiya Morya*, 48, pp. 5–9 (in Russian).
4. Sebakh, L.K., Petrenko, O.A., Zhugaylo, S.S. and Tsyntaryuk, E.A., 2006. Influence of Industrial Exploitation of the Sand Deposits on the State of the Lake Donuzlav Ecosystem. In: B. N. Panov, ed., 2006. *Current Problems of the Azov-Black Sea Basin Ecology. Proceeding of the 2nd International Conference. Kerch, 26–27 June 2006*. Kerch: YugNIRO, pp. 71–79 (in Russian).
5. Zhugaylo, S.S., Avdeeva, T.M., Pugach, M.N. and Adzhiumerov, E.N., 2018. Current State of Water Quality and Bottom Sediments in Lake Donuzlav. *Aquatic Bioresources and Environment*, 1(1), pp. 32–38. doi:10.47921/2619-1024_2018_1_1_32 (in Russian).

6. Ivanyutin, N.M., 2019. Current Ecological State of Lake Donuzlav. *Water and Ecology: Problems and Solutions*, (3), pp. 47–58. doi:10.23968/2305-3488.2019.24.3.47-58 (in Russian).
7. Dyakov, N.N. and Fomin, V.V., eds., 2021. *Modern Hydrometeorological and Hydrochemical Regimes of the Donuzlav Bay*. Sevastopol, 464 p. (in Russian).
8. Ryabushko, V.I., Shchurov, S.V., Kovrigina, N.P. and Popov, M.A., 2021. Hydrological, Hydrochemical and Hydrobiological Studies of Lake Donuzlav (Western Crimea, Black Sea) based on the Results of Expeditions in 2018. *Ecological Safety of Coastal and Shelf Zones of Sea*, (2), pp. 80–93. doi:10.22449/2413-5577-2021-2-80-93 (in Russian).
9. Lomakin, P.D., Ryabushko, V.I., Chepyzhenko, A.I. and Schurov, S.V., 2021. Control of the Current System and Fields of the Total Suspended Matter Concentration and Dissolved Organic Matter Concentration in Lake Donuzlav in May 2019. *Monitoring Systems of Environment*, (1), pp. 87–94. doi:10.33075/2220-5861-2021-1-87-94 (in Russian).

Submitted 20.07.2022; accepted after review 10.10.2023;
revised 1.02.2023; published 24.03.2023

About the authors:

Vitaly I. Ryabushko, Chief Research Associate, A. O. Kovalevsky Institute of Biology of the Southern Seas of RAS (2 Nakhimov Av., Sevastopol, 299011, Russian Federation), Dr. Sci. (Biol.), **ORCID ID: 0000-0001-5052-2024, Scopus Author ID: 7801673501, Researcher ID: H-4163-2014**, *rabushko2006@yandex.ru*

Sergey V. Shchurov, Research Associate, A. O. Kovalevsky Institute of Biology of the Southern Seas of RAS (2 Nakhimov Av., Sevastopol, 299011, Russian Federation), **ORCID ID: 0000-0002-8913-2637**, **Scopus Author ID: 57214992790, Researcher ID: AAC-9044-2022**, *skrimea@mail.ru*

Nelya P. Kovrigina, Senior Research Associate, A. O. Kovalevsky Institute of Biology of the Southern Seas of RAS (2 Nakhimov Av., Sevastopol, 299011, Russian Federation), Ph.D. (Geogr.), **ORCID ID: 0000-0002-6734-8285, Scopus Author ID: 6507114864,** *mariculture@mail.ru*

Aleksei I. Chepyzhenko, Senior Research Associate, Marine Hydrophysical Institute of RAS (2 Kapitanskaya St., Sevastopol, 299011, Russian Federation), Ph.D. (Techn.), **Researcher ID: AAG-7929-2020**, **Scopus Author ID: 6504344211**, **Istina Researcher ID (IRID): 6647872**, *ecodevice@yandex.ru*

Contribution of the authors:

Vitaly I. Ryabushko – setting goals and objectives of a comprehensive study, editing the manuscript

Sergey V. Shchurov – organization and management of the expedition, material collection, hydrological work

Nelya P. Kovrigina – hydrochemical work

Aleksei I. Chepyzhenko – complex of hydrophysical studies

All the authors have read and approved the final manuscript.

Original article **DOI**: 10.29039/2413-5577-2023-1-104-112

The Field of Colored Dissolved Organic Matter Content and its Relationship with Salinity in the Open Azov Sea Water

P. D. Lomakin *, D. D. Zavyalov

Marine Hydrophysical Institute of RAS, Sevastopol, Russian Federation
* *e-mail: p_lomakin@mail.ru*

Abstract
Based on the materials of a series of expeditions carried out by Marine Hydrophysical Institute (Sevastopol) and Southern Scientific Research Institute of Marine Fisheries and Oceanography (Kerch) during 2002–2013, a regression equation was obtained indicating the presence of a fairly close inverse correlation relationship between salinity and the concentration of colored dissolved organic matter in the open waters of the Sea of Azov. It is shown that the closeness of the correlation dependence between these values depends significantly on the presence of dissolved organic matter of anthropogenic origin in the waters of the studied region. Using this equation, according to the known average monthly salinity fields, the concentration fields of colored dissolved organic matter were calculated and the regularities of their structure and intra-annual variability were analyzed. It is found that the field of the studied matter is characterized by low concentration and relative homogeneity. In the open water area of the sea, salinity variations determined by the intra-annual variation in the runoff volume of the Don and Kuban Rivers do not significantly affect the spatiotemporal variability in the field of colored dissolved organic matter. It is shown that a close inverse correlation between the content of colored dissolved organic matter and salinity is an indicator of the good quality of water. A weak or positive correlation between these quantities is a sign of the presence of dissolved organic substances of anthropogenic nature in the aquatic environment.

Keywords: colored dissolved organic matter, salinity, correlation, pollution, Sea of Azov

Acknowledgements: The work was performed under state assignment no. 0555-2021-0005 “Complex interdisciplinary research of oceanologic processes, which determine fun ctioning and evolution of the Black and Azov Sea coastal ecosystems”.

For citation: Lomakin, P.D. and Zavyalov, D.D., 2023. The Field of Colored Dissolved Organic Matter Content and its Relationship with Salinity in the Open Water of the Sea of Azov. *Ecological Safety of Coastal and Shelf Zones of Sea*, (1), pp. 104–112. doi:10.29039/2413-5577-2023-1-104-112

Поле концентрации окрашенного растворенного органического вещества и его связь с соленостью в открытых водах Азовского моря

П. Д. Ломакин *, Д. Д. Завьялов

Морской гидрофизический институт РАН, Севастополь, Россия
** e-mail: p_lomakin@mail.ru*

Аннотация

На основе материалов серии экспедиций, проведенных Морским гидрофизическим институтом (г. Севастополь) и Южным научно-исследовательским институтом морского рыбного хозяйства и океанографии (г. Керчь) в 2002–2013 гг., получено уравнение регрессии, свидетельствующее о наличии достаточно тесной обратной корреляционной связи между соленостью и концентрацией окрашенного растворенного органического вещества в открытых водах Азовского моря. Показано, что теснота корреляционной зависимости между этими величинами существенным образом зависит от наличия в водах рассматриваемого региона растворенной органики антропогенного происхождения. При помощи данного уравнения по известным полям средней месячной солености рассчитаны поля концентрации окрашенного растворенного органического вещества, проанализирована их структура и внутригодовая изменчивость. Выявлено, что поле исследуемого вещества характеризуется низкой концентрацией и однородностью. В открытой акватории моря вариации солености, определяемые внутригодовым ходом объема стока рек Дон и Кубань, не оказывают существенного влияния на пространственно-временную изменчивость поля окрашенного растворенного органического вещества. Показано, что тесная обратная корреляционная связь между содержанием окрашенного растворенного органического вещества и соленостью – индикатор хорошего качества вод. Слабая или положительная корреляционная зависимость между этими величинами – признак наличия в водной среде растворенных органических веществ антропогенной природы.

Ключевые слова: окрашенное растворенное органическое вещество, соленость, корреляция, загрязнение, Азовское море

Благодарности: работа выполнена в рамках государственного задания по теме № 0555-2021-0005 «Комплексные междисциплинарные исследования океанологичес- ких процессов, определяющих функционирование и эволюцию экосистем прибрежных зон Черного и Азовского морей».

Для цитирования: *Ломакин П. Д., Завьялов Д. Д.* Поле концентрации окрашенного растворенного органического вещества и его связь с соленостью в открытых водах Азовского моря // Экологическая безопасность прибрежной и шельфовой зон моря. 2023. № 1. С. 104–112. EDN XDLBGE. doi:10.29039/2413-5577-2023-1-104-112

Introduction

The content of the dissolved organic carbon (DOC) and the colored dissolved organic matter (fDOM) are regarded as the main representative indicators of the dissolved organic matter content in sea water [1]. On the shelf of the oceans and seas, which are desalinated by river waters, in the areas of runoff fronts and frontal zones, the concentration fields of each of these indicators are associated with the salinity by a close inverse correlation with the correlation coefficient up to –0.95 [2, 3]. This correlation is due to the high concentration of the dissolved organic matter of terrigenous origin in the coastal waters, desalinated by mainland waters.

The content of this matter reduces abruptly in river mouths on a natural marginal filter and then falls noticeably at the limit of the runoff frontal zones [4, 5].

Outside coastal runoff frontal zones in the open waters of oceans and seas, such relationships and their properties are less studied. Thus, in the article [6], an inverse dependence of the concentration of dissolved organic carbon on salinity, DOC(S), was found in the open part of the Black Sea in the vertical structure of waters. This correlation, analyzed at a qualitative level by the authors of the cited work, was used by them to interpret biochemical processes in the deep-sea zone.

Note that the relationship between the indicators of the dissolved organic matter content and salinity is important and useful in a number of applied and theoretical areas of oceanology. For example, they enable us to get an idea of the structure of a poorly studied field of the dissolved organic matter content based on salinity arrays, as well as to track the trajectories of river water distribution on shelves and beyond.

The purposes of this article:

– to obtain an equation for the correlation dependence of fDOM concentration on salinity in the waters of the Sea of Azov, which are located outside the main runoff frontal zones and are not directly affected by river runoff;

– based on this equation and the known average monthly salinity fields, to calculate the content fields of the considered quantity, to identify the features of their structure and intra-annual variability;

– to evaluate the influence of the anthropogenic component of the fDOM content field on the tightness of the correlation dependence of this substance's concentration on salinity.

Initial data and research methods

The water area under consideration is a part of the sea characterized by maximum salinity, which includes open waters, as well as waters of the western and southern coastal areas, where the average monthly salinity is more than 10. According to the atlas[1)], isohaline 10 is a limit of coastal runoff haline zones observed along the northern and eastern coasts of the Sea of Azov and in Taganrog Bay.

The quantity under study is the optical indicator of the content of dissolved organic matter, fDOM. Its dimension is presented in optical calibration units – quinine sulfate (quinine sulfate unit, QSU) [7].

The empirical material used for the analysis is a sample of instrumental synchronous observations of salinity and fDOM concentration (54 soundings in total). They were carried out in a number of expeditions of Marine Hydrophysical Institute (Sevastopol) and Southern Research Institute of Marine Fisheries and Oceanography

[1)] NOAA, 2006. *Climatic Atlas of the Sea of Azov 2006*. International Ocean Atlas and Informational Series, Vol. 10. Available at: https://www.nodc.noaa.gov/OC5/AZOV2006/start.html [Accessed: 12 March 2023].

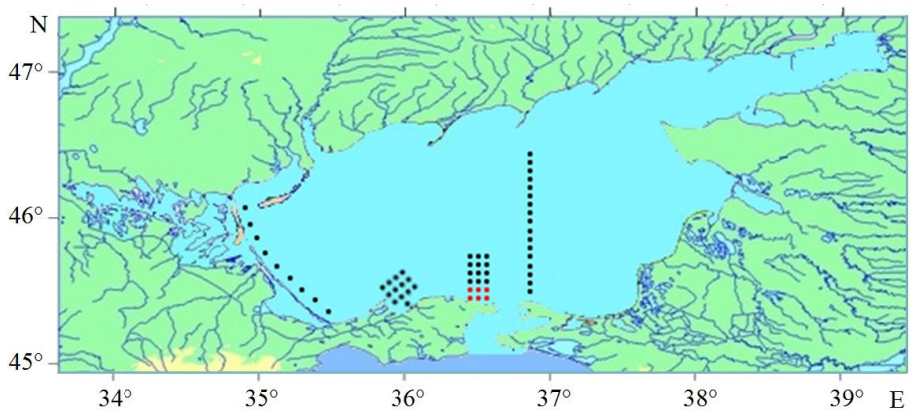

Fig. 1. Map of stations with simultaneous registration of fDOM concentration and salinity (2002–2013)

(Kerch) over the time interval from 2002 to 2013. The observations covered the central, western, and southwestern parts of the sea and the region of the Kerch pre-strait region (Fig. 1).

All analysed data were obtained using the Kondor portable optical sounding complex (ecodevice.com.ru/ecodevice-catalogue/multiturbidimeter-kondor). At each sounding with a depth step of 0.1 m, the salinity and fDOM concentration were recorded synchronously *in situ*. The error of salinity measurements was ±0.01 PSU. The measurement error of fDOM content was ±0.2 QSU. The range of studied depths was 1.5–10.5 m.

The relationship between salinity and fDOM concentration was calculated using the pair correlation method. Using the resulting regression equation, the average monthly climatic fields of salinity for the considered area of the Sea of Azov [1)], which were built on representative samples of actual data, were digitized and then recalculated into concentration fields of the studied quantity.

As an example, Fig. 2 shows the average monthly salinity field for June.

Discussion of the results

In Fig. 3, *a* in the S,fDOM coordinate system, the original data sample and the chart of the correlation between the analyzed quantities are shown, which implies that they are independent (correlation coefficient R = –0.14).

In the upper right corner of the coordinate plane, there is a separate cloud of points that clearly do not fit into the main field, illustrating the tendency for the fDOM concentration to decrease with increasing salinity.

It turned out that the singular points (there are six in total), which were distinguished by the maximum concentration of fDOM (45–61 QSU) and high salinity (12.9–13.3 PSU) (circled in Fig. 3), corresponded to the stations located in the area of wastewater discharge of the Bondarenkovo Treatment Facilities in the city of Kerch (red dots in Fig. 1). These data characterized coastal waters polluted by sewage runoff and were excluded from the original sample.

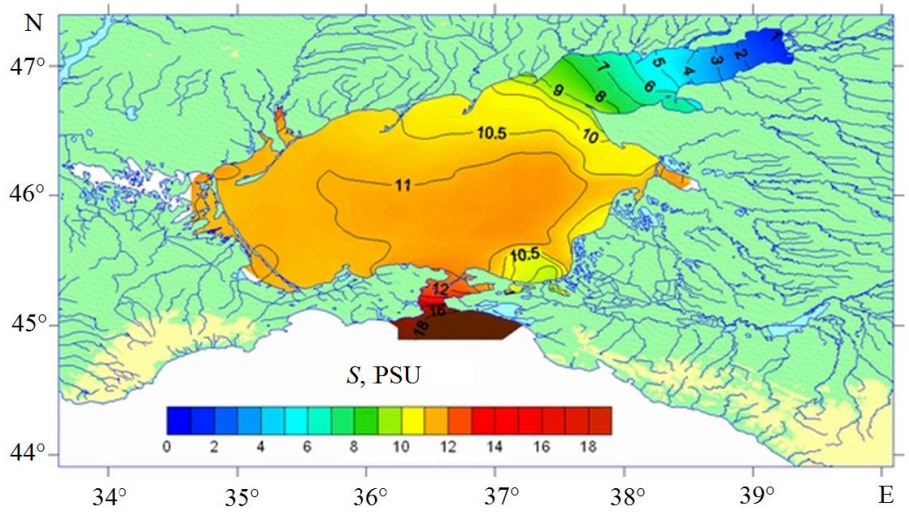

Fig. 2. Average monthly salinity in the surface layer (0 m) of the Sea of Azov in June [1)]

Based on the filtered sample, a typical inverse and rather close correlation was found between the studied quantities, correlation coefficient R = –0.63 (regression equation fDOM = –5.92·S + 90.26; N = 48 (Fig. 3, *b*)).

The result shown in Fig. 3 indicates the following. The dependence fDOM(S) responds to the presence of dissolved organic matter of anthropogenic origin in the studied waters and is a good indicator of the pollution of the aquatic environment by this substance. A close inverse correlation dependence fDOM(S) and, accordingly, a sufficiently high (in modulus) correlation coefficient are indicators of good water quality.

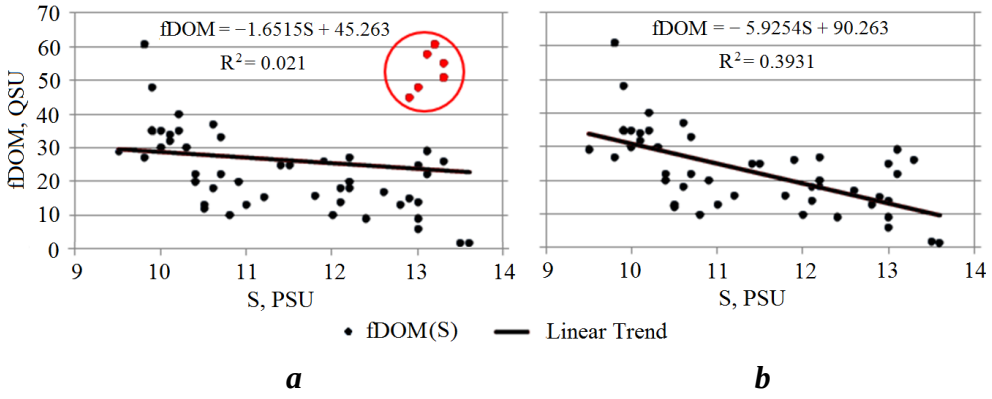

Fig. 3. fDOM(S) correlation dependence charts for the studied water area of the Sea of Azov: *a* – original sample; *b* – filtered sample

A weak negative or positive correlation between the analyzed quantities is a sign of the presence of dissolved organic substances of an anthropogenic nature in the aquatic environment.

Let us consider the factors that determine the structural features and temporal variability of salinity and fDOM in the Sea of Azov.

The main factor that determines the salinity regime of the predominant part of the sea area and, accordingly, the structure and intra-annual variability of the salinity and concentration fDOM fields, is related to the runoff volume of the Don River. The maximum runoff of this river is observed in May. In the remaining months of the year, the hydrological regime of the Don is characterized by a low water period [2)].

In the eastern coastal region of the Sea of Azov, the salinity field [1)] is determined by the runoff of the Kuban River, which reaches maximum values in the summer months during intense floods due to snowmelt in the Caucasus Mountains [8].

Accordingly, the maximum desalination of the predominant part of the sea area, characterized by an average monthly salinity of 11–11.5 PSU in the central part, is observed in May and June (Fig. 2). In the remaining months of the year, the salinity of the waters of the study area is 11.5–12.5 PSU [1)] and varies slightly with time [8].

In the considered area of the sea, the average monthly salinity fields in the surface layer are uniform. The difference in salinity at the boundaries is 1.5–2.5 PSU. Also, the range of the intra-annual variation of the average monthly salinity is estimated with a small interval of 0.5–0.7 PSU.

Fig. 4 shows the fDOM distributions calculated by us on the basis of the obtained regression equation fDOM(S) and average monthly salinity fields [1)] for March and June to illustrate the features of the structure and intra-annual variability of the characteristics of the field of the studied quantity.

It can be seen that in the months related to the extreme phases of intra-annual variations in the runoff of the Don River, which determines the maximum range of intra-annual fluctuations in water salinity in the Sea of Azov, the structure of the fDOM content field in the considered water area changes insignificantly. It is homogeneous. The concentration of the analyzed substance is almost unaffected by intra-annual variations; it is minimal over the entire area of the sea and varies in the range of 25–30 QSU. According to [9], the concentration of fDOM in the waters of Taganrog Bay, in the northern and eastern desalinated coastal areas of the Sea of Azov, is maximum and varies in the range of 30–300 QSU.

The area of the areal of the minimum concentration of the considered quantity undergoes significant changes during the year. In July–March, during the low water period of the Don and the Kuban, under conditions of minimal sea desalination, it is the largest and equals 70–80% of the area of the entire sea (Fig. 4, *a*). In May–June, during floods in the Don and the Kuban, the area occupied by waters with a minimum content of fDOM is the smallest – 50–60% of the area of the entire water body of the Sea of Azov (Fig. 4, *b*).

[2)] Rodionov, N.A., 1958. [*Hydrology of the Mouth Area of the Don*]. Leningrad: Gidrometeoizdat, 95 p. (in Russian).

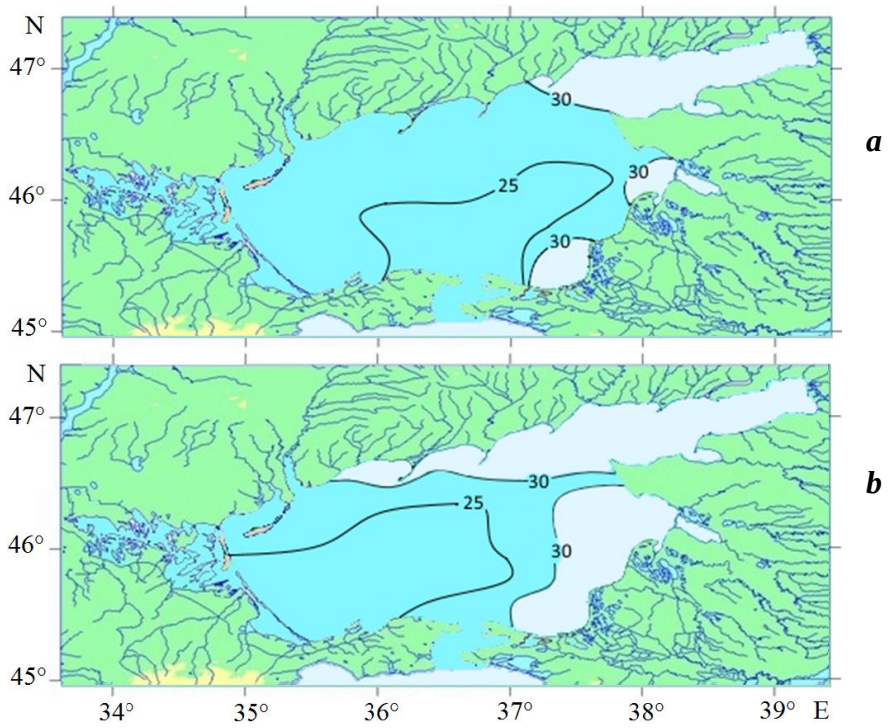

Fig. 4. Concentration of fDOM, QSU, at the surface in the open part of the Sea of Azov in March (*a*) and June (*b*)

Stability of the fDOM field structure and significant intra-annual fluctuations in the area of distribution of the waters of maximum salinity can be explained as follows. According to the classical ideas of K.N. Fedorov [5], there is an abrupt change in the properties of desalinated waters at the limit of the runoff frontal zones. The influence of these waters becomes insignificant and disappears in the open sea.

The sharply increasing runoff of the Don and the Kuban is accompanied by desalination of coastal waters and inflow of a large amount of fDOM, which is mainly concentrated within the runoff frontal zone. A small proportion of this substance penetrates into the open part of the sea. During the flood, the area of the runoff zone increases, and, accordingly, the area of the Sea of Azov with maximum salinity decreases.

Conclusion

Based on the materials of a series of expeditions carried out in 2002–2013, a rather close inverse correlation was revealed between salinity and fDOM concentration (coefficient R = –0.63) in the open waters of the Sea of Azov and in the water area adjacent to its western and southern coasts.

It has been established that the correlation fDOM(S) responds to the presence of dissolved organic matter of anthropogenic origin in the studied waters and

is a good indicator of the pollution of the aquatic environment by this substance. A close inverse correlation fDOM(S) is an indicator of good water quality. A weak or positive correlation between the considered quantities is a sign of the presence of dissolved organic substances of an anthropogenic nature.

Using the obtained regression equation, the fDOM content fields were calculated and plotted using average monthly salinity maps.

It is shown that in the waters of the salinized part of the Sea of Azov, due to the insignificant spatial and temporal variability of salinity, the average monthly fDOM fields are uniform and change little over time. They are characterized by a low concentration of 25–30 QSU and hardly react to sea desalination caused by the intra-annual variability in the runoff volume of the Don and the Kuban rivers. During floods on these rivers in May–June, the area of the water body with low fDOM content is minimal and occupies 50–60% of the entire area of the Sea of Azov. At all other times, during low water periods in the Don and the Kuban, it increases to 70–80 %.

REFERENCES

1. Agatova, A.I., Lapina, N.M. and Torgunova, N.I., 2018. Features of the Distribution of Organic Matter in the Waters of the Black Sea. In: A. P. Lisitsyn, ed., 2018. *The Black Sea System*. Moscow: Nauchny Mir, pp. 146–170. doi:10.29006/978-5-91522-473-4.2018 (in Russian).
2. Pugach, S.P. and Pipko, I.I., 2012. [Dynamics of Dissolved Coloured Organic Matter on the East Siberian Sea Shelf]. *Doklady Akademii Nauk*, 447(6), pp. 671–674 (in Russian).
3. Kari, E., Merkouriadi, I., Walve, J., Leppäranta, M. and Kratzer, S., 2018. Development of Under-Ice Stratification in Himmerfjärden Bay, North-Western Baltic Proper, and their Effect on the Phytoplankton Spring Bloom. *Journal of Marine Systems*, 186, pp. 85–95. doi:10.1016/j.jmarsys.2018.06.004
4. Lisitsyn, A.P., 1994. A Marginal Filter of the Oceans. *Okeanologiya*, 34(5), pp. 735– 747 (in Russian).
5. Fedorov, K.N., 1986. *The Physical Nature and Structure of Oceanic Fronts*. New York: Springer, 333 p.
6. Kaiser, D., Konovalov, S., Schulz-Bull, D.E. and Waniek, J.J., 2017. Organic Matter along Longitudinal and Vertical Gradients in the Black Sea. *Deep Sea Research Part: Oceanographic Research Papers*, 129, pp. 22–31. doi:10.1016/j.dsr.2017.09.006
7. Saraceno, G.F., Pellerin, B.A., Downing, D.D., Boss, E., Bachand, P.A.M. and Bergamaschi, B.A., 2009. High-Frequency in situ Optical Measurements during a Storm Event: Assessing Relationships between Dissolved Organic Matter, Sediment Concentrations, and Hydrologic Processes. *Journal of Geophysical Research. Biogeosciences*, 114(G4), G00F09. doi:10.1029/2009JG000989
8. Ilyin, Yu.P., Repetin, L.N., Belokopytov, V.N. and Goryachkin, Yu., 2012. *Hydrometeorological Conditions of the Ukrainian Seas. Vol. 2.* Sevastopol: ECOSY-Gidrofizika, 421 p. (in Russian).
9. Lomakin, P.D. and Zavyalov, D.D., 2021. Field of Colored Dissolved Organic Matter in the Azov Sea Coastal Waters. *Proceedings of the T.I.Vyazemsky Karadag Scientific Station – Nature Reserve of the Russian Academy of Sciences*, 6(3), pp. 14–21. doi:10.21072/eco.2021.19.02 (in Russian).

Submitted 16.08.2022; accepted after review 28.10.2022;
revised 1.02.2023; published 24.03.2023

About the authors:

Pavel D. Lomakin, Leading Research Associate, Marine Hydrophysical Institute of RAS (2 Kapitanskaya St., Sevastopol, 299011, Russian Federation), Dr.Sci. (Geogr.), professor, **ResearcherID: V-7761-2017**, **Scopus Author ID: 6701439810**, **IstinaResearcherID (IRID): 18321047**, *p_lomakin@mail.ru*

Dmitry D. Zavyalov, Junior Research Associate, Marine Hydrophysical Institute of RAS (2 Kapitanskaya St., Sevastopol, 299011, Russian Federation), *evilfence@ya.ru*

Contribution of the authors:

Pavel D. Lomakin – general task statement, collection of source information, interpretation of the results, article test writing

Dmitry D. Zavyalov – calculations, interpretation of the results, drawing-up of illustrations

All the authors have read and approved the final manuscript.

Original article **DOI**: 10.29039/2413-5577-2023-1-113-123

Taxonomic Composition of Polychaete Worms in the Mussel-Oyster Farm Area (the Black Sea, Sevastopol)

E. V. Lisitskaya *, N. A. Boltachova

A.O. Kovalevsky Institute of Biology of the Southern Seas of RAS, Sevastopol, Russia
**e-mail: e.lisitskaya@gmail.com*

Abstract

Studies were conducted in 2015–2019 in the mussel and oyster farm area. Data were obtained on the species composition of polychaete worms in bottom sediments under the farm, in fouling of farm constructions, and in plankton at the larval stages of development. A total of 48 polychaete species belonging to 25 families were identified. At the same time 23 species were found on the bottom under the farm, 24 species were found in the fouling of mussel collectors and oyster cages, and larvae of 25 species of polychaete worms were found in plankton. In the benthos, *Micronephthys longicornis* dominated in terms of occurrence and abundance, while in mussel collectors and oyster cages, species of the family Nereididae (*Nereis zonata*, *Platynereis dumerilii*, *Alitta succinea*) prevailed. The species composition of polychaete taxocene inhabiting the bottom under the farm and that in the fouling of the farm constructions differed significantly (the Czekanowski – Sørensen index was 0.26). In the benthos under the farm, 66 % of the species were deposit feeders by diet type, carnivores and omnivores were much fewer, whereas filter feeders were represented by only one species. Omnivores species dominated in the fouling (44 %), deposit feeders species were four times fewer, and filter feeders species were three times more than in the benthos. *Hydroides dianthus* (25 %) and *Polydora websteri* (67 %) found on and in mussel and oyster shells were highly abundant.

Keywords: Annelida, macrozoobentos, larvae Polychaete, the Black Sea

Acknowledgments: The work was performed under state assignment of the Federal Research Center of the IBSS on topic “Regularities of formation and anthropogenic transformation of biodiversity and bioresources of the Azov-Black Sea basin and other regions of the World Ocean” (registration no. 121030100028-0) and “Research of control mechanisms of production processes in biotechnological complexes for the purpose of development of scientific bases of obtaining biologically active substances and technical products of marine genesis” (registration no. 121030300149-0). We thank S. V. Shchurov, I. Y. Eremin, V. A. Grintsov, and M. V. Makarov for their help in collecting the material.

For citation: Lisitskaya, E.V. and Boltachova, N.A., 2023. Taxonomic Composition of Polychaete Worms in the Mussel -Oyster Farm Area (the Black Sea, Sevastopol). *Ecological Safety of Coastal and Shelf Zones of Sea*, (1), pp. 113–123. doi:10.29039/2413-5577-2023-1-113-123

Таксономический состав многощетинковых червей района мидийно-устричной фермы (Черное море, Севастополь)

Е. В. Лисицкая *, Н. А. Болтачева

ФГБУН ФИЦ «Институт биологии южных морей им. А. О. Ковалевского РАН», Севастополь, Россия
**e-mail: e.lisitskaya@gmail.com*

Аннотация

В результате исследований, выполненных в 2015–2019 гг. в районе мидийно-устричного хозяйства, получены данные о видовом составе многощетинковых червей, обитающих в донных отложениях под фермой, в обрастаниях конструкций фермы, а также в планктоне на пелагической стадии развития. Всего идентифицировано 48 видов полихет, относящихся к 25 семействам. При этом на дне под фермой обнаружено 23 вида, в обрастании мидийных коллекторов и устричных садков – 24, в планктоне – личинки 25 видов многощетинковых червей. В бентосе по встречаемости и численности преобладал *Micronephthys longicornis*, а на мидийных коллекторах и устричных садках – представители семейства Nereididae: *Nereis zonata, Platynereis dumerilii, Alitta succinea*. Таксоцены полихет, обитающих на дне под фермой и в обрастании конструкций фермы, существенно различались по видовому составу (индекс Чекановского – Съеренсена составлял 0.26). По типу питания в бентосе под фермой 66 % видов относились к детритофагам, хищников и полифагов было намного меньше, а сестонофаги представлены только одним видом. В обрастании преобладали виды-полифаги – 44 %, видов-детритофагов было в четыре раза меньше, а сестонофагов – в три раза больше, чем в бентосе. Высокой встречаемостью характеризовались обнаруженные на створках и в створках мидий и устриц *Hydroides dianthus* (25 %) и *Polydora websteri* (67 %).

Ключевые слова : Annelida, макрозообентос, личинки Polychaeta, Черное море

Благодарности: работа выполнена в рамках государственного задания ФИЦ ИнБЮМ по темам: «Исследование механизмов управления продукционными процессами в биотехнологических комплексах с целью разработки научных основ получения биологически активных веществ и технических продуктов морского генезиса» (№ гос. регистрации 121030300149-0) и «Закономерности формирования и антропогенная трансформация биоразнообразия и биоресурсов Азово-Черноморского бассейна и других районов Мирового океана» (№ гос. регистрации 121030100028-0). Выражаем благодарность за помощь в сборе материала С. В. Щурову, И. Ю. Еремину, В. А. Гринцову, М. В. Макарову.

Для цитирования: *Лисицкая Е. В., Болтачева Н. А* . Таксономический состав многощетинковых червей района мидийно-устричной фермы (Черное море, Севастополь) // Экологическая безопасность прибрежной и шельфовой зон моря. 2023. № 1. С. 113–123. EDN QQGUXI. doi:10.29039/2413-5577-2023-1-113-123

Introduction

Recently, the number of marine bivalve farms off the Crimean coast has been increasing. Functioning mariculture farms have a complex and contradictory impact on the environment. Bottom communities are particularly affected. This is due to the fact that the products of the farmed molluscs are a source of large amounts of organic matter in the bottom sediments, which leads to changes in the physical-chemical and trophic conditions of invertebrates: both epifauna and infauna [1, 2].

To control the impact of mariculture farms on the environment, long-term studies are carried out of the biota and aquatic environment in the water area of mussel and oyster farms [3]. The scale of the impact can vary depending on the operation duration and production volume as well as on the characteristics of the water area. A 5-fold increase in macrozoobenthos abundance and a 3.2-fold increase in biomass were recorded off the coast of the Caucasus in the area where the mussel farms were operating for five years. In contrast, the species diversity index decreased by an average of 2.7 times [1)]. There is evidence of both a negative impact on zoobenthos under marine farms and absence of such an impact [1, 4, 5]. Thus, mussel and oyster farms are an important habitat-forming factor.

Meanwhile, farm hydraulic engineering systems and structures can be seen as a kind of analogue of artificial reefs. Artificial reefs are known to be located both on the bottom and in the water column. They serve as a substrate for larval settlement of bottom organisms, create shelters for fish and invertebrates, and can attract and concentrate various hydrobionts [1]. Artificial reefs provide conditions for the formation of highly productive communities and the preservation of aquatic biodiversity.

Most published materials on hydrobionts colonising artificial reefs include fish and molluscs [1]. For polychaetes, there is less data and it mainly refers to polychaetes-perforators and mollusc shell foulers [6–9].

The aim of this work is to study the taxa of polychaetes inhabiting the mussel-oyster farming area, namely in the fouling of the farm structures, on the bottom under the farm and in plankton during the pelagic stage of development.

Material and methods

The mussel-oyster farm is located on the outer roadstead of Sevastopol Bay. The coordinates of the farm's outermost points are 44°37′02.2″N 33°29′53.7″E, 44°37′05.6″N 33°29′51.5″E, 44°37′13.3″N 33°30′07.1″E, 44°37′07.8″N 33°30′11.0″E (Fig. 1). The farm occupies a water area of 4 ha, and the depths in the area are 10–16 m.

[1)] Abaev, V.Yu., 2001. [*Impact of Mussel Farming on the Ecosystems of the Anapa Shelf of the Black Sea. Extended Abstract of Doctoral Dissertation*]. Krasnodar, 18 p. (in Russian).

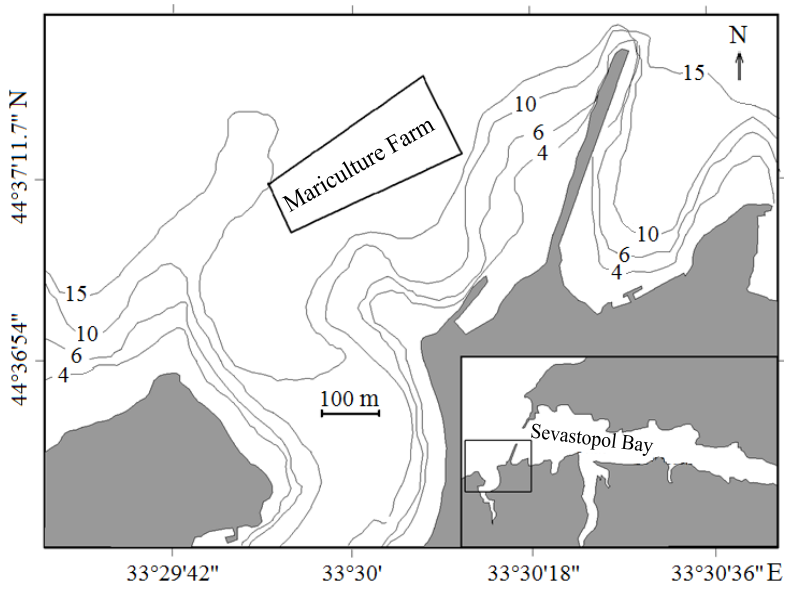

F i g . 1 . Schematic map of the study area

The substrate is silty sand. Mussel collectors were installed in 2014, and in 2015, two lines of oyster cages were also placed in the water area of the mariculture farm. By 2018, the marine farm produced up to 100,000 oysters and 50 tonnes of mussels per year [3, 10].

Macrozoobenthos samples from the substrate were collected monthly under the plantation from April 2015 to May 2016 in duplicate using a grab sampler with a grab area of 0.04 m^2. The material was further processed in the laboratory according to the standard method: it was washed through a sieve (mesh size 0.5 mm), fixed with 4 % formaldehyde solution. Species composition of polychaetes, their density (N, ind.$\cdot m^{-2}$), biomass (B, g$\cdot m^{-2}$) and occurrence (P, %) were determined [6]. Qualitative macrozoobenthos samples (12 collections) were taken under the farm during the summer periods of 2018 and 2019. From the samples, polychaetes were selected and their species was determined. The fouling of the farm structures was also used as study material. Samples were collected four times a year (seasonally) in triplicate in 2017–2018. The fragments of the mussel collectors and oyster cages were placed in baths of fresh water for 15 min, the washes were sieved (gauze mesh size 100 μm), and polychaetes were isolated [11]. The presence of polychaetes in and on the shells of cultured molluscs was taken into account.

Meroplankton was sampled in the water area of the mussel-oyster farm on a monthly basis in 2015–2019. The material was collected with a Juday net (inlet diameter 36 cm, gauze mesh size 135 μm) in the water layer from the bottom to the surface. Polychaete larvae were selected and identified alive using MBS-9 and Mikmed-5 light microscopes [12].

Literature data were used for taxonomic identification and trophic grouping of polychaetes [13–15].

The frequency of species occurrence was calculated as a percentage of the number of samples in which the species was detected in relation to the total number of collected samples. In the polychaete taxocene, species with an occurrence rate of 50 % or more were classified as an index species [2] (according to V. P. Vorobiov, "constant"), species with an occurrence rate of 25 % to 50 % were classified as characteristic ones, and species found at less than 25 % of stations [3] were considered to be rare.

The Sørensen – Czekanowski index was used to assess the similarity of the species composition of polychaetes in different habitats, $I_{cs} = \frac{2c}{a+b}$ where c is the number of species shared by both lists; a and b are the number of species in each list.

Results and discussion

During the study period, 48 polychaete species belonging to 25 families were identified in macrozoobenthos, fouling and plankton samples collected from the mussel-oyster farm area (table). The most numerous species belonged to the families Spionidae (8), Nereididae and Syllidae (5 species each), Syllidae (4). The other families were represented by one or two species.

Among the macrobenthic organisms under the farm, polychaetes of 23 species were found. Twenty-four species of polychaetes were recorded in the fouling of mussel collectors and oyster cages. Larvae of 25 polychaete species were recorded in the plankton during the entire study period [12]. Only two species, *Allita succinea* and *Pholoe inornata*, were shared by all three studied habitats (benthos, fouling and plankton).

The macrozoobenthos under the farm was dominated by small errant forms of polychaetes. The leading species of this taxon (50–100 % occurrence) included *Micronephthys longicornis*, *Heteromastus filiformis*, *Aricidea claudiae*. The occurrence of most species did not exceed 25 %. This taxocene was characterized by low quantitative indices, density ranged from 38–388 ind.·m^{-2}, biomass 0.04–3.13 g·m^{-2}. During 13 months, the mean polychaete density was 232 ± 29 ind.·m^{-2} and biomass was 0.57 ± 0.27 g/m^{-2}. The dominant species was *Micronephthys longicornis* with a maximum density of 260 ind.·m^{-2} and an average density of 145 ± 21 ind.·m^{-2}. This species is common in the Black Sea, it occurs quite often in silty substrates at depths up to 65 m and forms high-density settlements [14]. Out of the large polychaetes, *Nephtys hombergii* was recorded in quantitative collections and *Cirriformia tentaculata* and *Polycirrus jubatus* – in qualitative collections. The first of these species is eurybiontic and widespread. Due to its high settlement density it forms an independent biocenosis in the Black Sea [14]. The other two species are less common, they do not form large aggregations and prefer silty substrates and shallower waters. In general, almost all the polychaetes found in the bottom biotope, with the exception of *Syllis hyalina* and

[2] Zenkevitch, L.A. and Brozky, V.A., 1937. Some Data on the Ecology of Dominants in the Bentos of the Barents Sea. *Uchenye Zapiski MGU*, 13, pp. 203–226 (in Russian).
[3] Vorobiov, V.P., 1949. [*Benthos of the Sea of Azov*]. Simferopol: Krymizdat, 193 p. (in Russian).

Taxonomic composition of polychaetes in the area of mariculture

Taxonomic composition	Occurrence		In plankton
	in benthos, %	in fouling, %	
Alitta succinea (Leuckart, 1847)	8	83	+
Aricidea (Strelzovia) claudiae Laubier, 1967	62	-	-
Capitella capitata (Fabricius, 1780)	8	-	-
Capitellidae g. sp	8	-	+
Chaetozone caputesocis (Saint-Joseph, 1894)	qual.	-	-
Cirriformia tentaculata (Montagu, 1808)	qual.	-	-
Glycera sp.	8	-	-
Ctenodrilus serratus (Schmidt, 1857)	-	17	-
Dorvillea rubrovittata (Grube, 1855)	-	8	-
Eulalia viridis (Linnaeus, 1767)	-	8	-
Eunice vittata (Delle Chiaje, 1828)	qual.	-	-
Phyllodoce sp.	-	17	+
Genetyllis tuberculata (Bobretzky, 1868)	-	-	+
Harmothoe imbricata (Linnaeus, 1767)	-	92	+
Harmothoe reticulata (Claparède, 1870)	-	92	+
Hediste diversicolor (O.F. Müller, 1776)	-	-	+
Heteromastus filiformis (Claparède, 1864)	69	-	-
Hydroides dianthus (Verrill, 1873)	-	25	+
Lagis neapolitana (Claparède, 1869)	qual.	-	+
Lysidice ninetta Aud. Et H. M. Edw., 1833	-	17	+
Malacoceros fuliginosus (Claparède, 1870)	-	-	+
Magelona rosea Moore, 1907	15	-	+
Megadrilus purpureus (Schneider, 1868)	8	-	-
Melinna palmata Grube, 1870	8	-	-
Micronephthys longicornis (Perejaslavtseva, 1891)	100	-	-
Microspio mecznikowiana (Claparède, 1869)	-	-	+
Naineris laevigata (Grube, 1855)	qual.	-	-
Nephtys hombergii Savigny in Lamarck, 1818	23	-	+
Nereis zonata Malmgren, 1867	-	100	+

Continued

Taxonomic composition	Occurrence		In plankton
	in benthos, %	in fouling, %	
Nereididae g.sp.	8	-	+
Paraonidae g. sp.	8	-	-
Perinereis cultrifera (Grube, 1840)	-	33	-
Pholoe inornata Johnston, 1839	qual.	67	+
Phyllodoce mucosa Örsted, 1843	15	8	-
Platynereis dumerilii (Audouin Milne Edwards, 1834)	8	100	-
Polycirrus jubatus Bobretzky, 1868	qual.	-	-
Polydora cornuta Bosc, 1802	-	17	+
Polydora websteri Hartman in Loosanoff & Engle, 1943 *	-	67	+
Polyophthalmus pictus (Dujardin, 1839)	-	8	-
Prionospio cirrifera Wirén, 1883	8	-	-
Prionospio sp.	-	8	+
Protodorvillea kefersteini (McIntosh, 1869)	qual.	-	-
Sabellaria taurica (Rathke, 1837)	-	-	+
Salvatoria clavata (Claparède, 1863)	-	8	
Scolelepis (Scolelepis) squamata (O.F. Muller, 1806)	-	-	+
Spirobranchus triqueter (Linnaeus, 1758)	-	17	-
Spio decorata Bobretzky, 1870	-	-	+
Spionidae g. sp	23	-	+
Spirorbinae g. sp	qual.	qual.	+
Syllis hyalina Grube, 1863	8	8	-
Syllis prolifera Krohn, 1852	-	8	-
Syllidae gen. sp.	-	17	-
Trypanosyllis zebra (Grube, 1860)	-	17	-

* polychaetes found in oyster shells.

Note: "qual." – polychaetes from quality collections; "+" – species is found; "-" – species is not found.

Spirorbinae g. sp., are characteristic of silty substrates. Such substrates predominate in the area of the mussel-oyster farm.

In the area of mussel farms off the coast of the Caucasus (near Anapa) seven polychaete species were recorded [1)], five of which were also found during our survey (*Melinna palmatata*, *Pholoe inornata*, *Platynereis dumerilii*, *Eunice vitlala*, *Nephtys hombergii*). Still, *Mellina palmata* is the dominant species under the farm in the Anapa area, whereas in the Sevastopol area it is *Micronephthys longicornis*.

The species most frequently (50–100 % frequency) recorded in mussel collectors and oyster cages were *Nereis zonata*, *Platynereis dumerilii*, *Alitta succinea* (family Nereididae), as well as *Harmothoe imbricata*, *H. reticulata* (family Polynoidae), *Pholoe inornata* (family Sigalionidae). Characteristic species included *Hydroides dianthus* and *Polydora websteri* found on and in the shells of mussels and oysters. These polychaetes are known to cause significant damage to shellfish mariculture in many areas of the World Ocean [6–9]. These species are recent alien species to the Black Sea and their high occurrence indicates their successful acclimatisation in the Sevastopol water area. It is of interest that species considered very rare for the Black Sea were discovered: *Ctenodrilus serratus*[4)] and *Chaetozone caputexotic* [14].

At a mussel farm off the Caucasian coast of the Black Sea near Sochi, six species of polychaetes were observed in the collector fouling. As in our survey, *Alitta succinea*, *Nereis zonata*, and *Platynereis dumerilii* were common. The highest abundance was recorded for *A. succinea* [5)].

The species composition of taxocenes of polychaetes on the bottom under the farm and in the fouling of the farm structures differed significantly as indicated by the low value of the Sørensen – Czekanowski index (0.26). Out of the 24 polychaete species detected on the mariculture farm structures, 18 were not recorded in the sediments under the farm. The trophic structure of the polychaete taxa in these two habitats was represented by four trophic groupings: deposit feeders, filter feeders, predators and polyphages. However, the quantitative proportion of species in these groupings differed in the biotopes. In the benthos under the farm, the majority of species were deposit feeders. Predators and polyphages were much fewer, and filter feeders were represented by only one species (Fig. 2). The fouling was dominated by polyphagous species, with four times fewer deposit feeder species and three times more filter feeder species than in the benthos. A half of the deposit feeders in the benthos were surface deposit feeders and the other half were subsurface deposit feeders. In the fouling, the deposit feeding grouping is represented only by subsurface deposit species.

[4)] Yakubova, L.I., 1930. List of Archannelidae and Polychaeta in Sevastopol Bay of the Black Sea. *Izvestiya AN SSSR. Series 7. Otdeleniye Fiziko-Matematicheskikh Nauk*, (9), pp. 863–881 (in Russian).

[5)] Yakhontova, I.V., 2008. [*Community of Mussel Collector Fouling in the Eastern Black Sea. Extended Abstract of Ph. D. Dissertation, Biological Sciences*]. Moscow: VNIRO, 25 p. (in Russian).

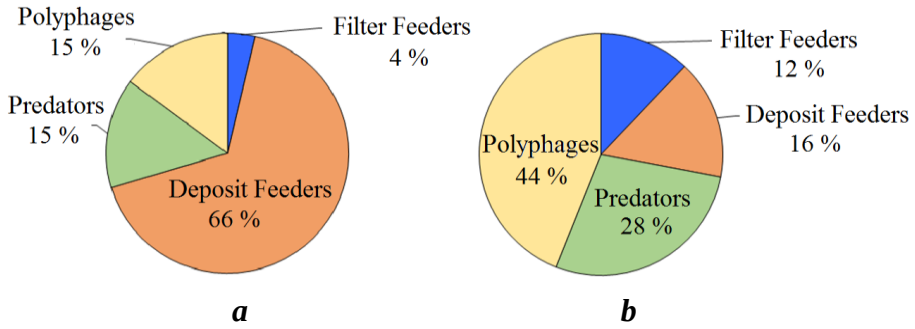

Fig. 2. Trophic structure of polychaetes taxocene in the benthos under the farm (*a*) and on the collectors (*b*)

Thus, the difference in the taxonomic composition of polychaetes in the benthos under the farm and on the collectors is due to the significant difference in these substrates as well as the trophic preferences of the species inhabiting these biotopes.

Pelagic larvae of polychaete worms were found in the mariculture area as well as in adjacent areas off the coast of southwestern Crimea during all seasons of the year [16]. Their taxonomic composition corresponded to the periods of adult reproduction. In winter, the plankton was dominated by larvae of *Harmothoe imbricata*; in spring, their diversity increased, with the appearance of *Harmothoe reticulata*, *Pholoe inornata*, *Allita succinea*, and *Nereis zonata*. In summer, the *Nephtys hombergii* nectochaetes dominated. Larvae of polychaetes of the family Spionidae (*Polydora cornuta*, *Malacoceros fuliginosus*, *Spio decorata*, *Prionospio* sp.) dominated in plankton from April to October. Larvae of polychaetes that settle on and in the shells of growing molluscs were recorded: *Polydora websteri* – from June to October, *Hydroides dianthus* – in October to November [12]. Seven species of Polychaeta were found in plankton alone, three of them – *Malacoceros fuliginosus*, *Scolepis squamata*, *Microspio mecznikowiana* – are relatively rare for the Black Sea. The polychaete *Sabellaria taurica* inhabits a peculiar biotope (sand with coarse shells) that is not represented in the study area.

Since many polychaete species have a pelagic developmental stage in their life cycle, the formation of polychaete taxa in the fouling of farm structures is mainly due to the deposition of larvae from plankton in mariculture waters. The similarity of polychaete taxa of the fouling and plankton is significantly higher than that of the fouling and benthos as indicated by the Sørensen – Czekanowski index (0.50).

Conclusion

A total of 48 polychaete species were identified from surveys carried out in 2015–2019 in the area of the mussel-oyster farm. However, 23 species were found on the bottom under the farm, 24 – in the fouling of mussel collectors and oyster cages, and the larvae of 25 polychaete species – in plankton. Recent alien species were noted: *Hydroides dianthus* and *Polydora websteri*, as well as species

rare for the Black Sea: *Ctenodrilus serratus* and *Chaetozone caputexotic*. The polychaete taxocenes are distinctive in each of the studied biotopes. The species compositions of polychaete taxa on the bottom under the farm and in the farm structure fouling differed significantly (the Sørensen – Czekanowski index being 0.26). On the mariculture farm structures, 18 species of polychaete worms were found that were not recorded in the bottom sediments under the farm. In the benthos under the farm, 66 % of the species were deposit feeders. Predators and polyphages were much fewer, and filter feeders were represented by only one species. Polyphagous species predominated in the fouling with 44 %, deposit feeders were four times fewer and filter feeders were three times more than in the benthos. Thus, the creation of a mussel-oyster farm, which provides additional substrate for polychaetes and the settlement of their pelagic larvae, contributes to the species richness of Polychaeta in the study area.

REFERENCES

1. Aleksandrov, B.G., 2008. *The Hydrobiological Basis for Managing of the Black Sea Coastal Ecosystems State*. Kiev: Naukova dumka, 343 p. (in Russian).
2. Kruglikov, O.E. and Ivanov, M.V., 2008. [Effect of the Sonostrov Mussel Farm on Benthos Communities]. In: M. P. Kirpichnikov, ed., 2008. [*Proceedings of the Scienific Conference Dedicated to the 70th Anniversary of N. A. Pertsov Belomor Biological Station, 9–10 August 2008*]. Moscow: Izd. "Grif i K", pp. 70–74 (in Russian).
3. Kapranov, S.V., Kovrigina, N.P., Troshchenko, O.A. and Rodionova, N.Yu., 2020. Long-Term Variations of Thermohaline and Hydrochemical Characteristics in the Mussel Farm Area in the Coastal Waters off Sevastopol (Black Sea) in 2001–2018. *Continental Shelf Research*, 206, 104185. doi:10.1016/j.csr.2020.104185
4. Ivanov, M.V. and Chivilev, S.M., 2007. The Long-Term Benthic Succession under the White Sea Mussel Farms. *Vestnik of Saint Petersburg University. Series 3. Biology*, (4), pp. 63–72 (in Russian).
5. Boltacheva, N.A., Makarov, M.V., Bondarenko, L.V. and Kovaleva, M.A., 2018. The Macrozoobenthos under Clam Farm (the Black Sea, Sevastopol Region). *Marine Biological Journal*, 3(1), pp. 9–22. doi:10.21072/mbj.2018.03.1.02 (in Russian).
6. Rodewald, N., Snyman, R. and Simon, C.A., 2021. Worming its Way in – *Polydora websteri* (Annelida: Spionidae) Increases the Number of Non-Indigenous Shell-Boring Polydorin Pests of Cultured Molluscs in South Africa. *Zootaxa*, 4969(2), pp. 255–279. doi:10.11646/zootaxa.4969.2.2
7. Sun, Y., Wong, E., Keppel, E., Williamson, J.E. and Kupriyanova, E.K., 2017. A Global Invader or a Complex of Regionally Distributed Species? Clarifying the Status of an Invasive Calcareous Tubeworm *Hydroides dianthus* (Verrill, 1873) (Polychaeta: Serpulidae) Using DNA Barcoding. *Marine Biology*, 164, 28. doi:10.1007/s00227-016-3058-9
8. Martinelli, J.C., Lopes, H.M., Hauser, L., Jimenez-Hidalgo, I., King, T.L., Padilla-Gamiño, J.L., Rawson, P., Spencer, L.H., Williams, J.D. et al., 2020. Confirmation of the Shell-Boring Oyster Parasite *Polydora websteri* (Polychaeta: Spionidae) in Washington State, USA. *Scientific Reports*, 10, 3961. doi:10.1038/s41598-020-60805-w
9. Waser, A.M., Lackschewitz, D., Knol, J., Reise, K., Wegner, K.M. and Thieltges, D.W., 2020. Spread of the Invasive Shell-Boring Annelid *Polydora websteri* (Polychaeta, Spionidae) into Naturalised Oyster Reefs in the European Wadden Sea. *Marine Biodiversity*, 50, 63. doi:10.1007/s12526-020-01092-6

10. Pospelova, N.V., Priimak, A.S. and Ryabushko, V.I., 2021. Chemical Composition of Mussel Mytilus galloprovincialis Cultivated at the Seashore of Sevastopol (Black Sea). *Ecological Safety of Coastal and Shelf Zones of Sea*, (4), pp. 67–80. doi:10.22449/2413-5577-2021-4-67-80 (in Russian).
11. Lisitskaya, E.V. and Shchurov, S.V., 2020. The Polychaetes Role in Fouling Community on the Mussel-Oysters Farm (Crimea, the Black Sea). *Problems of Fisheries*, 21(1), pp. 74–83 (in Russian).
12. Lisitskaya, E.V., 2017. Taxonomic Composition and Seasonal Dynamics of Meroplankton in the Area of Mussel-Oyster Farm (Sevastopol, Black Sea). *Marine Biological Journal*, 2(4), pp. 38–49. doi:10.21072/mbj.2017.02.4.04 (in Russian).
13. Kiseleva, M.I., 1981. [*Benthos of Soft Bottoms of the Black Sea*]. Kiev: Naukova dumka, 168 p. (in Russian).
14. Kiseleva, M.I., 2004. *Polychaetes (Polychaeta) of the Azov and Black Seas*. Apatity: Izd-vo Kol'skogo Nauchnogo Tsentra RAN, 409 p. (in Russian).
15. Jumars, P.A., Dorgan, K.M. and Lindsay, S.M., 2015. Diet of Worms Emended: an Update of Polychaete Feeding Guilds. *Annual Review of Marine Science*, 7, pp. 497–520. doi:10.1146/annurev-marine-010814-020007
16. Ryabushko, V.I., Shchurov, S.V., Kovrigina, N.P., Lisitskaya, E.V. and Pospelova, N.V., 2020. Comprehensive Research of the Environmental Status of Coastal Waters of Sevastopol (Western Crimea, Black Sea). *Ecological Safety of Coastal and Shelf Zones of Sea*, (1), pp. 104–119. doi:10.22449/2413-5577-2020-1-103-118 (in Russian).

Submitted 28.07.2022; accepted after review 2.12.2023;
revised 1.02.2023; published 24.03.2023

About the authors:

Elena V. Lisitskaya, Senior Research Associate, A.O. Kovalevsky Institute of Biology of the Southern Seas of RAS (2 Nakhimov Av., Sevastopol, 299011, Russian Federation), Ph.D. (Biol.), **ORCID ID: 0000-0002-8219-4616, Scopus Author ID: 6504112143, ResearcherID: T-1970-2017,** *e.lisitskaya@gmail.com*

Natalya A. Boltachova, Leading Research Associate, A.O. Kovalevsky Institute of Biology of the Southern Seas of RAS (2 Nakhimov Av., Sevastopol, 299011, Russian Federation), Ph.D. (Biol.), **ORCID ID: 0000-0003-0618-1992, Scopus Author ID: 36149089700,** *nboltacheva@mail.ru*

Contribution of the authors:

Elena V. Lisitskaya – statement of the research problem, analysis of the composition and abundance of polychaete worms in the fouling and plankton, formation of the article

Natalya A. Boltachova – analysis of the composition and abundance of polychaete worms in the bentos, preparation of graphic materials, editing of the manuscript

All the authors have read and approved the final manuscript.

Original article **DOI**: 10.29039/2413-5577-2023-1-124-136

Effect of Bicomponent ZnO-$ZnFe_2O_4$ Nanoparticles on Mediterranean Mussel (*Mytilus galloprovincialis*) Hemocytes under *in vitro* Conditions

M. S. Podolskaya [1]*, A. A. Tkachuk [1], A. Yu. Andreyeva [1], E. S. Kladchenko [1], E. S. Chelebieva [1], A. A. Mosunov [2]

[1] *A.O. Kovalevsky Institute of Biology of the Southern Seas of RAS, Sevastopol, Russia*

[2] *Sevastopol State University, Sevastopol, Russia*

**e-mail: podolskaya_m99@bk.ru*

Abstract

The present work investigates the toxic effect of bicomponent ZnO-$ZnFe_2O_4$ nanoparticles, which are the main active component of the domestic antifouling coating, on marker indicators of Mediterranean mussel (*Mytilus galloprovincialis*) hemolymph cells (hemocytes) under *in vitro* experimental conditions. The following indicators were evaluated: mortality, cellular composition and production of reactive oxygen species. In the experiment, hemocytes were incubated for 1 and 2 hours in 1 mL of sterile seawater containing nanoparticles of different concentrations: 0.03, 0.3 and 3 mg/mL. The data were analyzed using the flowing cytometry. It was shown that ZnO-$ZnFe_2O_4$ nanoparticles had an effect on the cellular composition of the hemolymph: the proportion of agranulocytes decreased and hour exposure to 0.03 mg/mL nanoparticles reduced the level of production of reactive oxygen species by 2.5 times compared to the control ($p \leq 0.05$). Incubation of hemocytes with a maximum concentration of nanoparticles (3 mg/mL) led to cell death within 1 hour after exposure. No acute toxic effects on hemocytes with the use of 0.03 mg/mL and 0.3 mg/mL of zinc oxide and zinc ferrite nanoparticles were observed.

Keywords: nanoparticles, Mediterranean mussel, hemocytes, reactive oxygen species

Acknowledgements: the synthesis of nanoparticles (ZnO-$ZnFe_2O_4$) was carried out under RSF project no. 21-13-00498 “Environmentally safe and highly effective antifouling coatings based on bicomponent metal nanoparticles and their oxides”. Assessment of the toxicity of nanoparticles on the body of mussels (analysis of hemocyte parameters) was carried out at the expense of the state task of FRC IBSS No. 121102500161-4 “Patterns of the organization of the immune system of commercial hydrobionts and the study of the influence of environmental factors on the functioning of their protective systems”.

For citation: Podolskaya, M.S., Tkachuk, A.A., Andreyeva, A.Yu., Kladchenko, E.S., Chelebieva, E.S. and Mosunov, A.A., 2023. Effect of Bicomponent ZnO-$ZnFe_2O_4$ Nanoparticles on Mediterranean Mussel (*Mytilus galloprovincialis*) Hemocytes under *in vitro* Conditions. *Ecological Safety of Coastal and Shelf Zones of Sea*, (1), pp. 124–136. doi:10.29039/2413-5577-2023-124-136

Влияние бикомпонентных наночастиц ZnO-$ZnFe_2O_4$ на гемоциты средиземноморской мидии (*Mytilus galloprovincialis*) в условиях эксперимента *in vitro*

М. С. Подольская [1]*, А. А. Ткачук [1], А. Ю. Андреева [1], Е. С. Кладченко [1], Э. С. Челебиева [1], А. А. Мосунов [2]

[1] *Институт биологии южных морей имени А.О. Ковалевского РАН, Севастополь, Россия*

[2] *Севастопольский государственный университет, Севастополь, Россия*
**e-mail: podolskaya_m99@bk.ru*

Аннотация

Исследовано токсическое действие бикомпонентных наночастиц ZnO-$ZnFe_2O_4$, являющихся основным действующим компонентом отечественного противообрастающего покрытия, на маркерные показатели клеток гемолимфы (гемоциты) средиземноморской мидии (*Mytilus galloprovincialis*) в экспериментальных условиях *in vitro*. Оценивались следующие показатели: смертность, клеточный состав и продукция активных форм кислорода. В эксперименте гемоциты инкубировали в течение 1 и 2 ч в 1 мл стерильной морской воды, содержащей наночастицы в различных концентрациях: 0.03, 0.3 и 3 мг/мл. Данные анализировали с помощью метода проточной цитометрии. Установлено, что действие наночастиц ZnO-$ZnFe_2O_4$ оказало влияние на клеточный состав гемолимфы: снижалась доля агранулоцитов, воздействие 0.03 мг/мл наночастиц при часовой инкубации снижало уровень продукции активных форм кислорода в 2.5 раза по сравнению с контрольной пробой ($p \leq 0.05$). Инкубация гемоцитов с максимальной концентрацией наночастиц (3 мг/мл) привела к гибели клеток уже через 1 ч после воздействия. Острого токсического воздействия на гемоциты при применении 0.03 мг/мл и 0.3 мг/мл наночастиц оксида цинка и феррита цинка не наблюдалось.

Ключевые слова: наночастицы, средиземноморская мидия, гемоциты, АФК

Благодарности: синтез наночастиц (ZnO-$ZnFe_2O_4$) был выполнен в рамках выполнения проекта РНФ № 21-13-00498 «Экологически безопасные и высокоэффективные противообрастающие покрытия на основе бикомпонентных наночастиц металлов и их оксидов». Оценка токсичности наночастиц на организм мидий (анализ параметров гемоцитов) проводился за счет средств госзадания ФИЦ ИнБЮМ № 121102500161-4 «Закономерности организации иммунной системы промысловых гидробионтов и исследование влияния факторов внешней среды на функционирование их защитных систем».

Для цитирования: Влияние бикомпонентных наночастиц ZnO-$ZnFe_2O_4$ на гемоциты средиземноморской мидии (*Mytilus galloprovincialis*) в условиях эксперимента *in vitro* / М. С. Подольская [и др.] // Экологическая безопасность прибрежной и шельфовой зон моря. 2023. № 1. С. 124–136. EDN BPTQRT. doi:10.29039/2413-5577- 2023-124-136

Introduction

Biofouling is a natural process involving the attachment of micro- and macroorganisms to various substrates in the aquatic environment [1)]. Moreover, habitation of fouling organisms on the surfaces of hydraulic structures causes significant damage to shipping, oil platforms and industry as a whole [1, 2]. Global damage from marine fouling currently exceeds $50 billion per year [3]. The main task of antifouling coatings is to prevent the formation of a biological film, which is the first stage of biofouling [4]. At the same time, such coatings must be safe with respect to non-target organisms. Antifouling coatings widely used in the past were based on such biocides as tributyltin and copper, which proved to be highly toxic to marine organisms and were disallowed [5–7].

One of the innovative methods of protection against biofouling is the use of coatings based on metal oxide nanostructures [8]. The most commonly used nanoparticles are of such metals as zinc, aluminum, iron, titanium, silver and copper, as well as their oxides [9]. These nanoparticles have proven antibacterial, anticorrosive and antifouling properties [10].

Their low toxicity to aquatic organisms is an important quality of new antifouling components. Nevertheless, the data available in the publications are insufficient to make an unambiguous conclusion about the toxicity of nanoparticles to marine organisms. It is known that the toxicity of nanoparticles depends on the type of metal, size, shape and surface charge of the particles [11]. Among possible mechanisms of the toxic effect of nanoparticles on the organisms of hydrobionts, it is possible to single out the production of reactive oxygen species (ROS), which is a consequence of the disproportionately large surface area of nanoparticles [12]. ROS overproduction, which exceeds the ability of cells to provide antioxidant protection, causes oxidative stress, which leads to disturbances in the structure of the cell membrane, mitochondria, and oxidation of proteins and DNA [13, 14]. Thus, a study of aluminum oxyhydroxide (boehmite) exposure to nanoparticles revealed no acute toxicity to *Daphnia magna* (Straus, 1820) [15]. At the same time, the study of titanium dioxide nanoparticles showed the ability of nanoparticles to accumulate in the bodies of daphnia [16]. The impact of copper oxide nanoparticles led to the behavior disorder of the mollusk *Scrobicularia plana* (da Costa, 1778) [17]. Also, the impact of zinc oxide nanoparticles had a negative influence on the development of marine fish *Oryzias melastigma* larvae (McClelland, 1839) [18].

Currently, the development of antifouling coatings based on nanoparticles is considered to be a promising area. Previously, a new antifouling paint component was created, which contained $ZnO\text{-}ZnFe_2O_4$ nanoparticles obtained

---

[1)] Korobkov, V.A., Levin, V.S., Lukoshkov, A.V. and Serebrenitsky, P.P., 1981. [*Underground Technology*]. Leningrad: Sudostroenie, 240 p. (in Russian).

by electrical explosion of twisted zinc and iron wires in oxygen-containing atmosphere. ZnO nanoparticles are able to absorb visible light and inhibit the growth of microorganisms due to the photocatalytic process [19]. The composition is a domestic development and has proven antifouling properties [20], but there is no data on its safety in relation to marine organisms. Since the method we use to obtain nanoparticles is quite original [21], and, as we know, the particles of the studied composition were obtained for the first time, detailed studies of their physical and chemical properties, as well as the mechanisms of biological action, provide the subject for our future research.

Bivalve molluscs are convenient model objects to study the effect of nanoparticles, as they lead an attached mode of life and are filter-feeding organisms [22]. The functional state of molluscs is assessed by morphological and physiological parameters of hemolymph cells, hemocytes, which, in turn, are cellular immunity effectors [23]. The cellular immune response is based on the production of reactive oxygen species (ROS) by hemocytes, phagocytosis and encapsulation of foreign substances [24, 25]. Mollusc hemocytes react to the action of stimuli with a respiratory burst, which represents a sharp increase in the production of ROS by cells that cause oxidative stress in pathogenic organisms [26]. Hemocytes are a generally accepted model to assess the physiological state of molluscs [6].

Studying the toxicity of new paint components based on nanoparticles, determining acceptable concentration ranges, and understanding the effect of nanoparticles on immune system effectors form a relevant objective. In connection with the above, the purpose of this work is to evaluate the toxic effect of ZnO-$ZnFe_2O_4$ nanoparticles on the functional parameters of hemocytes of the hemolymph of the bivalve mollusc *Mytilus galloprovincialis*.

Materials and Methods

Mature, four years old mussels (*M. galloprovincialis*) weighing 12.9 ± 2.3 g, 57.8 ± 1.8 mm in size, were selected in the amount of 210 pieces in the Sevastopol coastal area (water temperature 15–20 °C, salinity 17–18 PSU, oxygen content 7.2–8.5 mg/L). The mussels were delivered to the laboratory in plastic containers with no water. The molluscs were acclimated to laboratory conditions in aquaria with a stocking density of 3–5 L per individual for 7 days. The conditions close to the point of material collection were maintained in the aquaria: temperature 23.3 ± 0.1 °C; salinity 18.2 ± 0.02 PSU; pH 8.1 ± 0.01; oxygen ontent 7.7 ± 0.1 mg/L. The oxygen content and water temperature were monitored using a portable oxygen meter with a temperature sensor *ST*300*D* (Ohaus, USA). Salinity and pH were controlled using a portable conductometer-salinometer sensION 5 HACH (USA) and pH-meter ST2100-F (Ohaus, USA). Throughout the experiment, including the period of acclimation to laboratory conditions, the water was changed daily to remove metabolites while maintaining the salinity value. The molluscs were fed with a mixture of microalgae *Tetraselmis viridis* (strain IBSS-25 from the collection of the IBSS FRC Department of Biotechnology and Phytoresources)

at a rate of 5–10 mL of the mixture for every 50 L of aquarium water. After acclimation, the hydrobionts were divided into 7 groups of 30 individuals in each group (one control group, three groups with incubation for 1 hour (groups 1.1, 1.2, and 1.3), three groups with incubation for 2 hours (groups 2.1, 2.2, and 2.3).

The effect of nanoparticles on mollusk hemocytes was studied under *in vitro* conditions. For this purpose, hemolymph was taken with a sterile syringe from the adductor muscle of 10 individuals and combined into one sample. To obtain hemocytes, the composite sample was washed three times in sterile sea water by centrifugation (500 g, 5 min). The pellet was used for further analysis. All work on washing and preparing cells for analysis was carried out at +4 °C to prevent cell adhesion.

In the experiment, the cells were incubated in 1 mL of sterile sea water containing nanoparticles. Each sample contained $1 \cdot 10^6$ cells/mL. Different concentrations of bimetallic $ZnO\text{-}ZnFe_2O_4$ nanoparticles synthesized under the Russian Science Foundation project were used: 0.03 (the concentration is 10 times lower than the active one), 0.3 (the active concentration of the developed antifouling mixture) and 3 (the concentration is 10 times higher than the active one) mg/mL. Cells were incubated in a thermoshaker with cooling for microtubes (Biosan TS-100C) at +4 °C and 1,000 rpm. One part of the hemocyte samples in the range of the studied concentrations of nanoparticles (groups 1.1 (the concentration of nanoparticles in the sample is 0.03 mg/mL), 1.2 (0.3 mg/mL), and 1.3 (0.03 mg/mL)) was incubated for 1 h, the other one (groups 2.1 (the concentration of nanoparticles in the sample is 0.03 mg/mL), 2.2 (0.3 mg/mL), and 2.3 (0.03 mg/mL)) – for 2 h. A sample of hemocytes in sea water without nanoparticles served as a control. After incubation, the cells of the experimental samples were washed from nanoparticles in sterile sea water by centrifugation (500 g, 5 min).

Analysis of the functional parameters of hemocytes was carried out on a flow cytometer Cytomics FC 500 (Beckman Coulter, USA), equipped with a single-phase argon laser (wavelength 488 nm). For analysis by flowing cytometry, a suspension was prepared with a concentration of hemocytes $(1–2) \cdot 10^6$ cells per 1 mL.

To identify the types of hemocytes, the prepared suspension of hemolymph cells was stained with the dye SYBR Green I (SGI). The final concentration of SGI in the sample makes 10 μmol/L. Stained cells were incubated for 40 min in the dark at +4 °C. The content of DNA in hemocytes was analyzed on the basis of histograms of the dye fluorescence distribution in channel *FL*1 using the program *Flowing Software* 5.2. The abscissa axis on the histogram of the dye fluorescence distribution displayed the DNA content in the cells, and the ordinate axis – the number of cells.

The ability of hemocytes to spontaneous production of ROS was evaluated based on the assessment of the fluorescence intensity of the 2-7-dichlorofluorescein-diacetate (*DCF-DA*) dye. Then, 1 mL of hemocyte suspensions were incubated with 10 μl of *DCF-DA* solution for 40 min in the dark. The final dye concentration in the sample made 10 μmol/L. The dye fluorescence was analyzed in channel *FL*1.

Hemocyte survivorship rate was determined using propidium iodide (PI), a fluorescent dye for nucleic acids. 10 µl of PI solution (Sigma Aldrich) was added to 1 mL of hemocyte suspension and incubated in the dark for 40 min at 4 °C. The proportion of dead cells in the total number of hemocytes was estimated from PI fluorescence histograms in channel *FL2* of the cytometer.

When processing the results, the normality of the distribution was controlled using the Kolmogorov–Smirnov test. Differences among the groups were analyzed using *RStudio* software version 4.1.0.

The distribution of functional parameters of hemocytes did not obey the normal distribution law, so the data were analyzed using the nonparametric Mann–Whitney test. The results are expressed as mean ± standard error of the mean.

Results

Significant differences between the control (hemocyte sample in sea water without nanoparticles) and experimental (hemocyte samples with different concentrations of nanoparticles and incubation time (groups 1.1, 1.2, 1.3, 2.1, 2.2 and 2.3) groups of hemocytes in terms of the number of dead cells were not detected, although there was a tendency towards an increase in their number as a result of exposure to nanoparticles (Fig. 1).

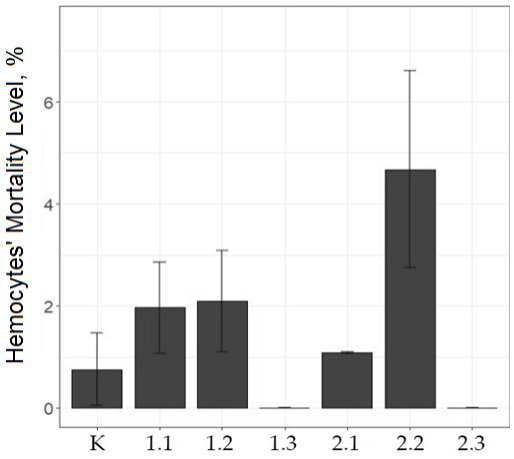

Fig. 1. Effect of ZnO-$ZnFe_2O_4$ nanoparticles on the mortality of Mediterranean mussel (*M. galloprovincialis*) hemocytes. K – control; 1.1 – incubation 1 h, concentration 0.03 mg/mL; 1.2 – incubation 1 h, concentration 0.3 mg/mL; 1.3 – incubation 1 h, concentration 3 mg/mL; 2.1 – incubation 2 h, concentration 0.03 mg/mL; 2.2 – incubation 2 h, concentration 0.3 mg /mL; 2.3 – incubation 2 h, concentration 3 mg/mL

Since the dye enters the cells through the damaged membrane, the absence of data on the diagram at the maximum concentration (3 mg/mL) indicates that the hemolymph cells were destroyed and died right after the first hour of exposure and were removed by other hemocytes through phagocytosis.

Fig. 2 and 3 show the effect of nanoparticles on the size and granularity of mussel hemolymph cells. No significant differences revealed among the groups may indicate that the nanoparticles present in the samples did not have any significant effect on the size and granularity of hemocytes. However, there was a tendency towards a decrease in the size of agranulocytes with an increase in the concentration of nanoparticles.

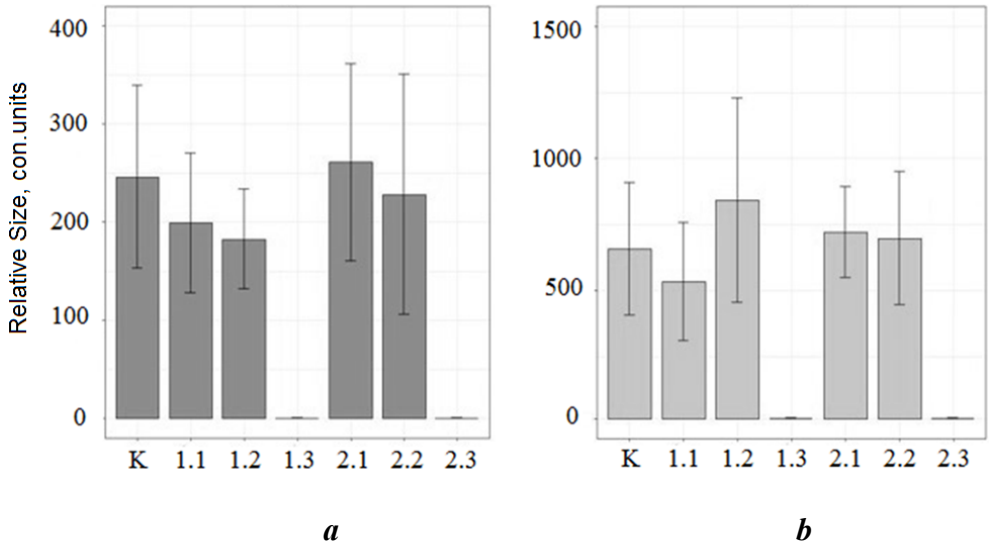

F i g . 2 . Effect of ZnO-$ZnFe_2O_4$ nanoparticles on the relative size of hemocytes of Mediterranean mussel (*M. galloprovincialis*): *a* – that of agranulocytes; *b* – that of granulocytes. For the other nomenclatures see Fig. 1

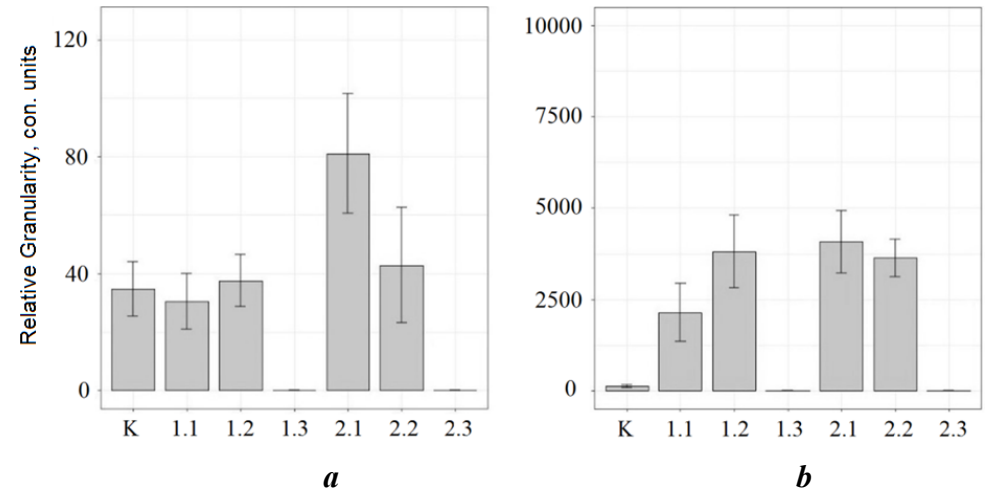

F i g . 3 . The effect of ZnO-$ZnFe_2O_4$ nanoparticles on the relative granularity of Mediterranean mussel (*M. galloprovincialis*) hemocytes: *a* – that of agranulocytes; *b* – that of granulocytes. For the other nomenclatures see Fig. 1

As a result of the incubation of hemocytes with nanoparticles, there were slight changes in the level of relative granularity of hemocytes: the values of lateral scattering in agranulocytes increased with an increase in the concentration of nanoparticles, while in granulocytes, on the contrary, there was a tendency to an increase in the level of the cytoplasm granularity depending on the concentration (Fig. 3). At the same time, changes in the values of side scattering between the control and experimental groups were not significant.

Nanoparticles affected the spontaneous production of ROS by hemolymph cells significantly. The fluorescence intensity of agranulocytes and granulocytes stained with *DCF-DA* fluorescent dye decreased depending on the concentration of nanoparticles in the medium (Fig. 4). The production of ROS by agranulocytes decreased by 2.5 times from 182.3 ± 69.7 relative fluorescence units (RFU) in the control sample to 72.1 ± 28.2 RFU in a sample with an hourly incubation containing nanoparticles with the concentration of 0.03 mg/mL ($p \leq 0.05$). An increase in the production of ROS was observed only during a two-hour *incubation* when both populations of cells were exposed to nanoparticles with the concentration of 0.3 mg/mL. Nevertheless, the changes were statistically insignificant.

Discussion

The results of the work indicate that the active concentration of nanoparticles (0.3 mg/mL) did not have any significant effect on the hemocytes of the Mediterranean mussel *M. galloprovincialis*. No significant differences in the functional parameters of cells were revealed between the control and experimental groups.

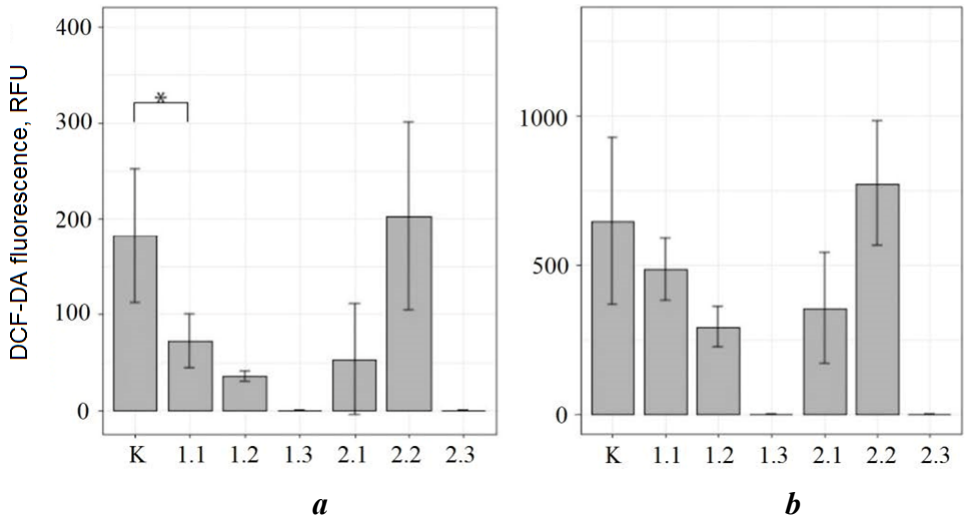

Fig. 4. The effect of $ZnO\text{-}ZnFe_2O_4$ nanoparticles on DCF-DA fluorescence intensity of the Mediterranean mussel (*M. galloprovincialis*) hemocytes: *a* – in agranulocytes, relative fluorescent units, RFU; *b* – in granulocytes, RFU. For the other nomenclatures see Fig. 1

There was a tendency towards an increase in the proportion of granulocytes and a decrease in the proportion of agranulocytes. A slight increase in cell size and granularity was also observed. The concentration of nanoparticles 10 times lower than the active one (0.03 mg/mL) also had no significant effect on the functional parameters of mussel hemocytes. At the same time, exposure to nanoparticles during one-hour incubation reduced the level of the production of ROS by 2.5 times compared to the control sample. Incubation of hemocytes with a concentration of nanoparticles 10 times higher than the active one (3 mg/mL) led to cell death as early as 1 h after exposure.

It is known that hemocytes of bivalve molluscs play an important functional role in the organism, being responsible for cell-mediated immunity through phagocytosis and production of cytotoxic molecules of various nature [23]. During the incubation of hemocytes with nanoparticles, there was a tendency to increase the size and degree of granularity of hemocytes, which may indicate active phagocytosis of nanoparticles. In this case, the formation of phagosomes with nanoparticles led to an increase in the heterogeneity of the content of the hemocyte cytoplasm and, as a consequence, to an increase in the lateral scattering index. Changes in the shape of cells containing different amounts of nanoparticles also affected the amount of sample direct scattering. Intense absorption of nanoparticles by hemocytes is likely to be able to reduce the overall phagocytic capacity of hemocytes, which can lead to the weakening of the innate immune system of bivalves [27]. Similarly to our results, the effect of Ag and TiO_2 nanoparticles on the hemolymph of the oyster *Crassostrea virginica* also led to a decrease in cell phagocytosis after 2 h of exposure [28].

An increase in the concentration of nanoparticles in the one-hour incubation group led to a decrease in the production of ROS, while in the two-hour group, on the contrary, it induced the production of ROS (Fig. 4). Since nanoparticles are able to independently generate ROS, an increase in ROS content in cells should be considered as the development of oxidative stress in hemocytes [29, 30]. It is also known that nanoparticles taken up by hemocytes can affect immune functions such as phagocytosis and production of ROS [31]. At the same time, it was revealed that phagocytosis of foreign particles causes an increase in the production of ROS [32]. Mitochondria are the main source of ROS [33]. The production of ROS by hemocytes is an important protective function of the innate immunity of bivalves. Once inside the cell, nanoparticles can depolarize the mitochondrial membrane and disrupt its functions [29]. In response to this exposure, mitochondria increase the production of ROS, causing oxidative stress [34]. As it is known, phagocytosis is an energy-consuming process, and this can also be the cause of ROS generation [35]. Previously, a study of the effect of carbon soot nanoparticles on hemocytes of the mussel *M. galloprovincialis* under *in vitro* conditions for 0.5–4 h (1–10 μg/mL) also showed an increase in the production of ROS in the cell [23]. On the contrary, in another study by the same researcher devoted to the effect of TiO_2 and SiO_2 nanoparticles on the mussel hemocytes, no significant toxic effect on the cell was revealed [36]. When mussel hemocytes were exposed to TiO_2 nanoparticles, a significant increase in the production of ROS

and a decrease in the membrane potential of mitochondria, which were observed when exposed to maximum concentrations, were noted [35].

Conclusion

Thus, it can be concluded that the toxicity of nanoparticles mainly depended on their concentration and time of exposure. The results showed that an acute toxic effect occurred with a concentration of 3 mg/mL, at which cell death took place within an hour of incubation. In groups 1.1, 1.2 and 1.3 with hourly incubation, a decrease in the production of ROS was observed, and in groups 2.1, 2.2 and 2.3 with two-hour incubation, on the contrary, it increased, which may indicate the mechanisms of cell adaptation to stress. No specific cell response was observed when exposed to nanoparticles with concentrations of 0.03 and 0.3 mg/mL, which makes it possible to use such concentrations in the aquatic environment.

REFERENCES

1. Zvyagintsev, A.Y., Poltarukha, O.P. and Maslennikov, S.I., 2015. Fouling on Technical Water Supply Marine Systems and Protection Method Analysis of Fouling on Water Conduits (Analitical Review). *Water: Chemistry and Ecology*, (1), pp. 30–51 (in Russian).
2. Abacharaev, M.M. and Abacharaev, I.M., 2011. Perspective Developments on Marine Fouling Control. *Vestnik of Astrakhan State Technical University. Series: Marine engineering and technologies*, (3), pp. 7–9 (in Russian).
3. Zvyagintsev, A.Yu., 2005. *Marine Fouling in the North-West Part of Pasific Ocean*. Vladivostok: Dalnauka, 432 p. (in Russian).
4. Nurioglu, A.G., Esteves, A.C.C. and de With, G., 2015. Non-Toxic, Non-Biocide-Release Antifouling Coatings Based on Molecular Structure Design for Marine Applications. *Journal of Materials Chemistry B*, 3(32), pp. 6547–6570. doi:10.1039/C5TB00232J
5. Castritsi-Catharios, J., Alambritis, G., Miliou, H., Cotou, E. and Zouganelis, G., 2014. Comparative Toxicity of "Tin Free" Self-Polishing Copolymer Antifouling Paints and Their Inhibitory Effects on Larval Development of a Non-Target Organism. *Materials Sciences and Applications*, 5, pp. 158–169. doi:10.4236/msa.2014.53020
6. Meador, J.P., 2000. *Predicting the Fate and Effects of Tributyltin in Marine Systems*. In: G. W. Ware, ed., 2000. Reviews of Environmental Contamination and Toxicology. New York: Springer. Vol. 166, pp. 1–48.
7. Legg, M., Yücel, M.K., Garcia de Carellan, I., Kappatos, V., Selcuk, C. and Gan, T.H., 2015. Acoustic Methods for Biofouling Control: A Review. *Ocean Engineering*, 103, pp. 237–247. doi:10.1016/j.oceaneng.2015.04.070
8. Shanmugasundaram, T., Radhakrishnan, M., Gopikrishnan, V., Pazhanimurugan, R. and Balagurunathan, R., 2013. A Study of the Bactericidal, Anti-Biofouling, Cytotoxic and Antioxidant Properties of Actinobacterially Synthesised Silver Nanoparticles. *Colloids and Surfaces B: Biointerfaces*, 111, pp. 680–687. doi:10.1016/j.colsurfb.2013.06.045
9. Lozhkomoev, A.S., Bakina, O.V., Glazkova, E.A., Svarovskaya, N.V. and Lerner, M.I., 2018. Patterns of the Formation of Antimicrobial Micro/Nanocomposites during the Oxidation of Bimetallic Al/Zn Nanoparticles. *Russian Journal of Physical Chemistry A*, 92(12), pp. 2530–2534. doi:10.1134/S0036024418120270
10. Palza, H., 2015. Antimicrobial Polymers with Metal Nanoparticles. *International Journal of Molecular Sciences*, 16(1), pp. 2099–2116. doi:10.3390/ijms16012099

11. Hoshyar, N., Gray, S., Han, H. and Bao, G., 2016. The Effect of Nanoparticle Size on in vivo Pharmacokinetics and Cellular Interaction. *Nanomedicine*, 11(6), pp. 673–692. doi:10.2217/nnm.16.5
12. Hu, W., Culloty, S., Darmody, G., Lynch, S., Davenport, J., Ramirez-Garcia, S., Dawson, K.A., Lynch, I., Blasco, J. et al., 2014. Toxicity of Copper Oxide Nanoparticles in the Blue Mussel, *Mytilus edulis*: a Redox Proteomic Investigation. *Chemosphere*, 108, pp. 289–299. doi:10.1016/j.chemosphere.2014.01.054
13. Xia, T., Kovochich, M., Brant, J., Hotze, M., Senpf, J., Oberley, T., Sioutas, C., Yeh, J.I., Wiesner, A.E. et al., 2006. Comparison of the Abilities of Ambient and Manufactured Nanoparticles to Induce Cellular Toxicity according to an Oxidative Stress Paradigm. *Nano Letters*, 6(8), pp. 1794–1807. doi:10.1021/nl061025k
14. Hsin, Y.-H., Chen, C.-F., Huang, S., Shih, T.-S., Lai, P.-S. and Chueh, P.J., 2008. The Apoptotic Effect of Nanosilver is Mediated by a ROS-and JNK-Dependent Mechanism Involving the Mitochondrial Pathway in NIH3T3 Cells. *Toxicology Letters*, 179(3), pp. 130–139. doi:10.1016/j.toxlet.2008.04.015
15. Svarovskaya, N.V., Bakina, O.V., Glazkova, E.A., Lerner, M.I., Lozhkomoev, A.S., Serova, A.N. and Khorobraya, E.G., 2013. Evaluation of the Toxicity of Nanostructural Aluminium Oxyhydroxide with the Help of Hydrobionts Svarovskaya. *Chemistry for Sustainable Development*, 21(4), pp. 411–414. Available at: https://sibran.ru/en/journals/issue.php?ID=150645&ARTICLE_ID=150654 [Accessed: 18 February 2023].
16. Zhu, X., Wang, J., Zhang, X., Chang, Y. and Chen, Y., 2010. Trophic Transfer of TiO_2 Nanoparticles from Daphnia to Zebrafish in a Simplified Freshwater Food Chain. *Chemosphere*, 79(9), pp. 928–933. doi:10.1016/j.chemosphere.2010.03.022
17. Miller, R.J., Lenihan, H.S., Muller, E.B., Tseng, N., Hanna, S.K. and Keller, A.A., 2010. Impacts of Metal Oxide Nanoparticles on Marine Phytoplankton. *Environmental Science and Technology*, 44(19), pp. 7329–7334. doi:10.1021/es100247x
18. Cong, Y., Jin, F., Wang, J. and Mu, J., 2017. The Embryotoxicity of ZnO Nanoparticles to Marine Medaka, *Oryzias melastigma*. *Aquatic Toxicology*, 185, pp. 11–18. doi:10.1016/j.aquatox.2017.01.006
19. Allahverdiyev, A.M., Abamor, E.S., Bagirova, M. and Rafailovich, M., 2011. Antimicrobial Effects of TiO_2 and Ag_2O Nanoparticles against Drug-Resistant Bacteria and Leishmania Parasites. *Future Microbiology*, 6(8), pp. 933–940. doi:10.2217/fmb.11.78
20. Mosunov, A.A. and Evstigneev, V.P., 2021. Nanoparticles in Marine Antifouling Coatings: a Case Study. *Journal of Physics: Conference Series*, 2094(2), 022041. doi:10.1088/1742-6596/2094/2/022041
21. Bakina, O., Glazkova, E., Rodkevich, N., Mosunov, A., Chzhou, V. and Lerner, M., 2022. Electroexplosive Synthesis of Composite $ZnO/ZnFe_2O_4$/Zn Nanoparticles with Photocatalytic and Antibacterial Activity. *Materials Science in Semiconductor Processing*, 152, 107076. doi:10.1016/j.mssp.2022.107076
22. Canesi, L., Ciacci, C., Betti, M., Fabbri, R., Canonico, B., Fantinati, A., Marcomini, A. and Pojana, G., 2008. Immunotoxicity of Carbon Black Nanoparticles to Blue Mussel Hemocytes. *Environment International*, 34(8), pp. 1114–1119. doi:10.1016/j.envint.2008.04.002
23. Andreyeva, A.Y., Kladchenko, E.S., Kukhareva, T.A. and Sakhon, E.G., 2019. Analysis of Cell Cycle and Morphological and Functional Abnormalities of *Mytilus galloprovincialis* Lam., 1819 (Bivalvia) Hemocytes from Coastal Ecosystems near Sevastopol, Crimea. *Inland Water Biology*, 12(2), pp. 96–103. doi:10.1134/S1995082919060038
24. Canesi, L., Gallo, G., Gavioli, M. and Pruzzo, C., 2002. Bacteria–Hemocyte Interactions and Phagocytosis in Marine Bivalves. *Microscopy Research and Technique*, 57(6), pp. 469–476. doi:10.1002/jemt.10100

25. Koutsogiannaki, S. and Kaloyianni, M., 2010. Signaling Molecules Involved in Immune Responses in Mussels. *Invertebrate Survival Journal*, 7(1), pp. 11–21. Available at: https://www.isj.unimore.it/index.php/ISJ/article/view/204/119 [Accessed: 18 February 2023].

26. Tiscar, P.G. and Mosca, F., 2004. Defense Mechanisms in Farmed Marine Molluscs. *Veterinary Research Communications*, 28(suppl. 1), pp. 57–62. doi:10.1023/B:VERC.0000045379.78547.23

27. Jovanović, B. and Palić, D., 2012. Immunotoxicology of Non-Functionalized Engineered Nanoparticles in Aquatic Organisms with Special Emphasis on Fish–Review of Current Knowledge, Gap Identification, and Call for Further Research. *Aquatic Toxicology*, 118, pp. 141–151. doi:10.1016/j.aquatox.2012.04.005

28. Chalew, T.E.A., Galloway, J.F. and Graczyk, T.K., 2012. Pilot Study on Effects of Nanoparticle Exposure on *Crassostrea virginica* Hemocyte Phagocytosis. *Marine Pollution Bulletin*, 64(10), pp. 2251–2253. doi:10.1016/j.marpolbul.2012.06.026

29. Dayem, A.A., Hossain, M.K., Lee, S.B., Kim, K., Saha, S.K., Yang, G.-M., Choi, H.Y. and Cho, S.-G., 2017. The Role of Reactive Oxygen Species (ROS) in the Biological Activities of Metallic Nanoparticles. *International Journal of Molecular Sciences*, 18(1), 120. doi:10.3390/ijms18010120

30. Sokolova, I.M., 2013. Energy-Limited Tolerance to Stress as a Conceptual Framework to Integrate the Effects of Multiple Stressors. *Integrative and Comparative Biology*, 53(4), pp. 597–608. doi:10.1093/icb/ict028

31. Barmo, C., Ciacci, C., Canonico, B., Fabbri, R., Cortese, K., Balbi, T., Marcomini, A., Pojana, G., Gallo, G. et al., 2013. In Vivo Effects of n-TiO_2 on Digestive Gland and Immune Function of the Marine Bivalve *Mytilus galloprovincialis*. *Aquatic Toxicology*, 132–133, pp. 9–18. doi:10.1016/j.aquatox.2013.01.014

32. Donaghy, L., Lambert, C., Choi, K.-S. and Soudant, P., 2009. Hemocytes of the Carpet Shell Clam (*Ruditapes decussatus*) and the Manila Clam (*Ruditapes philippinarum*): Current Knowledge and Future Prospects. *Aquaculture*, 297(1–4), pp. 10–24. doi:10.1016/j.aquaculture.2009.09.003

33. Starkov, A.A., 2008. The Role of Mitochondria in Reactive Oxygen Species Metabolism and Signaling. *Annals of the New York Academy of Sciences*, 1147(1), pp. 37–52. doi:10.1196/annals.1427.015

34. Wang, T., Huang, X., Jiang, X., Hu, M., Huang, W. and Wang, Y., 2019. Differential in vivo Hemocyte Responses to Nano Titanium Dioxide in Mussels: Effects of Particle Size. *Aquatic Toxicology*, 212, pp. 28–36. doi:10.1016/j.aquatox.2019.04.012

35. Davies, L.C., Rice, C.M., McVicar, D.W. and Weiss, J.M., 2019. Diversity and Environmental Adaptation of Phagocytic Cell Metabolism. *Journal of Leukocyte Biology*, 105(1), pp. 37–48. doi.org/10.1002/JLB.4RI0518-195R

36. Canesi, L., Ciacci, C., Gallo, G., Marcomini, A. and Pojana, G., 2010. *In vitro* Effects of Suspensions of Selected Nanoparticles (C60 fullerene, TiO_2, SiO_2) on *Mytilus* Hemocytes. *Aquatic Toxicology*, 96(2), pp. 151–158. doi:10.1016/j.aquatox.2009.10.017

Submitted 9.08.2022; accepted after review 5.12.2022;
revised 1.02.2023; published 24.03.2023

About the authors:

Maria S. Podolskaya, Acting Junior Research Associate, A.O. Kovalevsky Institute of Biology of the Southern Seas of RAS (2 Nakhimov Av., Sevastopol, 299011, Russian Federation), **ORCID ID: 0000-0001-8185-3985**, *podolskaya_m99@bk.ru*

Anastasia A. Tkachuk, Junior Research Associate, A.O. Kovalevsky Institute of Biology of the Southern Seas of RAS (2 Nakhimov Av., Sevastopol, 299011, Russian Federation), **ORCID ID**: **0000-0002-4017-7164**, *aatkachuk86@gmail.com*

Alexandra Yu. Andreyeva, Head of the Laboratory of Ecological Immunology of Hydrobionts, A.O. Kovalevsky Institute of Biology of the Southern Seas of RAS (2 Nakhimov Av., Sevastopol, 299011, Russian Federation), Ph.D. (Biol.), **ORCID ID: 0000-0001-7845-0165, ResearcherID: Z-6151-2019, Scopus AuthorID: 57191916535**, *andreevaal@gmail.com*

Ekaterina S. Kladchenko, Research Associate, A.O. Kovalevsky Institute of Biology of the Southern Seas of RAS (2 Nakhimov Av., Sevastopol, 299011, Russian Federation), **ORCID ID: 0000-0001-9476-6573, ResearcherID: U-7749-2019, Scopus AuthorID: 57205560752**, *Kladchenko_Ekaterina@bk.ru*

Elina S. Chelebieva, Senior Research Associate, A.O. Kovalevsky Institute of Biology of the Southern Seas of RAS (2 Nakhimov Av., Sevastopol, 299011, Russian Federation), Ph.D. (Biol.), **ORCID ID: 0000-0002-7662-2573, ResearcherID: H-3359-2014, Scopus AuthorID: 56549997100**, *elina.chelebieva@gmail.com*

Andrey A. Mosunov, Leading Research Associate, Sevastopol State University (33 Universitetskaya St., Sevastopol, 299053, Russian Federation), Ph.D. (Phys.-Math.), **ORCID ID: 0000-0002-1390-5832, ResearcherID: R-5570-2016, Scopus AuthorID: 36802573200**, *aamosunov@sevsu.ru*

Contribution of the authors:

Maria S. Podolskaya – preparation of the text of the article, conducting experimental studies, qualitative data analysis and interpretation, processing and description of the study results, preparation of graphic materials, review of literature on the study topic

Anastasia A. Tkachuk – formalized data analysis, literature review on the study topic, conducting experimental studies, text editing

Alexandra Y. Andreyeva – formulation and research task statement, development of the concept, development of methods for conducting experimental studies, formulation of conclusions, editing of the text

Ekaterina S. Kladchenko – preparation of graphic materials, conducting experimental studies, editing text

Elina S. Chelebieva – conducting experimental studies, text editing

Andrey A. Mosunov – synthesis of nanoparticles, text editing

All the authors have read and approved the final manuscript.

Original article **DOI**: 10.29039/2413-5577-2023-1-137-145

Thermoprofilemeter for Measuring the Vertical Temperature Distribution in the Upper 100-Meter Layer of the Sea and its Testing in the Arctic Basin

P. V. Gaisky *, I. E. Kozlov

Marine Hydrophysical Institute of RAS, Sevastopol, Russia
** e-mail: gaysky@inbox.ru*

Abstract

The paper describes the technical and methodological aspects of development of an experimental sample of a distributed temperature sensor. The thermoprofilemeter is created for Arctic studies of the thermal near-surface structure of marine environment, including vertical temperature profiles, detection of thermocline and internal waves. The temperature-sensitive part of the sensor built on the basis of continuous spatially modulated conductors measures 48 m. The spatial-averaged resolution is 1.5 m. The sensor can be used in static and dynamic measurement modes, including sounding and towing. Control of the depth of the measuring part is carried out using hydrostatic pressure sensors located at the ends of the sensor. The specialized software provides the display with measuring information in the form of instantaneous temperature profiles as well as in the form of the dynamics of temperature isolines with reference to depth and time, in telemetric mode and during post-processing. The calculated isolines provide automatic control of the spatial vertical displacement of the thermocline, and the amplitude and period of internal waves. An experimental sample of the device was used in Arctic studies in 2021.

Keywords: distributed temperature sensor, thermoprofilemeter, isotherm, heat storage, thermocline, internal waves, temperature field, heat exchange, termistor chain.

Acknowledgements: The research was performed under state assignment on topic no. 0555-2021-0004 (creation of the thermoprofilemeter) and RSF grant no. 21-17-00278 (*in situ* measurements of internal waves in the Arctic Ocean).

For citation: Gaisky, P.V. and Kozlov, I.E., 2023. Thermoprofilemeter for Measuring the Vertical Temperature Distribution in the Upper 100-Meter Layer of the Sea and its Testing in the Arctic Basin. *Ecological Safety of Coastal and Shelf Zones of Sea*, (1), pp. 137–145. doi:10.29039/2413-5577-2021-3-137-145

Термопрофилемер для измерения вертикального распределения температуры в верхнем 100-метровом слое моря и его испытания в Арктическом бассейне

П. В. Гайский *, И. Е. Козлов

Морской гидрофизический институт РАН, Севастополь, Россия
** e-mail: gaysky@inbox.ru*

Аннотация
Описаны технические и методические аспекты разработки экспериментального образца распределенного датчика температуры – термопрофилемера. Измеритель создан для исследований термической приповерхностной структуры морской среды в Арктике, включая контроль вертикальных профилей температуры по глубине, обнаружение термоклина и определение параметров внутренних волн. Длина термочувствительной части датчика, построенной на базе непрерывных пространственно-модулированных проводников, составляет 48 м. Пространственно-осредненное разрешение – 1.5 м. Датчик может использоваться в статическом и динамическом режимах измерений, включая зондирование и буксировку. Контроль заглубления измерительной части осуществляется с помощью гидростатических датчиков давления, расположенных на концах датчика. Специализированное программное обеспечение измерителя осуществляет отображение измерительной информации в виде мгновенных профилей температуры, а также динамики изолиний температуры с привязкой к пространству и времени в телеметрическом режиме и при постобработке. По пространственному положению и смещению рассчитанных изолиний по глубине во времени обеспечивается автоматический контроль местонахождения термоклина, амплитуды и периода внутренних волн. Экспериментальный образец измерителя использовался в арктических исследованиях 2021 г.

Ключевые слова: распределенный датчик температуры, термопрофилемер, изотерма, теплозапас, термоклин, внутренние волны, поле температуры, теплообмен, термокоса

Благодарности: работа выполнена в рамках государственного задания по теме № 0555-2021-0004 (создание термопрофилемера) и гранта РНФ № 21-17-00278 (выполнение натурных измерений внутренних волн в Арктике).

Для цитирования: *Гайский П. В., Козлов И. Е.* Термопрофилемер для измерения вертикального распределения температуры в верхнем 100-метровом слое моря и его испытания в Арктическом бассейне // Экологическая безопасность прибрежной и шельфовой зон моря. 2023. № 1. С. 137–145. EDN CWVFVA. doi:10.29039/2413-5577-2021-3-137-145

Introduction

Studies of the dynamics of temperature changes in the aquatic environment of the Arctic region are becoming increasingly important due to an active development of the region and the development of climatic anomalies [1, 2]. Along with the tasks of controlling the heat reserve and heat transfer processes in the aquatic environment, there is a need for a qualitative study of the transfer, distribution and dynamics of mixing of water masses, taking into account currents, internal

waves [3–7] and other phenomena of hydrological, meteorological, geological and anthropogenic nature.

One of the tools for such studies is distributed temperature sensors – spatially discrete thermistor chains [8–10] and distributed thermoprofilemeters [11, 12]. With increased requirements for accuracy and speed of measurements, in some cases, thermoprofilemeters are preferable. The operation of thermoprofilemeters is based on the interrogation of analog conductor sensors. Therefore, with appropriate metrological calibration and implementation of electronic circuits of the primary measuring transducer, unlike serial digital analogues, thermoprofilemeters can successfully operate in a wide temperature range. Structurally, thermoprofilemeters can have adaptive spatial resolution. Polling of all distributed sensors in a thermoprofilemeter is carried out simultaneously. The experience of using thermoprofilemeters in expeditionary studies has shown their reliability both in telemetric applications and in long-term autonomous applications. Since the electronics of the meter is designed for operating temperature ranges from –40 to +60 °C, and the mechanical loads on the temperature-sensitive sensor cable are limited by its specific technical design (load-carrying protection and sheath), a thermoprofilemeter can be quite successfully used in seasonal working conditions of the Arctic research.

Equipment

Since the main measuring purpose of the designed sensor is the temperature processes in the Arctic region, occurring at depths of up to 100–150 m, an ideal distributed measuring device for vertical instantaneous temperature profiles would be a sensor of an appropriate length. An experimental device 48 m long was made from 32 distributed sections of 1.5 m each. Control of internal waves at the boundary of the detected thermocline with a depth of more than 50 m is supposed to be carried out using a measuring device in the towed-sounding mode (due to the supply of cable-rope). Provided that the sensor body is straight, its vertical orientation and reference of temperature measurements in depth are controlled by hydrostatic pressure sensors located at the extreme upper and lower points of the measuring device. In the manufacture of pressure measuring channels, the Honeywell MLH300PSL06A sensors were used. In the manufacture of the temperature sensor part, copper conductors (∅ 0.18 mm wire) were used, laid according to orthogonal functions [11, 12] in a protective polyamide tube ∅ 6–10 mm with a parallel internal load-bearing steel cable. A submersible microcontroller electronics unit provides channel switching and analog-to-digital conversion of measuring information with the transmission of primary data frames via a cable-rope to an onboard computer device via a standard RS232/485 serial interface. The body of the electronics unit is made of stainless steel and polyacetate (POM-C). A block diagram and a general view of the measuring device are shown in Fig. 1 and 2, respectively.

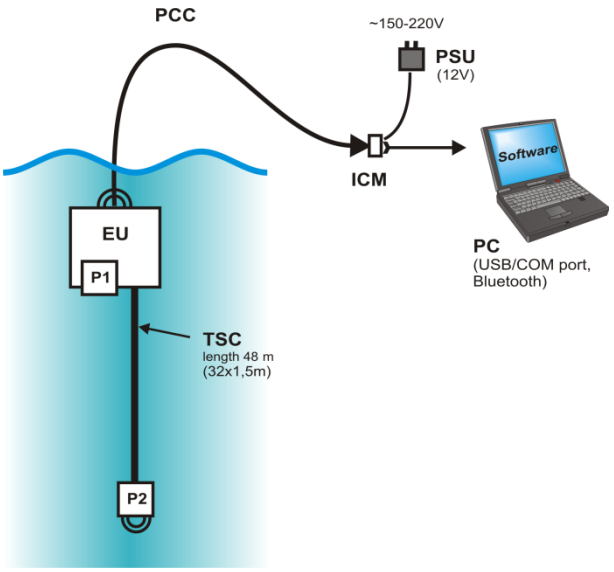

Fig. 1. Device block diagram

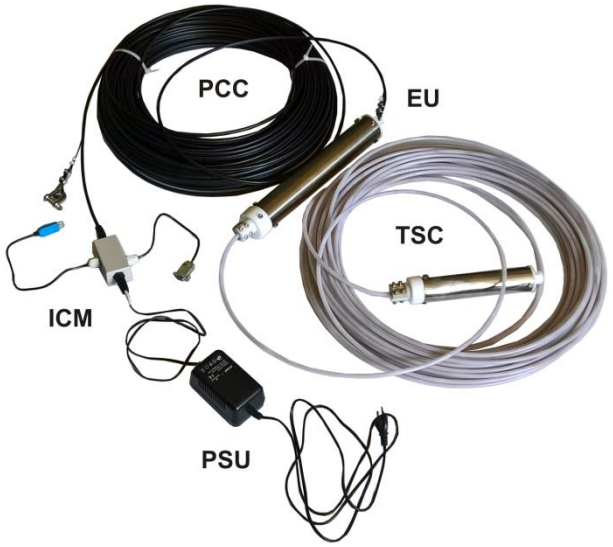

Fig. 2. General view of the device

The main structure of the measuring device includes:

– a temperature-sensitive submersible sensor cable (TSC);

– a submersible electronics unit (EU);

– hydrostatic pressure sensors built into EU and TSC (S1 and S2), calculated for depths of up to 200 m (readings up to 100 m);

– a connecting power and communication cable (PCC);

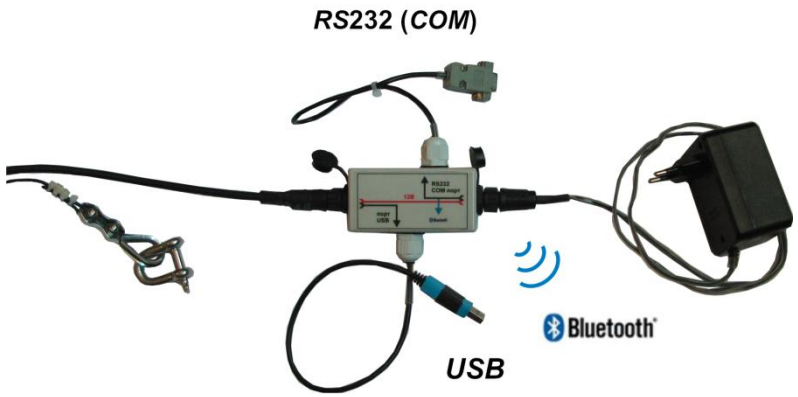

F i g . 3 . Interface conversion module (ICM) view and connection

– an interface conversion module (ICM)

– an external power conversion and stabilization unit from ~ 220 V to 12 V (PSU);

– specialized software for primary registration and processing of measuring device data for a PC (software).

To ensure flexibility of connecting the measuring device to a computer device, a multi-interface module (Fig. 3), which provides the ability to use standard COM, USB and Bluetooth ports (via virtual COM) was developed.

Results

A functional diagram of the developed electronics unit of the measuring device is shown in Fig. 4. The measuring channels of the device are polled in the switching mode. For distributed sensor conductors, a parallel current-potential switching (K_i and K_u) is used. The pressure sensors are polled by a separate switch (K_uS). Analog-to-digital conversion is carried out using a 24-bit sigma-delta converter by Analog Devices.

A functional diagram of the ICM is shown in Fig. 5. This module uses ready-made interface conversion solutions, standard drivers and available system options for setting up and connecting external devices to a PC.

Specialized software for recording, processing and displaying measuring device data [1)] operates in MS Windows operating systems.

[1)] Gaisky, P.V., 2022. [*Program for Registration and Processing of Thermoprofilemeter Measurement Data "THERMOPROF"*]. Sevastopol: MHI. State Registration no. 2022611315.

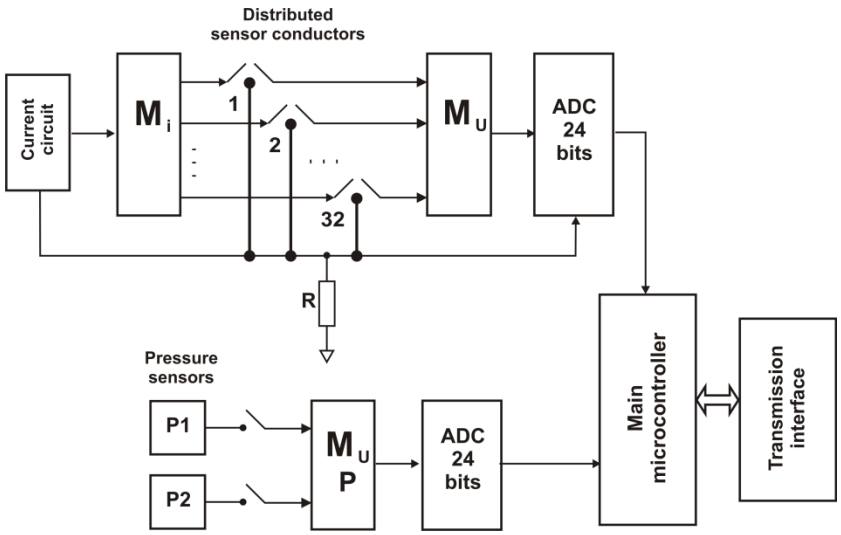

F i g . 4 . Functional diagram of the device electronics unit

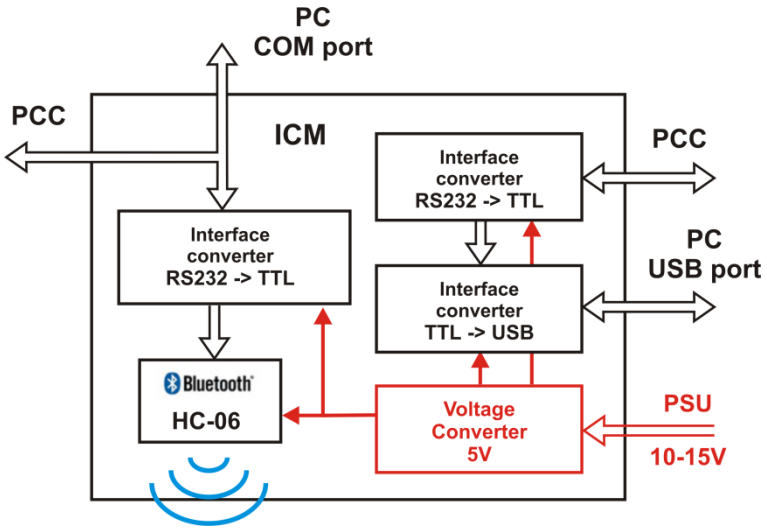

F i g . 5 . Interface conversion module functional diagram

Based on the results of metrological verifications, as well as on the requirements established by the terms of reference, the technical and metrological characteristics of the experimental sample of the device were formulated:

– TSC length – 48 m;

– number of sections – 32 pcs.;

– spatial-averaged resolution of TSC – 1.5 m;

– period of measuring the profile and orientation in depth (polling frequency) – 2 s;

– measurement error of temperature averaged over the TSC section ±0.1 °C in the range from 0 to +25 °C;

– depth measurement error at the installation points of pressure sensors (S1 and S2) – 0.1 dBa (0.1 m) in the range from 0 to 100 m;

– digital temperature resolution – 0.0007 °C;

– digital pressure resolution – 0.00008 dBa;

– average inertia of TCS in liquid – 30 s;

– power supply of the submersible part (TSC and EU) according to the PCC – direct voltage from 10 to 15 V (up to 2 W);

– PCC length – 40÷100 m;

– measuring device weight (TSC, EU, PCC, ICM, PSU) – up to 15 kg;

– external dimensions of the measuring device in the packaging kit – 0.6 × 0.6 × 0.2 m.

Fig. 6 shows a fragment of records of measurements carried out in the deep-water area during the Arctic expedition [13]. The result is displayed as temperature isolines of a vertical profile with reference to depth and time. The developed thermoprofilemeter was used in the towed-sounding mode from the ship. The figure clearly shows fluctuations of isothermal surfaces. The fluctuation of the 4 and 6 °C isotherms from 11:10 to 11:20 about 30 m high in the 10–50 m layer is most

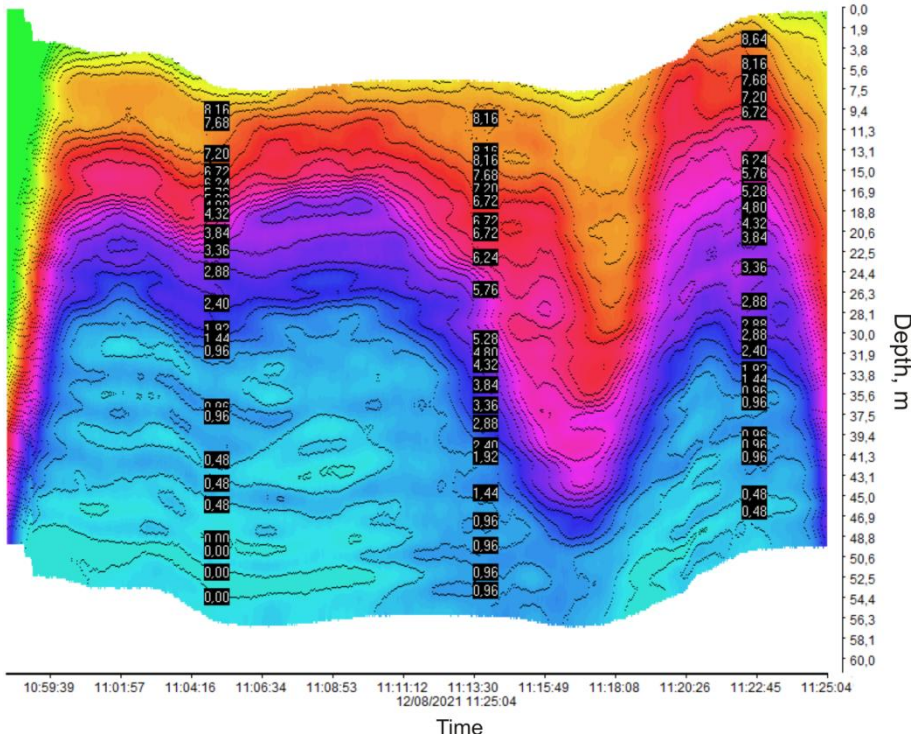

Fig. 6. Example of measurement recording by a sensor in the Arctic in towed-sounding mode in temperature isolines

pronounced, and, according to the authors, is associated with the passage of a short-period internal wave in the measurement area. During this experiment, the ship moved 1 km with an average drift speed of 66.7 cm/s. The maximum sounding in depth according to the data of pressure sensors located at the ends of the measuring device was carried out up to +7 m to the length of the thermoprofilemeter. The measuring system in the telemetric mode monitored the depth of the thermoprofilemeter and the position of the thermocline, and the algorithms for controlling spatial displacements of the isolines monitored the amplitude and the internal wave period. At the same time, the figure clearly shows thermal inertia of the distributed sensor in the first 20 seconds after the dive. Obviously, when evaluating observational data in dynamic modes and in the presence of gradients, it must be taken into account. For an objective analysis of the lengths of detected internal waves, it is necessary to simultaneously control the speed of outboard currents.

Conclusion

The developed experimental sample of the measuring device passed primary full-scale tests and provided researchers in expeditionary work with high-quality operational information. Further modernization of the design of the measuring device will increase the mechanical load capacity of the sensor cable and overall reliability. Taking into account the technical modification, additional methods of using thermoprofilemeters for Arctic research are considered, including an autonomous installation and the possibility of long-term measurements in towed mode.

The measurement results obtained with the help of thermoprofilemeters are characterized by greater accuracy and less discreteness (both temporal and spatial) compared to common thermal pendants made in the form of a string of digital temperature sensors. Specialized software algorithms provide efficiency in the visual display of telemetric measurement information.

References

1. Ivanov, V.V., Arkhipkin, V.S., Lemeshko, E.M., Myslenkov, S.A., Smirnov, A.V., Surkova, G.V., Tuzov, F.K., Chechin, D.G. and Shestakova, A.A., 2022. Changes in Hydrometeorological Conditions in the Barents Sea as an Indicator of Climatic Trends on the Eurasian Arctic on the 21st Century. *Vestnik Moskovskogo Universiteta. Seria 5, Geografia*, (1), pp. 13–25 (in Russian).
2. Ashik, I.M., Alekseev, V.V., Bloshkina, E.V., Kulakov, M.Yu., Makhotin, M.S., Tarasenko, A.D. and Filchuk, K.V., 2022. State and Development Prospects of the Hydrological Monitoring System of the Arctic Ocean. *Arctic and Antarctic Research*, 68(1), pp. 8–25. doi:10.30758/0555-2648-2022-68-1-8-25 (in Russian).
3. Bukatov, A.A., Solovei, N.M. and Pavlenko, E.A., 2021. Free Short-Period Internal Waves in the Arctic Seas of Russia. *Physical Oceanography*, 28(6), pp. 599–611. EDN MYIODE. doi:10.22449/1573-160X-2021-6-599-611
4. Svergun, E.I., Zimin, A.V. and Zhegulin, G.V., 2022. Observations of the Second Mode Internal Waves in the White and Barents Seas. *Physical Oceanography*, 29(2), pp. 172–181. doi:10.22449/1573-160X-2022-2-172-181
5. Morozov, E.G. and Paka, V.T., 2010. Internal Waves in a High-Latitude Region. *Oceanology*, 50(5), pp. 668–674. doi:10.1134/S0001437010050048

6. Kozlov, I., Kudryavtsev, V., Zubkova, E.V., Zimin, A.V. and Chapron, B., 2015. Characteristics of Short-Period Internal Waves in the Kara Sea Inferred from Satellite SAR Data. *Izvestiya: Atmospheric and Oceanic Physics*, 51(9), pp. 1073–1087. doi:10.1134/S0001433815090121
7. Kozlov, I.E., Kudryavtsev, V.N., Zubkova, E.V., Atadjanova, O.A., Zimin, A.V., Romanenkov, D.A., Chapron, B. and Myasoedov, A.G., 2014. Generation Sites of Nonlinear Internal Waves in the Barents, Kara and White Seas from Spaceborn SAR Observations. *Sovremennye Problemy Distantsionnogo Zondirovaniya Zemli iz Kosmosa*, 11(4), pp. 338–345 (in Russian).
8. Ocherednik, V.V., Baranov, V.I., Zatsepin, A.G. and Kyklev, S.B., 2018. Thermochains of the Southern Branch, Shirshov Institute of Oceanology, Russian Academy of Sciences: Design, Methods, and Results of Metrological Investigations of Sensors. *Oceanology*, 58(5), pp. 661–671. doi:10.1134/S0001437018050090
9. Nikolaev, N.I., Vasilyeva, N.V. and Nikolaeva, I.V., 2021. Development of a Device for Remote Monitoring of "Thermo-Braid" Temperature Environment. *Science and Business: Development Ways*, (11), pp. 17–23 (in Russian).
10. Tolstosheev, A.P., Lunev, E.G. and Motyzhev, S.V., 2014. [Analysis of the Results of in situ Experiments with Thermoprofiling Drifting Buoys in the Black Sea and other Areas of the World Ocean]. *Morskoy Gidrofizicheskiy Zhurnal*, (5), pp. 9–32 (in Russian).
11. Gaisky, V.A. and Gaisky, P.V., 2001. Distributed Thermoprofilometers and their Capabilities in Oceanographic Investigations. *Physical Oceanography*, 11(6), pp. 543–577. doi:10.1007/BF02509846
12. Gayskiy, V.A. and Gayskiy, P.V., 2018. *Use of Distributed Sensors for Sea Temperature Measurements*. Sevastopol: IPTS, 175 p. https://doi.org/10.33075/978-5-6040795-4-6 (in Russian).
13. Kopyshov, I.O., Kozlov, I.E., Zhuk, V.R., Artamonova, A.V., Silvestrova, K.P., Mekhova, O.S., Korzhenovskaya, A.I., Frey, D.I., Jamalova, A.G., Gaisky, P.V. et al., 2021. Study of High-Amplitude Internal Waves in the Kara Gate Strait in August 2021. In: MRC MSU, 2021. *Proceedings of X International Conference "Marine Research and Education", 25–29 October 2021*. Tver: OOO "PoliPRESS", pp. 238–241 (in Russian).

Submitted 18.08.2022; accepted after review 11.10.2022;
revised 1.02.2023; published 24.03.2023

About the authors:

Pavel V. Gaisky, Leading Research Associate, Head of Innovation Marine Instrument Engineering Laboratory of SCU, Marine Hydrophysical Institute of RAS (2 Kapitanskaya St., Sevastopol, 299011, Russian Federation), Ph.D. (Tech.), **Scopus Author ID: 7801588003, SPIN-code: 7789-0658,** *gaysky@inbox.ru*

Igor E. Kozlov, Leading Research Associate, Head of Polar Marine Research Laboratory, Marine Hydrophysical Institute of RAS (2 Kapitanskaya St., Sevastopol, 299011, Russian Federation), Ph.D. (Phys.-Math.), **ORCID ID**: **0000-0001-6378-8956**, **ResearcherID: G-1103-2014**, **Scopus Author ID: 49963767500**, *ik@mhi-ras.ru*

Contributions of the authors:

Pavel V. Gaisky – development and production of the device, development of the software

Igor E. Kozlov – testing the device during an Arctic expedition, analysis of measurement data

All the authors have read and approved the final manuscript.